

AN ABSTRACT OF THE THESIS OF

Jennifer L. Stone-Sundberg for the degree of Doctor of Philosophy in Chemistry
presented on December 3, 2001.

Title: A Contribution to the Development of Wide Band-Gap Nonlinear Optical
and Laser Materials

Abstract approved: Redacted for privacy
Douglas A. Keszler

The primary focus of this work is on examining structure-property relationships of interest for high-power nonlinear optical and laser crystals. An intuitive and simply illustrated method for assessing the nonlinear optical potential of structurally characterized noncentrosymmetric materials is introduced. This method is applied to materials including common quartz and tourmaline and then extended to synthetic materials including borates, silicates, aluminates, and phosphates. Particularly, the contributions of symmetric tetrahedral and triangular anionic groups are inspected. It is shown that both types of groups significantly contribute to the optical frequency converting abilities of noncentrosymmetric crystals. In this study, several known materials are included as well as several new materials. The roles of the orientation, composition, and packing density of these anionic groups are also discussed.

The structures and optical properties of the known materials BPO_4 , NaAlO_2 , $\text{LaCa}_4\text{O}(\text{BO}_3)_3$, and tourmaline; the new compounds $\text{La}_{0.8}\text{Y}_{0.2}\text{Sc}_3(\text{BO}_3)_4$ and $\text{Ba}_2\text{B}_{10}\text{O}_{17}$; and the laser host $\text{Sr}_3\text{Y}_{0.75}\text{Yb}_{0.25}(\text{BO}_3)_3$ are described.

Copyright © December 3, 2001 by
Jennifer Stone-Sundberg

A Contribution to the Development of Wide Band-Gap Nonlinear Optical and

Laser Materials

by

Jennifer L. Stone-Sundberg

A THESIS

Submitted to

Oregon State University

In partial fulfillment of

The requirements for the

Degree of

Doctor of Philosophy

Completed December 3, 2001

Commencement June 2002

Doctor of Philosophy dissertation of Jennifer L. Stone-Sundberg presented on
December 3, 2001.

APPROVED:

Redacted for privacy

Major Professor, representing Chemistry

Redacted for privacy

Head of Department, representing Chemistry

Redacted for privacy

Dean of the Graduate School

I understand that my dissertation will become part of the permanent collection of Oregon State University libraries. My signature below authorizes release of my dissertation to any reader upon request.

Redacted for privacy

Jennifer L. Stone-Sundberg, Author

ACKNOWLEDGEMENTS

I am particularly indebted to my major professor Dr. Douglas Keszler for his enthusiasm, support, and unending supply of good ideas in seeing me to the completion of this degree.

I also thank Drs. Judith Kissick, Gerard Aka, Andree Kahn-Harrari, Ben Clark, Uma Sitharaman, Joseph Nibler, Thomas Plant, John Emmett, Elizabeth Austin-Minor, Roger Neilsen, Alex Yokochi, Greg Peterson, and Tom Reynolds for many useful discussions, helpful suggestions, and for taking the time to listen.

Others who have been tremendously helpful include Jeff Barber (thanks for all of the great lunch sessions!), Tim Thomas, Erwin Schutfort, Ted Hinke, Nipaka Sukpirom, Sangmoon Park, Elisabeth Reino, Linda White, and the current Keszler group members Jeremy Anderson, Mike Hrushka, and Cheolhee Park.

Finally, I want to acknowledge my husband, Garth Sundberg, for his selflessness in helping and supporting me through this process. I will always remember the patience and kindness you have shown me.

CONTRIBUTION OF AUTHORS

This work would not have been possible without the help of several collaborators. These collaborators and their respective contributions are given here. Michael Hrushka assisted in the crystal growth and characterization of YLSB for chapter 2. Jeffrey Barber and Joseph Nibler assisted in designing and executing the SHG measurements of the tourmaline crystal in Chapter 6. Erwin Schutfort performed the ICP analyses of the tourmaline in Chapter 6. Gerard Aka was involved in the crystal growth of $\text{Ba}_2\text{B}_{10}\text{O}_{17}$ while Andree Kahn-Harari and Thomas Reynolds provided many useful discussions in the writing of Chapter 7. The crystal studied in Chapter 8 was grown by Romain Gaume, Paul-Henri Haumesser, Bruno Viana, Gerard Aka, and Andree Kahn-Harari of ENSCP-CNRS.

TABLE OF CONTENTS

CHAPTER 1: INTRODUCTION	1
Overview	1
The nonlinear optical effect and second-harmonic generation ..	4
Influences on the refractive index of a material	4
Description of the polarizability of a material	6
Second-harmonic generation and the effect of crystal symmetry	7
Phase matching	10
The coherence length l_c	10
The phase matching angle θ_{pm}	10
Types of phase matching	11
Effect on SHG from identity, orientation, and packing of oxoanions	13
A survey of current nonlinear optical crystals and their applications	16
Frequency-doubling crystals currently in use	16
Applications of frequency-doubling crystals	18
Development and characterization of new SHG materials	19
References	21
CHAPTER 2: $\text{La}_{0.75}\text{Y}_{0.25}\text{Sc}_3(\text{BO}_3)_4$: A NEW TRIGONAL HUNTITE .	23
Abstract	24
Introduction	25
Experimental	27
Synthesis and crystal growth	27

TABLE OF CONTENTS (continued)

Elemental analysis	27
Structure analysis	28
Unit cell and intensity data collection	28
Solution and refinement	29
Differential thermal analysis	33
Optical second-harmonic generation studies	33
Results and Discussion	35
Structure	35
Frequency conversion	35
Thermal analysis	41
Summary and Future Work	43
Acknowledgements	43
References	44
CHAPTER 3: $\text{LaCa}_4\text{O}(\text{BO}_3)_3$ (LaCOB): OPTICAL SECOND- HARMONIC GENERATION FROM TRIANGULAR OXOANIONS	47
Abstract	48
Introduction	49
Experimental	50
Results and Discussion	59
Acknowledgement	62
References	63

TABLE OF CONTENTS (continued)

CHAPTER 4: BPO ₄ : OPTICAL SECOND-HARMONIC GENERATION FROM WIDE BAND-GAP TETRAHEADRAL GROUPS		65
Abstract		66
Introduction		67
Experimental		68
Synthesis and powder characterization		68
Powder synthesis		68
Powder SHG measurements		68
Single crystal growth		69
X-ray studies		69
Unit-cell determination and data collection		69
Structure refinement		70
Results and Discussion		74
Structure		74
SHG properties		78
Summary		85
Acknowledgement		85
References		86
CHAPTER 5: STRUCTURE AND SECOND- HARMONIC GENERATION FOR NaAlO ₂		88
Abstract		89
Introduction		90
Experimental		91
Synthesis and powder characterization		91
Powder synthesis		91

TABLE OF CONTENTS (continued)

Powder SHG measurements	91
Crystal growth	92
X-ray studies	92
Results and Discussion	97
Structure	97
SHG properties	102
Powder SHG measurements	102
Calculation of d_{ijk}	102
Acknowledgement	107
References	108
CHAPTER 6: TOURMALINE: STRUCTURE, COMPOSITION, AND OPTICAL SECOND-HARMONIC GENERATION	
	110
Abstract	111
Introduction	112
Experimental	115
X-ray analysis	115
Unit cell and intensity data collection	115
Refinement	115
Elemental analyses	119
Electron microprobe	119
Inductively coupled plasma spectroscopy (ICP) .	119
FTIR study to determine the presence of OH	120
SHG characterization	121
Determination of the phase-matching angle	122
Determination of types of phase-matching	122
Determination of conversion efficiency (d_{eff})	122
Determination of surface-damage threshold	123
Results and Discussion	124
Structure and elemental composition	124
Optical characterization	130

TABLE OF CONTENTS (continued)

Determination of the phase-matching angle	130
Determination of types of phase-matching	131
Determination of conversion efficiency (d_{eff})	132
Determination of surface-damage threshold	132
Summary	135
Acknowledgements	136
References	137
CHAPTER 7: NONLINEAR OPTICAL BORATE CRYSTAL	
$\text{Ba}_2\text{B}_{10}\text{O}_{17}$	140
Abstract	141
Introduction	142
Experimental	144
Results	146
Conclusions	155
Acknowledgements	156
References	157
CHAPTER 8: $\text{Sr}_3\text{Y}_{0.814}\text{Yb}_{0.186}(\text{BO}_3)_3$: STRUCTURE OF	
Yb-DOPED BORATE LASER MATERIAL	159
Abstract	160
Introduction	161
Experimental	162
Crystal growth	162
X-ray analysis	164

TABLE OF CONTENTS (continued)

Unit cell parameters and data collection	164
Structure refinement	165
Elemental analysis	170
Results and Discussion	171
Structure	171
Elemental analysis	171
Acknowledgements	173
References	174
 BIBLIOGRAPHY	 176

LIST OF FIGURES

Figure	Page
1.1. Illustration of Snell's law of refraction	4
1.2. Illustration of refractive index versus frequency	6
1.3. Polarization directions and angles in a Type I phase-matched negative uniaxial crystal	12
1.4. D_{3h} oxoanion BO_3^{3-}	15
2.1. Modified Kurtz-Perry powder SHG setup	34
2.2. Drawing of YLSB structure	36
2.3. Simulated Cu-K α powder pattern for YLSB	38
2.4. YLSB structure: view down the c axis	40
2.5. DTA of YLSB	42
3.1. LaCOB viewed down the c -axis	60
3.2. LaCOB viewed down the a -axis	61
4.1. Unit-cell drawing of BPO_4	75
4.2: Powder diffraction patterns for BPO_4	76
4.3. BPO_4 viewed down the c axis	80
4.4. Illustration of tetrahedra orientation in BPO_4	81
4.5. Rotation of a tetrahedral group by 90° about one of the Cartesian axes produces an orientation that is centrosymmetrically related to the original resulting in the sum of the β values for the two orientations equaling zero, or $\beta(1,2,3) = -\beta'(1,2,3)$	82
4.6. Drawing of a unit-cell of α -quartz	83

LIST OF FIGURES (continued)

Figure	Page
5.1. Structure of NaAlO ₂ viewed approximately down the <i>a</i> -axis	98
5.2. NaAlO ₂ viewed down the <i>c</i> -axis	99
5.3. NaAlO ₂ viewed approximately down the <i>b</i> -axis	100
5.4. Illustration of tetrahedra orientation in NaAlO ₂	105
5.5. Rotation of a tetrahedral group by 90° about one of the Cartesian axes	106
6.1. Tourmaline structure viewed down the <i>c</i> axis	113
6.2. FTIR of tourmaline crystal	121
6.3. View down the optic axis of tourmaline	133
6.4. View orthogonal to the optic axis of tourmaline	134
7.1. Structure of Ba ₂ B ₁₀ O ₁₇ as viewed along <i>c</i>	147
7.2. B ₃ O ₈ ring	148
7.3. Calculated (top) and measured (bottom) X-ray powder patterns for Ba ₂ B ₁₀ O ₁₇	149
7.4. X-ray powder patterns for Ba _{2-x} Sr _x B ₁₀ O ₁₇	150
7.5. DTA of Ba ₂ B ₁₀ O ₁₇ ground glass	152
7.6. DTA of crystalline Ba _{2-x} Sr _x B ₁₀ O ₁₇	153
8.1. Boule of 15 at%-doped Yb:BOYS, grown on an iridium rod	163
8.2. Structure of Sr ₃ Y _{0.814} Yb _{0.186} (BO ₃) ₃ viewed along <i>c</i>	172

LIST OF TABLES

Table	Page
1.1. Properties of selected SHG crystals at 1064 nm	17
1.2. Applications of SHG crystals	18
2.1. Elemental analysis and stoichiometry for YLSB	28
2.2. Crystallographic data for YLSB	31
2.3. Positional and thermal parameters (B_{eq}) and occupancy for YLSB	32
2.4. Anisotropic displacement parameters for YLSB	32
2.5. Selected interatomic distances (\AA) and angles ($^\circ$) for YLSB	37
3.1. Crystallographic data for LaCOB	53
3.2. Positional and thermal parameters (B_{eq}) for LaCOB	54
3.3. Anisotropic displacement parameters for LaCOB	54
3.4. Selected interatomic distances (\AA) and angles ($^\circ$) for LaCOB	55
4.1. Experimental details for the structure solution of BPO_4 ...	72
4.2. Positional and isotropic displacement coefficients (B_{eq}) for BPO_4	73
4.3. Anisotropic displacement parameters for BPO_4	73
4.4. Interatomic distances (\AA) and angles ($^\circ$) for BPO_4	77
5.1. Crystallographic data for NaAlO_2	95
5.2. Positional and isotropic displacement parameters (B_{eq}) for NaAlO_2	96

LIST OF TABLES (continued)

Table	Page
5.3. Anisotropic displacement parameters for NaAlO ₂	96
5.4. Selected interatomic distances (Å) and angles (°) for NaAlO ₂	101
6.1. Crystallographic data for tourmaline crystal	117
6.2. Positional and isotropic displacement coefficients (B _{eq})	118
6.3. Electron-microprobe analysis of studied tourmaline crystal	119
6.4. ICP data for studied tourmaline crystal	120
6.5. Interatomic distances (Å) and angles (°) for tourmaline crystal	125
8.1. Crystal growth parameters for Yb:BOYS	163
8.2. Experimental details for the structure solution of Yb:BOYS	167
8.3. Positional and isotropic displacement parameters (B _{eq}) for Yb:BOYS	168
8.4. Anisotropic displacement parameters for Yb:BOYS	168
8.5. Interatomic distances(Å) and angles(°) for Yb:BOYS	169
8.6. Microprobe analysis of Yb:BOYS crystal	170

A CONTRIBUTION TO THE DEVELOPMENT OF WIDE BAND-GAP NONLINEAR OPTICAL AND LASER MATERIALS

CHAPTER 1

INTRODUCTION

Overview

In the time since the frequency doubling of light by a non-centrosymmetric medium was first demonstrated in 1961 by Franken et. al. (1) the development and applications of nonlinear optical (NLO) materials have blossomed. These materials open up the lasing wavelength range to higher energy frequencies than those obtainable by using current single-frequency solid-state, semiconductor, and gas lasers alone. This expanded lasing spectrum contributes to many vital laser applications in fields such as materials processing, medicine, and research.

Frequency doubling or second-harmonic generation (SHG), is a specific NLO response of noncentrosymmetric crystals when they are subjected to high-power coherent light, i.e., a laser beam. This NLO response derives from a

nonlinear, second-order effect of the dielectric polarization. This effect will be further described in the next section. In addition to lacking a center of symmetry, the material must exhibit transparency at both the input (or fundamental) and generated second-harmonic wavelengths, and must be able to withstand the power densities of the input and generated light beams to produce frequency-doubled light. Several other materials parameters must also be optimized to realize an effective and practical SHG crystal.

Researchers have investigated noncentrosymmetric inorganic and organic single crystals as well as poled chiral organic chromophores in polymeric systems (2) as potential sources of commercial SHG materials. Only the inorganic crystals have been found to exhibit favorable properties for application, and they will be the focus of this work. Within these crystals, the composition, geometry, relative orientation, and packing density of specific oxoanion groups are responsible for SHG.

Among NLO materials, borate crystals are unique in providing unsurpassed levels of power and high-frequency capabilities. Despite their relatively high level of development, numerous fundamental questions remain concerning the origins of their nonlinear response, particularly in those systems that contain an admixture of tetrahedral BO_4 and triangular BO_3 groups. In this work, some insight into the contribution of the tetrahedral groups to the nonlinear response is provided through examination of the structures and properties of BPO_4 and NaAlO_2 . Results from these studies have led to the first accounting of the nonlinearity of α -quartz and to a study of the properties of the common

mineral tourmaline. To extend the functional range of NLO borate crystals, two new examples, $\text{Ba}_2\text{B}_{10}\text{O}_{17}$ and $\text{La}_{0.75}\text{Y}_{0.25}\text{Sc}_3(\text{BO}_3)_4$, have been synthesized and characterized, the latter potentially exhibiting properties suitable for direct second-harmonic conversion to vacuum-ultraviolet wavelengths.

In the remainder of this chapter, some of the fundamental and practical aspects of second-harmonic generation will be addressed, a brief review of known materials will be given, and a scheme for development of new crystals will be presented.

The nonlinear optical effect and second-harmonic generation

Influences on the refractive index of a material

The refractive index (n) of a material is given as:

$$n = \frac{c}{v} \quad (1.1)$$

where c is the speed of light in vacuum and v is the velocity of light in the material. This implies that light will slow down in any medium more dense than a vacuum and that the velocity of light will decrease when it crosses a boundary between a less dense medium and a more dense medium. Along with velocity, the wavelength of light going from medium to medium changes in the following fashion,

$$\frac{\lambda_1}{\lambda_2} = \frac{v_1}{v_2} \quad (1.2)$$

and Snell's law of refraction (equation 1.3) describes the path of the light beam traveling from one medium to another and illustrated in Figure 1.1.

$$n_1 \sin \theta_1 = n_2 \sin \theta_2 \quad (1.3)$$

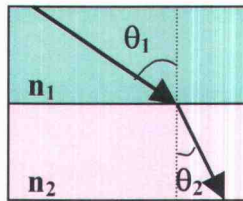


Figure 1.1. Illustration of Snell's law of refraction.

Media other than vacuum contain atoms, which become polarized when they interact with light. This polarization of the atoms and groups of atoms is responsible for the change of speed, wavelength, and direction of light from one medium to another.

The refractive index of a material varies with the frequency of the incident light. A material has several natural frequencies or absorption bands; these are frequencies at which photons are absorbed due to electron motion, vibrations of atoms, and vibrations of groups of atoms. Between two absorption bands the refractive index increases with increasing frequency of incident light. This frequency dependence of the refractive index is known as dispersion and is illustrated in Figure 1.2.

If the material is anisotropic, the refractive index is also dependent on the direction relative to the crystal axes that the incident light enters the crystal. The maximum difference in refractive index as a function of direction is known as birefringence. Other influences on the refractive index of a particular material include temperature, pressure, electric and magnetic fields, and the intensity of the incident light. Detailed descriptions of the dependence of the refractive index of a material on frequency can be found in references 3-7.

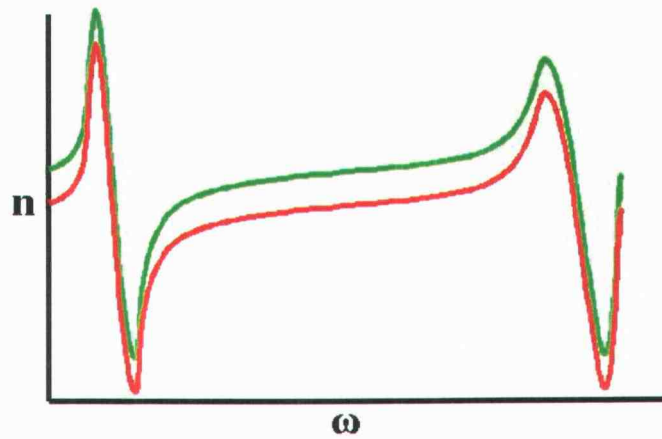


Figure 1.2. Illustration of refractive index versus frequency.

Description of the polarizability of a material

The polarization of a material by an electric field of incident light is not a linear phenomenon, though a linear approximation works for lower intensities of incident light. This polarization can be described with equation 1.4,

$$P_i = \alpha_{ij} E_j + 2d_{ijk} E_j E_k + 4\chi_{ijkl} E_j E_k E_l + \dots \quad (1.4)$$

where P is the polarization, E is the applied electric field, α is the linear or first-order polarizability term or susceptibility of the material, d is the first nonlinear polarizability term or the second-order susceptibility (quadratic polarizability), χ is the third-order susceptibility, and so on. The subscripts i, j, k, l indicate the direction (x, y, z) of the n th component of the polarization or electric field. The susceptibility terms sum over these directions, i.e., α_{ij} is a 3×3 matrix with 9 terms, d_{ijk} is a $3 \times 3 \times 3$ matrix with 27 terms, and χ_{ijkl} is a $3 \times 3 \times 3 \times 3$ matrix

with 81 terms). All even order terms of the series are non-zero only if the material lacks a center of symmetry.

Second-harmonic generation and the effect of crystal symmetry

This work deals exclusively with the second-order term and specifically the frequency-doubling (or second harmonic generation (SHG)) component of this term. Looking at only this term under frequency doubling conditions, the polarizability can be expressed as:

$$P_i^{2\omega=\omega+\omega} = d_{ijk} E_j^\omega E_k^\omega \quad (1.5)$$

Note that i , j , and k take on the integer values: 1 = x, 2 = y, and 3 = z in this notation. Since there is no physical significance to switching j and k in equation 1.5, $jk = kj$ can be substituted by l in the following fashion:

$$l = 1 \text{ when } j \text{ and } k = 1 \quad = \text{xx}$$

$$l = 2 \text{ when } j \text{ and } k = 2 \quad = \text{yy}$$

$$l = 3 \text{ when } j \text{ and } k = 3 \quad = \text{zz}$$

$$l = 4 \text{ when } j \text{ or } k = 2 \text{ and the other} = 3 \quad = \text{zy}$$

$$l = 5 \text{ when } j \text{ or } k = 1 \text{ and the other} = 3 \quad = \text{zx}$$

$$l = 6 \text{ when } j \text{ or } k = 1 \text{ and the other} = 2 \quad = \text{xy.}$$

For example, a d_{ijk} of d_{123} is the same as a d_{il} of d_{14} . Now the second harmonic polarization vector can be expressed as a 3x6 d_{il} matrix operating on the 6 x 1 E matrix:

$$\begin{pmatrix} P_x \\ P_y \\ P_z \end{pmatrix} = \begin{pmatrix} d_{11} & d_{12} & d_{13} & d_{14} & d_{15} & d_{16} \\ d_{21} & d_{22} & d_{23} & d_{24} & d_{25} & d_{26} \\ d_{31} & d_{32} & d_{33} & d_{34} & d_{35} & d_{36} \end{pmatrix} * \begin{pmatrix} E_x^2 \\ E_y^2 \\ E_z^2 \\ 2E_z E_y \\ 2E_z E_x \\ 2E_x E_y \end{pmatrix} \quad (1.6)$$

Depending on the symmetry of the crystal class, many of the d_{il} coefficients go to zero. Only the crystal class 1 in the triclinic system has no symmetry and therefore all 18 terms of the d_{il} matrix are non zero. Each of the other crystal classes has a unique set of present, equivalent, and absent d_{il} terms (6, 8, 9). As stated earlier, crystals with a center of symmetry do not have a second-order term (or any other even-ordered terms) in their polarizability. Mathematically it can be shown that this results in all components of the d_{il} tensor equaling zero (6-10).

For example, the first NLO material demonstrated, α -quartz, belongs to point group 32. For this particular symmetry, only the d_{11} , d_{12} , d_{14} , d_{25} , and d_{26} components are nonzero and are related as shown below.

$$\begin{pmatrix} d_{11} & -d_{11} & 0 & d_{14} & 0 & 0 \\ 0 & 0 & 0 & 0 & -d_{14} & -d_{11} \\ 0 & 0 & 0 & 0 & 0 & 0 \end{pmatrix}$$

Phase matching

To maximize the output SHG power, it is essential to match the phase of this produced SHG wave to that of the fundamental polarization wave. This implies the two wave velocities and hence their refractive indices must be identical (11-12). This phase matching of the waves will yield constructive summation with increasing crystal length and the desired end result of increasing SHG power, barring absorption effects. The relative output power of SHG of a crystal is dramatically controlled by whether or not directions exist in the crystal under the operational conditions that would allow the refractive indices of the fundamental and produced frequencies to be identical. Materials without such conditions are not phase-matchable and produce very low power levels of SHG frequencies. Methods such as quasi-phase-matching can be employed with such materials, but this requires the existence of a polar axis and very detailed crystal processing. The ratio of the power density of second-harmonic light to fundamental input light can be expressed as

$$\frac{P_{2\omega}}{P_{\omega}} \propto L^2 d_{ijk}^2 \frac{P_{\omega}}{area} e^{(-L[\alpha_{\omega} + \frac{\alpha_{2\omega}}{2}])} \left[\frac{\sin^2 \frac{1}{2} L \cdot \Delta k}{(\frac{1}{2} L \cdot \Delta k)^2} \right] \quad (1.7)$$

where P = power, L = NLO crystal length, d_{ijk} = NLO susceptibility, α = absorption, and $\Delta k = k_{2\omega} - 2k_{\omega}$ (measure of phase mismatch). Increasing $P_{2\omega}$ can be achieved by increasing the crystal length, increasing the susceptibility, increasing the input power, decreasing absorption at the fundamental and second-harmonic wavelengths, and decreasing Δk . At $\Delta k = 0$, the material is phase-matched.

The coherence length l_c

The crystal length at which the amplitude of the combination of the fundamental and SHG waves reaches its first maximum is defined as the coherence length (l_c). This length is described by equation 1.8:

$$l_c = \frac{\lambda_\omega}{4|n_{2\omega} - n_\omega|} \quad (1.8)$$

When the coherence length becomes infinite (or the difference between the refractive indices of the input and produced frequencies becomes zero), the material is phase-matched.

The phase matching angle θ_{pm}

The specific directions within a crystal that allow phase-matching are measured as an angular difference from the optic axis Z. This phase-matching angle is denoted θ_{pm} and can be described as a cone around the Z axis. Not every combination of x and y coordinates on the cone produces equivalent SHG power. Factoring in this projection on the x-y plane direction, another angle, ϕ , is necessary to describe the direction of maximum SHG power output within a crystal at a given fundamental frequency. An illustration of these directions is provided in Figure 1.3. Note that whether or not a noncentrosymmetric crystal can phase-match at a particular input frequency and what the phase-matching angle at that frequency is dependent on the nature of the material. If a material phase-matches either along the optic axis ($\theta_{pm} = 0^\circ$) or perpendicular to it ($\theta_{pm} = 90^\circ$), the crystal is deemed to be non critically phase-matched. Phase-matching at

all other angles is referred to as critical phase matching. Non-critical phase matching is considered desirable because considerable phase matching can occur over a much larger angular range centered about this phase-matching direction than for critically phase-matched directions (13). A θ_{pm} of 45° represents the least ideal angle for phase matching, resulting in a need for very precise optical alignment and minimal beam divergence in an actual system. This can be explained by considering spherical coordinates where it can be shown that n varies as $\cos 2\theta$. Hence the derivative $dn/d\theta$ reaches minima at $\theta = 0$ and 90° and a maximum at $\theta = 45^\circ$.

Types of phase matching

For uniaxial crystals, phase-matching is described as Type I or Type II, depending on whether the second-harmonic wave is formed from a single polarization of input light (Type I) or a combination of perpendicularly polarized light (Type II). The polarization of the second-harmonic wave is perpendicular to the input light in the case of Type I or to one of the components of the input light in the case of Type II. The waves will be polarized either in the direction of the optic axis along the ordinary refractive index sphere (o), or in the orthogonal direction along the axis of the extraordinary ellipsoid (e). The production of SHG requires the input of two photons of fundamental wavelength to make one photon of the frequency-doubled wavelength. This yields six possible and four unique combinations of polarizations of input (two parts) and output (one part) waves for phase-matching:

<u>Type I</u>	<u>Type II</u>
$o + o \rightarrow e$	$o + e \rightarrow e$ ($e + o \rightarrow e$)
$e + e \rightarrow o$	$e + o \rightarrow o$ ($o + e \rightarrow o$)

Uniaxial crystals, or crystals with two refractive indices at a given wavelength, can be deemed either positive or negative depending on whether the ordinary or extraordinary refractive index is larger, respectively. For negative uniaxial crystals, extraordinarily polarized light will always be produced and for positive uniaxial crystals ordinarily polarized light will always be produced. Refer to Figure 1.3 for the polarization directions.

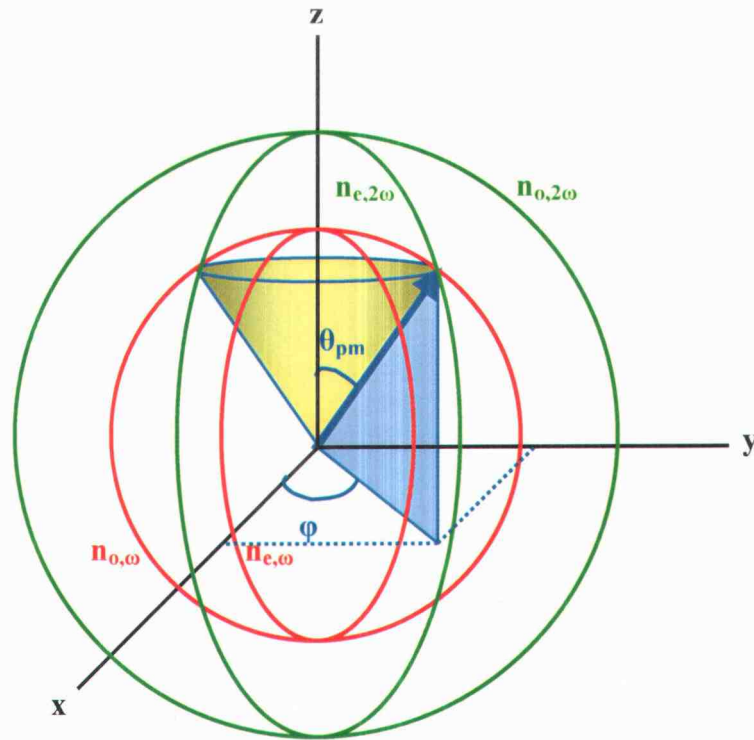


Figure 1.3. Polarization directions and angles in a Type I phase-matched negative uniaxial crystal.

Effect on SHG from identity, orientation, and packing of oxoanions

As stated earlier, the ratio of the second harmonic power density to the fundamental power density (eq. 1.7) in an SHG process is proportional to the square of the nonlinear coefficient d_{ijk} . The bulk SHG nonlinear optical coefficient (or second-order susceptibility) d_{ijk} of a material is dependent on the response of the microscopic, molecular level groups within the crystal. Specifically this response is determined by the nonlinearity or hyperpolarizability (β_{lmn}) of a microscopic group as well as the relative orientations and packing densities of a collection of the groups in a given crystal. These dependencies of d_{ijk} can be expressed with equation 1.9,

$$d_{ijk} = \frac{1}{V} \sum_1^N \sum_{lmn} R_{il} R_{jm} R_{kn} \beta_{lmn} \quad (1.9)$$

where the components of the hyperpolarizability tensor (β_{lmn}) are summed according to the directional cosines or orientation functions (R) of the individual groups and weighted by their number densities ($1/V$). Basically, materials with groups (in this case oxoanions) possessing large β_{lmn} components that are identically aligned and densely packed will have the largest d_{ijk} values.

Many optical properties, including second-order effects and the microscopic hyperpolarizability β_{lmn} , are influenced by the energy gaps and bond polarities of specific molecular-level groups. The microscopic hyperpolarizability tensor components can be determined by using a sum-over-states model as given in equation 1.10,

$$\beta_{nlm}(\omega, \omega) = \frac{1}{4} h^2 \sum_g \sum_{e, e'} \frac{\langle g | \mu_i | e \rangle \langle e | \mu_j | e' \rangle \langle e' | \mu_k | g \rangle}{(\omega_e - \omega_g - 2\omega)(\omega_{e'} - \omega_g - \omega)} \quad (1.10)$$

where $|g\rangle$ represents a ground electronic state, $|e\rangle$ and $|e'\rangle$ represent excited electronic states, and ω and 2ω represent fundamental and second-harmonic light energies, respectively, in the frequency-conversion process. Hence, by mixing states through the magnitudes of their transition moments weighted by the relevant energy gaps, a description of the polarization state of a molecular-level group can be obtained.

The molecular microscopic hyperpolarizability coefficients β_{lmn} exhibit lmn directional components that have the same symmetry characteristics as those associated with the bulk crystal macroscopic nonlinearity d_{ijk} (*cf.* eq. 1.6). In this work, for example, the nonlinear characteristics of structures containing trigonal BO_3 groups (Figure 1.4) will be considered. This group ideally exhibits D_{3h} symmetry, so the only nonzero components of the hyperpolarizability tensor are $\beta_{111} = -\beta_{122} = -\beta_{212}$. The hyperpolarizability coefficients β_{111} and β_{122} corresponding to induced hyperpolarization along x by light polarized orthogonal to x and y , respectively, have opposite signs. This result can readily be appreciated by considering the effects of polarized light on each of the bond dipoles in the group. For some collection of these groups, either aligned or misaligned, the second-order susceptibility (d_{ijk}) will correspond to projection of the individual hyperpolarizability coefficients (β_{lmn}) onto a conventionally defined Cartesian system (*cf.*, eq. 1.9). Conceptually, the hyperpolarizability derives largely from motions of electron density along bonding directions, so we can

follow the alignment or misalignment of these bonds to account for a macroscopic nonlinearity, relying on results from single-crystal diffraction experiments to define the microscopic structural arrangement.

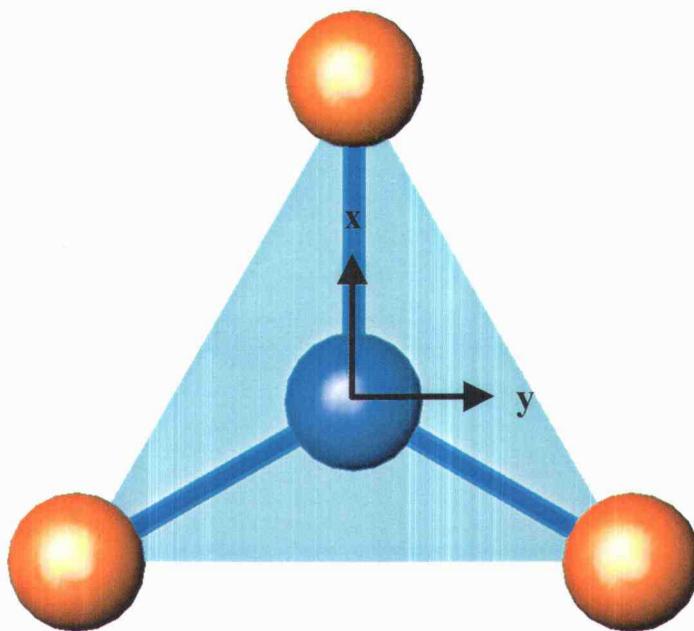


Figure 1.4. D_{3h} oxoanion BO_3^{3-}

Large band-gap energies for oxides produce transparency windows at high energies, i.e., from IR to UV, but a small microscopic hyperpolarizability. This can lead to a low SHG efficiency compared to an identical structure with different metals and a small band gap. Hence a balancing act must be performed to idealize transparency with SHG efficiency if short wavelength frequency

conversion is the end goal. This may be done by identifying materials with large band gaps but densely packed and preferentially oriented groups.

A survey of current nonlinear optical crystals and their applications

Frequency-doubling crystals currently in use

The goals in the development of new SHG crystals include the following: optimized transparencies and phase-matching conditions leading to the production of lasing at shorter wavelengths; improved SHG conversion efficiencies; and high optical damage thresholds for the production of higher powers over current technology. Presently, some of the most common SHG materials in use in laser systems include the following:

- | | |
|--|----------------------------------|
| - LBO – LiB_3O_5 | - KTP – KTiOPO_4 |
| - BBO – $\beta\text{-BaB}_2\text{O}_4$ | - KDP – KH_2PO_4 |
| - L2BO – $\text{Li}_2\text{B}_4\text{O}_7$ | - LiNbO_3 |
| - CLBO – $\text{CsLiB}_6\text{O}_{10}$ | - KNbO_3 |

A summary of their d_{eff} values, phase-matching angles, transparency windows, damage thresholds, crystal-growth technique, and comments on physical properties is given in Table 1.1.

Table 1.1. Properties of selected SHG crystals at 1064nm (6, 13 - 15).

Crystal	d_{eff} (pm/V)	θ_{pm}	Type I, II	Transmit (nm)	Damage* (J/cm ²)	Growth	Comments
LBO	1.17	0, 90	biaxial	160-2600	25	flux	
BBO	2.01 1.43	22.8 32.3	I II	198-2600	13	flux	
L2BO	0.07	30.5	I	160-3500	very high	Cz.	H ₂ O sol.
CLBO	0.49 0.95	29.2 42.1	I II	170-2600	25	Cz	hygroscop.
KTP	3.24		biaxial	350-4500	15	flux	
KDP	0.26 0.34	41.0 58.7	I II	177-1700	10	flux	H ₂ O sol.
LiNbO ₃	not phase-match- able at 1064 nm			330-5500	10	Cz.	
KNbO ₃	10.90	18.7	biaxial	400-4500	1.7	Cz.	

* $\tau_p = 10$ ns, $\lambda = 1064$ nm

LBO is currently the standard for high-power 1064 to 532-nm wavelength conversion because of its high damage threshold and non-critical phase-matching at 90°. However, it is not phase-matchable for fundamental wavelengths below 688 nm, limiting its usefulness to the production of near UV light. BBO possesses both Type I and Type II phase-matching over a wide range of angles, and it can be Type I phase-matched at a short-wavelength fundamental limit of 410 nm. Limitations of this crystal include difficulty of consistent quality crystal

growth and high angular sensitivity to phase-matching, requiring considerable precision and very little flexibility in the optical system. L2BO, CLBO, and KDP all have water-solubility problems, requiring care in the treatment and packaging. All three have relatively low d_{eff} values but very high damage thresholds and transparency windows. KTP, LiNbO₃, and KNbO₃ are very robust crystals with large d_{eff} values, but they are opaque in the ultraviolet range.

Applications of frequency-doubling crystals

Frequency doubling crystals can be found in laser systems for materials processing, medicine, data storage, and analytical research and detection. The advantages of using all solid-state laser systems incorporating SHG crystals include the following: virtually maintenance free systems; many electrically efficient systems; beam stability; simple operation; and compactness. A brief outline of some SHG crystal applications is given in Table 1.2.

Table 1.2. Applications of SHG crystals.

•Medical	•Materials Processing	•Analytical
Laser eye surgery	Micromachining	Flow cytometry
Cancer treatment (photodynamic therapy)	Microlithography	Detection
Stroke treatment (removal of blood clots) (16)	DVD mastering	

Development and characterization of new SHG materials

Development of a successful material for application in frequency doubling laser light depends on the optimization of certain highly desirable physical properties of a material. These desirable properties include the following: a melting or decomposition point above 700°C but not so high as to not be obtainable using conventional furnaces; congruent melting or straightforward solution growth; ease of large three-dimensional crystal growth; chemical, thermal, and physical stability; high purity of crystals; high damage threshold; wide transparency range (IR to UV); suitable birefringence for phase matching; and large d_{ij} nonlinear polarization coefficients. In order to have these desired properties in a material, certain composition and structure conditions must be met. For example, to achieve a wide transparency range from IR to UV, the materials should be synthesized from oxoanions of groups 13-16, such as borates, silicates, or phosphates, with charge compensation by cations from Groups 1 or 2 or the Lanthanides Sc^{3+} , Y^{3+} , or La^{3+} . Other anions such as fluorides and sulfides may have desirable optical properties, but crystals containing these anions are generally not as chemically and physically stable or easily manufactured. Also, sulfides do not have the transparency windows that we desire, and fluorides generally exhibit small nonlinear coefficients because of their wide band gaps (*cf.* eq. 1.7). For the production of frequency doubled light, the material must be noncentrosymmetric. Maximizing the efficiency of frequency conversion requires the optimization of the orientation of the anionic groups (the groups

should be similarly aligned) and their packing in the unit cell (number density) should be maximized.

The basic steps of materials development for this application include the following: review the literature and databases on existing materials for desirable compositions/structures that will potentially yield the desired properties; synthesize existing and new materials based on predictions; confirm/characterize structures and properties via analytical techniques such as powder diffraction, single crystal studies, differential thermal analysis (DTA), and SHG screening for d_{eff} and phase-matchability; scale up the crystal growth of any promising candidates from the characterization stages using Czochralski or flux-growth techniques; and finally optical characterization of large crystals with respect to phase-matching angles and type, damage threshold, d_{ij} values, and thermal response.

References

- (1) Franken, P. A.; Hill, A. E.; Peters, C. W.; and Weinreich, G. "Generation of optical harmonics." *Physical Review Letters* 7 (4) 118-119 (1961).
- (2) Prasad, Paras N.; and Williams, David J. "Introduction to nonlinear optical effects in molecules & polymers." John Wiley & Sons, Inc. (1991).
- (3) Nye, J. F. "Physical properties of crystals." Oxford University Press Inc. (1985).
- (4) Gay, P. "An introduction to crystal optics." Longman Group Limited. (1967).
- (5) Huard, Serge. "Polarization of light." John Wiley & Sons. (1997).
- (6) Zernike, Frits; and Midwinter, John E. "Applied nonlinear optics." John Wiley & Sons, Inc. (1973).
- (7) Baldwin, George C. "An introduction to nonlinear optics." Plenum Press (1969).
- (8) Yariv, Amnon; and Yeh, Pochi. "Optical waves in crystals." John Wiley & Sons, Inc. (1984).
- (9) Boyd, Robert W. "Nonlinear optics." Academic Press. (1992).
- (10) Bloembergen, Nicolaas. "Nonlinear optics, 4th Edition." World Scientific. (1996).
- (11) Giordmaine, J. A. "Mixing of light beams in crystals." *Physical Review Letters*. 8 (1) 19-20 (1962).
- (12) Maker, P. D.; Terhune, R. W.; Nisenoff, M.; and Savage, C. M. "Effects of dispersion and focusing on the production of optical harmonics." *Physical Review Letters*. 8 (1) 21-22 (1962).
- (13) CASIX Crystal Guide 1999. contact@casix.com.
- (14) Smith, A. V. "How to select nonlinear crystals and model their performance using SNLO software," <http://www.sandia.gov/imr1/XWEB1128/xxtal.htm> (2000).

(15) Dmitriev, V. G.; Gurzadyan, G. G.; Nikogosyan, D. N. "Handbook of nonlinear optical crystals." Springer-Verlag. (1991).

(16) Watts, Michael. "Giving a green light." Photonics Spectra. 35 (10) 106-110 (2001).

CHAPTER 2

 $\text{La}_{0.75}\text{Y}_{0.25}\text{Sc}_3(\text{BO}_3)_4$: A NEW TRIGONAL HUNTITE

Jennifer L. Stone-Sundberg, Michael A. Hruschka, and Douglas A. Keszler

To be submitted to the Journal of Solid State Chemistry (2001).

Abstract

A new noncentrosymmetric huntite borate with the formula $\text{La}_{0.75}\text{Y}_{0.25}\text{Sc}_3(\text{BO}_3)_4$ (YLSB) has been discovered and characterized. This material crystallizes in the space group $R32(h)$ with cell parameters $a=9.805(3)$, $c=7.980(2)$ Å, $V=664.4(2)$ Å³ and $Z=3$. This material is isostructural with $\text{YAl}_3(\text{BO}_3)_4$ (YAB) and contains nearly coplanar arrays of BO_3 groups extending perpendicular to the c axis. Second-harmonic generation data from powder and a calculated d_{ij} matrix are presented.

Introduction

The purpose of this study was to identify a new, widely transparent nonlinear optical material within the family of compounds $\text{LnM}_3(\text{BO}_3)_4$ (Ln = lanthanide, Y; M = Al, Ga, Sc). The trigonal, huntite derivative $\text{YAl}_3(\text{BO}_3)_4$ (YAB), for example, has been extensively studied as a self-frequency doubling laser host (1-9), and more than 100 papers have been published on this topic during the past decade. References 1-16 represent a partial survey of this literature. Interest in this material arises from its high frequency-conversion efficiency and the ability to dope lanthanide laser ions on the Y site. The major limitation, however, in developing the compound has been the difficulty in growing large, high-quality crystals. At present, the only known flux for the growth of YAB is a polymolybdate (2, 3, 11), but this flux suffers from problems of volatility and Mo incorporation into the crystals; the latter problem limits short-wavelength applicability.

To circumvent these crystal-growth problems, efforts have been directed to the development of the Sc huntite derivatives $\text{LnSc}_3(\text{BO}_3)_4$ (12-18). These materials exist for the lighter lanthanides La – Gd. The La derivative ($\text{LaSc}_3(\text{BO}_3)_4$, LSB), however, crystallizes in a monoclinic form of the huntite structure, providing only a very weak nonlinear susceptibility. Nevertheless, the compound melts congruently, and it is easily grown for the commercial production of high-efficiency Nd^{3+} -doped laser rods. For the heavier lanthanides, trigonal huntite phases can be identified, but as the size of the lanthanide

decreases, X-ray data provide evidence for an increasing occurrence of stacking faults, diminishing the integrity of the trigonal structure. The monoclinic structure of LSB can be converted to the trigonal form by doping with a smaller lanthanide, e.g., Gd. Indeed trigonal crystals of Nd:La_{0.8}Gd_{0.2}Sc₃(BO₃)₄ have been grown by the Czochralski method, but with very poor crystal quality. This poor quality could be associated with the aforementioned stacking faults or the growth method, since the mixed crystal cannot melt congruently.

To produce a widely transparent, trigonal huntite containing Sc, we have substituted Y for La in LSB, and a flux method has been utilized to produce a high-quality trigonal crystal. In this contribution, we describe the crystal structure and nonlinear optical properties of the new trigonal borate La_{0.75}Y_{0.25}Sc₃(BO₃)₄ (YLSB).

Experimental

Synthesis and crystal growth

A powder sample of YLSB was prepared by grinding together a stoichiometric ratio of La_2O_3 (Stanford Materials, 99.999%), Y_2O_3 (Stanford Materials, 99.99%), Sc_2O_3 (Stanford Materials, 99.99%), and B_2O_3 (Alfa AESAR, 99.98%). The sample was heated at 1073 K for 2 h in a platinum crucible followed by regrinding and heating at 1373 K for 96 h. The resulting powder exhibits an X-ray diffraction pattern indicative of the R32 structure of YAB.

Crystals were grown for elemental and X-ray structure analysis by using the flux LiBO_2 (Cerac, 99.9%); the mixture for crystal growth was 33 wt% YLSB and 67 wt% LiBO_2 . The sample was heated in a platinum crucible from room temperature to 1323 K at a rate of 60 K/h, soaked for two hours, cooled at a rate of 6 K/h to 1023 K, and then quenched to avoid crystallizing the flux. Colorless, transparent hexagonal crystals were observed in the glassy solidified melt. A transparent block of dimensions 0.1 x 0.3 x 0.5 mm was extracted and mounted on a glass fiber with epoxy for elemental analysis and structure determination.

Elemental analysis

An electron microprobe analysis (CAMECA SX-50 electron microprobe) was performed on the selected YLSB crystal. The operating conditions included an accelerating voltage of 15.2 kV and a beam current of 49.78 nA. Five sets of

qualitative and quantitative elemental analyses data were collected and averaged. A summary of these data, assuming stoichiometric amounts of B, is given in Table 2.1. The stoichiometry was calculated on the basis of 12 O atoms and 4 B atoms in each formula unit, consistent with the composition of members of the huntite family.

Table 2.1. Elemental analysis and stoichiometry for YLSB.

Element	Average Atomic %	# per Formula Unit (pfu)
B	(20.0)*	4
O	(60.0)**	12
Sc	14.59(8)	2.92
Y	1.11(6)	0.22
La	4.30(4)	0.86

* Calculated assuming 4 B pfu and 20 total atoms pfu.
 ** Calculated assuming 12 O pfu and 20 total atoms pfu.

Structure analysis

Unit cell and intensity data collection

All measurements were made on a single-crystal Rigaku AFC6R diffractometer with graphite-monochromated Mo K α radiation from a rotating-anode generator. Cell constants and an orientation matrix for data collection were obtained from a least-squares refinement by using 24 automatically-centered reflections in the range $20 \leq 2\theta \leq 35^\circ$. The cell constants correspond to a rhombohedral cell (hexagonal axes); Laue symmetry $-3m$ was determined on the

diffractometer. Intensity data were collected over the range of indices $-15 \leq h \leq 15$, $0 \leq k \leq 15$, $-12 \leq l \leq 12$ by using the ω - 2θ scan technique to a maximum 2θ value of 70° . Of the 2065 reflections collected, 380 were unique, and 380 had $F_o^2 \geq 3\sigma(F_o^2)$. The intensity of three standard reflections measured after every set of 400 reflections varied by an average of 1.0% during the collection.

Solution and refinement

The structure was solved by using programs from the TEXSAN crystallographic software package (26). On the basis of the systematic condition $hkil$, $-h+k+l = 3n$, the statistical analysis of the intensity distribution, packing considerations, and the successful solution and refinement of the structure (*vide infra*), the crystal was found to form in the noncentrosymmetric space group R32 [#155]. The La and Sc positions were derived from the direct methods program SIR92 (19), and the remaining atomic positions were determined from difference electron-density maps. After full-matrix refinement with isotropic displacement coefficients on each atom, the occupancies of the La and Sc sites were refined. No significant change in the Sc occupancy factor was observed, so it was subsequently fixed to unity. Occupancy of the La site was significantly reduced, indicating occupation of Y on the La site. Following refinement with isotropic displacement coefficients on each atom, an empirical absorption correction was applied with the program DIFABS (17), and the data were then averaged ($R_{int} = 0.042$). The final cycle of full-matrix least-squares refinement (20) with 380 observed reflections ($I > 3.00\sigma(I)$), anisotropic displacement coefficients on the O

atoms, and 28 variable parameters (secondary extinction coefficient = 2.7×10^{-6}), converged to the agreement factors $R = 0.022$ and $R_w = 0.031$. Refinement of the final La occupancy factor leads to the formula $\text{La}_{0.75}\text{Y}_{0.25}\text{Sc}_3(\text{BO}_3)_4$. The weighting scheme in the least-squares refinement was based on counting statistics and included a factor ($p = 0.040$) to reduce the weighting of the intense reflections. Plots of $\sum w (|F_o| - |F_c|)^2$ versus $|F_o|$, reflection order in data collection, $\sin \theta/\lambda$ and various classes of indices showed no unusual trends. The maximum and minimum peaks on the final difference electron-density map corresponded to 0.96 and 0.58% of the Sc atom, respectively. Crystal data are outlined in Table 2.2, positional and isotropic displacement coefficients are listed in Table 2.3, and anisotropic displacement coefficients are listed in Table 2.4.

Table 2.2. Crystallographic data for YLSB.

Formula Weight, amu	496.51
Crystal System	Rhombohedral
Space Group	R32(h) [155]
a , Å	9.805(3)
c , Å	7.980(2)
V , Å ³	664.4(2)
Z	3
D_{calc} , g cm ⁻³	3.722
F(000)	695
Diffractometer	Rigaku AFC6R
Radiation	Mo K α ($\lambda=0.71069$) graphite-monochromated
Data Collection	$\pm h, k, \pm l$
No. Observations (total, unique) ($F_o^2 \geq 3\sigma(F_o^2)$)	2065, 380 380
R	0.022
R_w	0.031
Maximum Shift in Final Cycle	0.00
GOF	1.07

$$R = \frac{\sum ||F_o| - |F_c||}{\sum |F_o|} = 0.022$$

$$R_w = \left[\frac{\sum w (|F_o| - |F_c|)^2}{\sum w F_o^2} \right]^{1/2} = 0.031$$

Table 2.3. Positional and thermal parameters (B_{eq}) and occupancy for YLSB.

Atom	Wy	x	y	z	B_{eq}^a
La ^b	3a	0	0	0	0.79(1)
Sc	9d	0.4572	0	0	0.56(2)
B(1)	3b	0	0	½	0.67(8)
B(2)	9e	0.5507(5)	0	½	0.72(6)
O(1)	9e	0.1405(4)	0	½	0.80(4)
O(2)	18f	0.5449(4)	0.8580(4)	0.4853(4)	1.16(4)
O(3)	9e	0.4081(5)	0	½	1.53(7)

$$^a B_{eq} = (8\pi/3)^2 \sum_i \sum_j U_{ij} a_i^* a_j^* a_i a_j$$

$$^b \text{occupancy} = 0.154/0.1667$$

Table 2.4. Anisotropic displacement parameters for YLSB.

Atom	U_{11}	U_{22}	U_{33}	U_{12}	U_{13}	U_{23}
O(1)	0.0069(9)	U_{11}	U_{11}	0.0061	-0.0014(5)	-0.0027
O(2)	0.020(1)	U_{11}	U_{11}	0.0104(9)	0.002(1)	0.0005(8)
O(3)	0.011(1)	U_{11}	U_{11}	0.0018	-0.0024(7)	-0.0131

Differential thermal analysis

A differential thermal analysis (DTA) scan was obtained on a TA Instruments Thermal Analysis DTA 1600°C Delta-T Cell interfaced with a PC by using the software Universal Analysis.

Optical second-harmonic generation studies

The experimental method of Kurtz and Perry (28) was used to measure powder SHG signals with a 1064-nm laser. The sample was ground and sieved by using a stack of mesh sizes 25, 45, 53, 63, 75, 106, 125, 150, 212, and 250 μm . Samples of KH_2PO_4 (KDP,) $\beta\text{-BaB}_2\text{O}_4$ (BBO), and α -quartz were prepared as reference materials in an identical fashion. The samples were pressed between glass microscope cover slides and secured with tape in 1-mm thick aluminum holders containing a 5-mm diameter hole. The samples were then placed in a light-tight box and excited with 20-mJ, 1064-nm pulses from a Q-switched New Wave Research Minilase-20 Nd:YAG laser. A cutoff filter was used to limit background flash-lamp light on the sample, and an interference filter (530 ± 10 nm) was used to select the second harmonic prior to detection with a photomultiplier tube attached to a Tektronix SC 504 80-MHz oscilloscope. Samples of Al_2O_3 (Stanford Materials, 99.999%) and α quartz were used to monitor and calibrate the instrumental setup. A photograph of the experimental setup is presented in Figure 2.1.

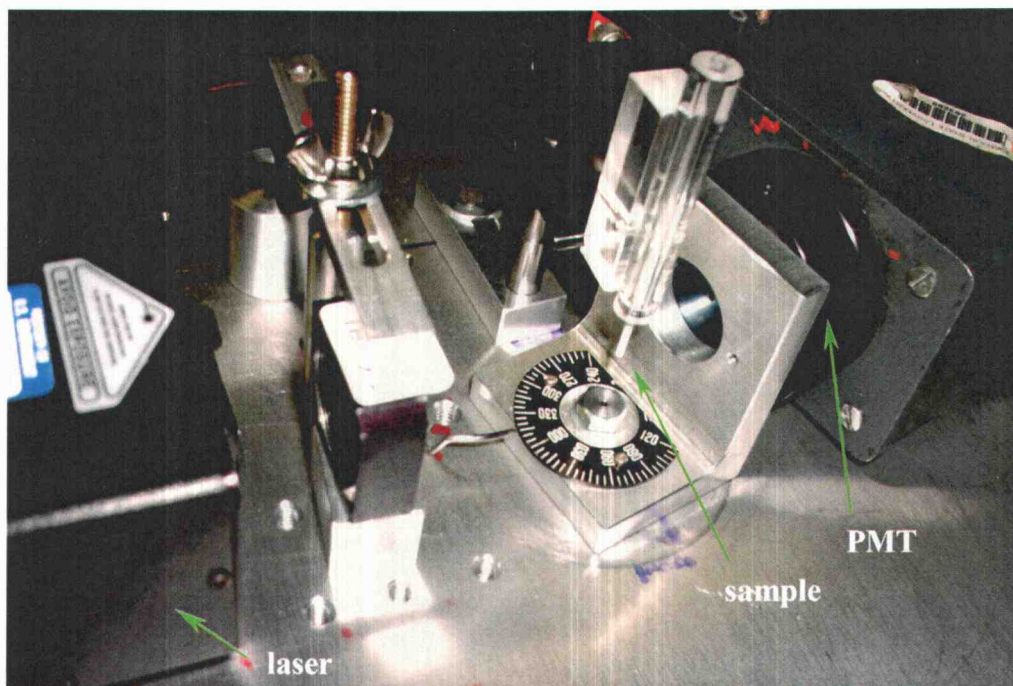


Figure 2.1. Modified Kurtz-Perry powder SHG setup.

Results and Discussion

Structure

The structure of YLSB is illustrated in Figure 2.2. It is a classical huntite type with nearly planar layers of BO_3 groups extending in the ab plane. The La, Y, and Sc atoms occupy six-coordinate sites between these layers with the La/Y atoms centering a distorted trigonal prism and the Sc atom centering a distorted octahedron. The La/Y sites are completely isolated one from the other, while the ScO_6 octahedra share edges. Connectivities between the dissimilar polyhedra occur only through vertex sharing.

Selected interatomic distances and angles are listed in Table 2.5. The prismatic, six-coordinate La/Y site has a La/Y-O bond length of 2.466(3) Å, which compares to a weighted average of 0.75 x La-O and 0.25 x Y-O distances from crystal radii (27) of 2.37 Å. The average Sc-O length 2.10(3) Å corresponds to the value, 2.105 Å, deduced from crystal radii, and the B-O distances are similar to the expected value of 1.37 Å.

X-ray diffraction patterns demonstrating the existence of the trigonal structure for YLSB are given in Figure 2.3.

Frequency conversion

The magnitude of the second-order nonlinearity of YLSB can be estimated from a calculation of the nonlinear d coefficients on the basis of an oriented-gas

model (29, 30). In this model, the magnitudes of these coefficients are associated primarily with the orientation of individual borate groups.

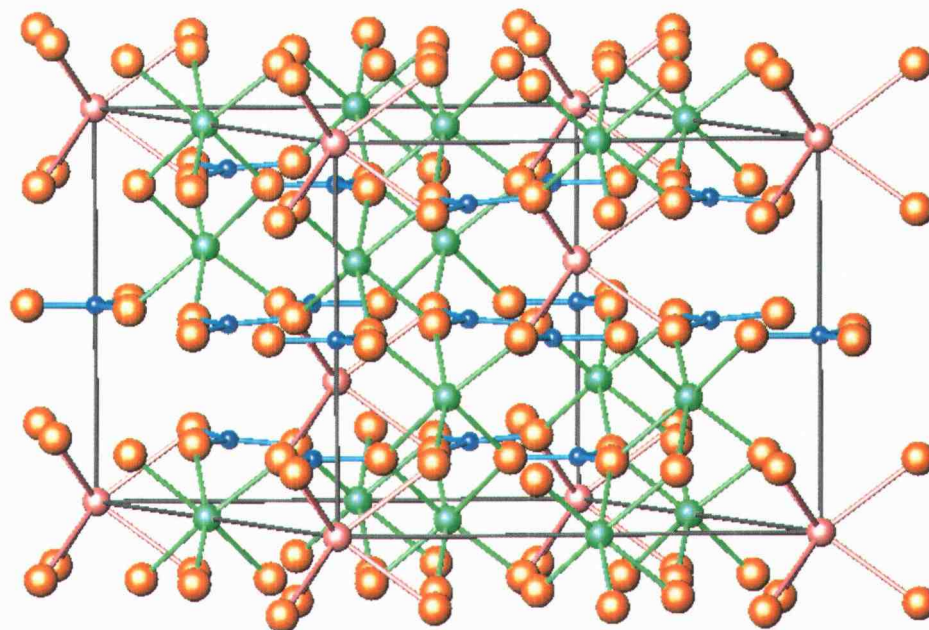


Figure 2.2. Drawing of YLSB structure. La atoms are rose, Sc atoms are green, B atoms are blue, and the O positions are orange.

Table 2.5. Selected interatomic distances (Å) and angles (°) for YLSB.

La - O(2) (x 6)	2.466(3)	O(2) - La - O(2)	125.1(2)
			88.8(1)
			72.7(2)
			139.7(2)
Sc - O(1) (x 2)	2.121(3)	O(1) - Sc - O(1)	168.0(2)
		O(1) - Sc - O(2)	92.8(1)
			94.8(1)
		O(1) - Sc - O(3)	76.6(2)
			94.6(1)
- O(2) (x 2)	2.061(5)	O(2) - Sc - O(2)	100.6(2)
		O(2) - Sc - O(3)	167.7(1)
			86.8(1)
- O(3) (x 2)	2.137(4)	O(3) - Sc - O(3)	87.65(6)
B(1) - O(1)	1.377(5)	O(1) - B(1) - O(1)	120
B(2) - O(2)	1.371(6)	O(2) - B(2) - O(2)	122.2(6)
- O(3)	1.358(9)	O(2) - B(2) - O(3)	118.9(3)

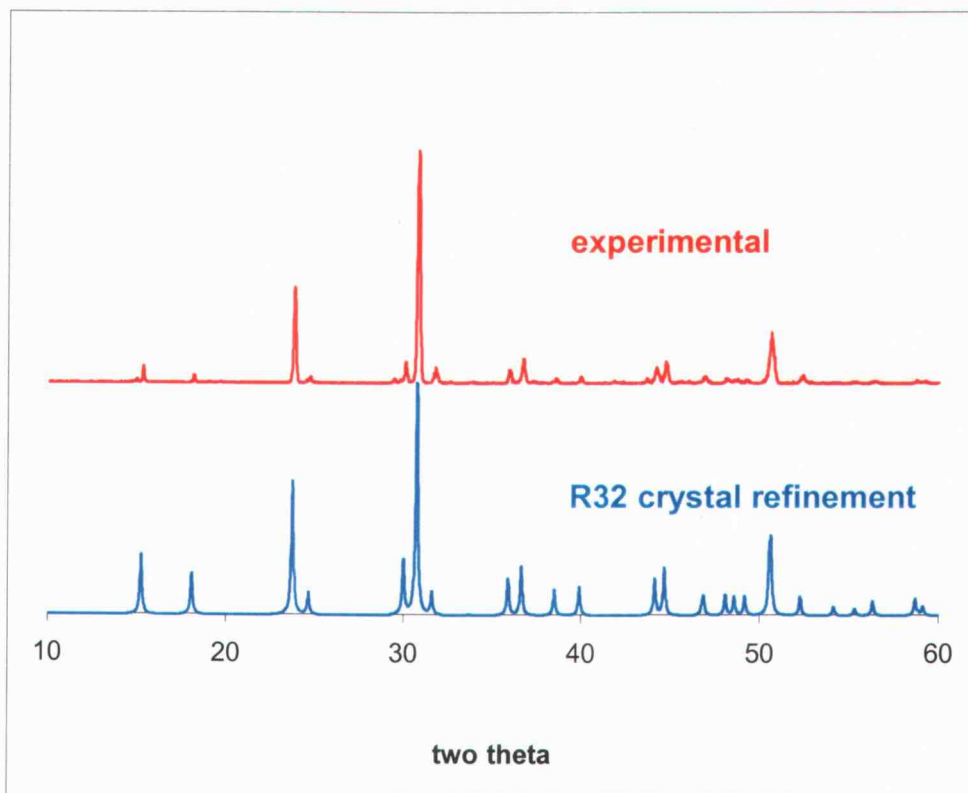


Figure 2.3. Simulated Cu-K α powder pattern for YLSB from single crystal data (top) and experimental Cu-K α X-ray powder diffraction pattern for YLSB.

By using eq. (2.1), the components of the hyperpolarizability tensor (β_{lmn}) are summed according to the orientations (R) of the individual groups and weighted by their number densities ($1/V$).

$$d_{ijk} = \frac{1}{V} \sum_1^N \sum_{lmn} R_{il} R_{jm} R_{kn} \beta_{lmn} \quad (2.1)$$

Application of eq. 2.1 to YLSB is quite straightforward. As shown in Figure 2.4, there are twelve BO_3 groups in a unit cell; three are centered by atom B(1) and nine are centered by atom B(2). The two types of groups are related by an approximate center of symmetry, so each such pair of B(1)- and B(2)-centered triangles will contribute nil to the d coefficient. Since the number of B(2) triangles is greater than that of B(1) triangles the net structural contribution to the d coefficient is $9-3/12 = 0.5$, i.e., the arrangement of BO_3 triangles is 50% of optimum. The same BO_3 group arrangement is observed in YAB, and its d_{11} coefficient has been reported to be 1.5 pm/V. The d_{11} value for YLSB may then be deduced from eq. 2.2.

$$d_{11}(\text{YLSB}) = \frac{\text{YLSB } \text{BO}_3 \text{ group number density}}{\text{YAB } \text{BO}_3 \text{ group number density}} \times 1.5 \text{ pm/V} \quad (2.2)$$

From the number densities of 1.8×10^{22} and $2.2 \times 10^{22} \text{ cm}^{-3}$ for YLSB and YAB, respectively, the predicted value of d_{11} for YLSB is 1.2 pm/V.

The second-harmonic signal (intensity) produced by YLSB powders from a 1064-nm fundamental wavelength corresponds to 0.67 x BBO. On the basis of eq. 2.3, these signals are proportional to the squares of the nonlinear d coefficients, assuming the phase matching lengths for the two materials are the same (28).

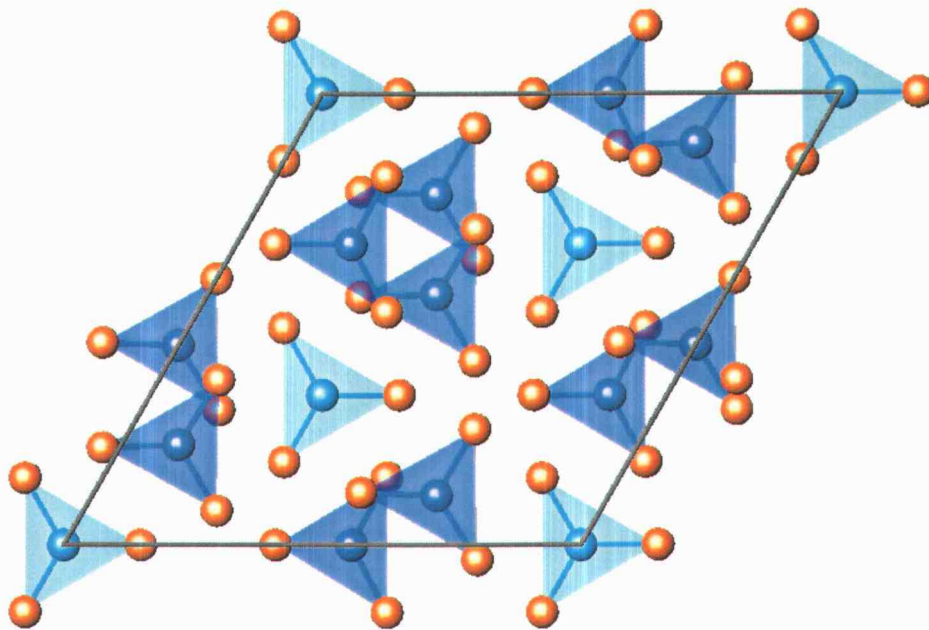


Figure 2.4. YLSB structure: view down the c axis. Light blue shaded circles represent B(1) atoms, and dark blue-shaded circles represent B(2) atoms.

$$\frac{I^{2\omega}(YLSB)}{I^{2\omega}(YAB)} = \frac{\langle d_{ijk}^{2\omega}(YLSB) \rangle^2}{\langle d_{ijk}^{2\omega}(YAB) \rangle^2} \quad (2.3)$$

From measurements of SHG signals, $I^{2\omega}(YLSB)/I^{2\omega}(BBO) = 0.6$, which leads to the ratio $d_{obs}(YLSB)/d_{obs}(BBO) = 0.8$. Since the reported d coefficient for BBO is 1.8 pm/V, the derived value for YLSB is 1.4 pm/V, a value in general agreement with that calculated above (1.2 pm/V).

Thermal analysis

The differential thermal analysis trace (Figure 2.5) exhibits a broad melting event starting at 1220° C and ending at 1478° C. On cooling, a sharp exotherm is observed at 1218° C. In principle, a solid solution such as $La_{1-x}Y_xSc_3(BO_3)_4$ ($x > 0$) will not exhibit congruent-melting behavior and a sharp endotherm on heating. The DTA trace is consistent with this behavior, and a flux must be used to grow crystals.

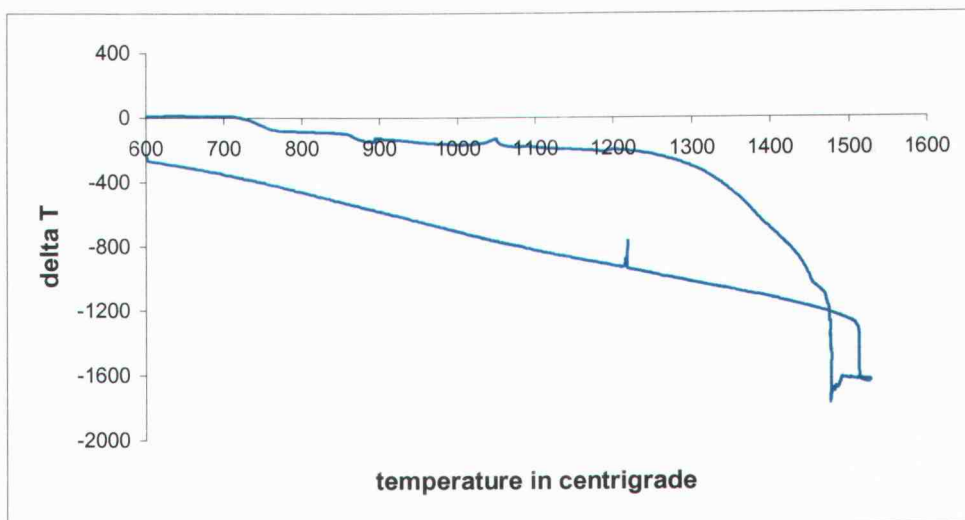


Figure 2.5. DTA of YLSB.

Summary and Future Work

The compound $\text{La}_{0.75}\text{Y}_{0.25}\text{Sc}_3(\text{BO}_3)_4$ has been established as the only trigonal example of a huntite other than YAB that can exhibit a transparency below 200 nm. These features coupled with a high nonlinearity and probable ease in crystal growth from a lithium-borate flux provide a unique opportunity for realizing a nonlinear optical crystal for direct second-harmonic generation of VUV light. In the context of the crystal growth, it is important to definitively establish the solubility limit of Y. There is a slight discrepancy in stoichiometry between the X-ray and microprobe results in that the La/Y ratio from the X-ray study is 3/1, whereas the corresponding microprobe ratio is 4/1. Refinement of cell parameters from X-ray data for compositions in the series $\text{La}_{1-x}\text{Y}_x\text{Sc}_3(\text{BO}_3)_4$ ($0.35 \geq x \geq 0.15$) is currently underway, and experiments are in progress for optimizing the lithium borate flux for the production of large crystals.

Acknowledgments

The authors would like to thank Professor Roger Neilson of the Department of Geosciences at Oregon State University for performing the elemental analysis. NSF is gratefully acknowledged for supporting the work.

References

- (1) Filimonov, A. A., Leonyuk N. I., Meissner, L. B., Timchenko, T. I., Rez, I. S. "Nonlinear Optical Properties of Isomorphic Family of Crystals with Yttrium-Aluminum Borate (YAB) Structure." *Kristall und Technik* 9 1 63-66 (1974).
- (2) Aka, Gerard; Viegas, Nathalie; Teisseire, Beatrice; Kahn-Harari, Andree; and Godard, Jean. "Flux Growth and Characterization of Rare-earth-doped Non-linear Huntite-type Borate Crystals: $Y_{1-x}Nd_x(Al_{0.7}Ga_{0.3})_3(BO_3)_4$ and $Y_{1-x}Yb_xAl_3(BO_3)_4$." *J. Mater. Chem.*, 5 (4) 583-587 (1995).
- (3) Aka, G., Viegas, N., Kahn-Harari, A., Vivien, D. "Optical Properties of Single Crystals of Gallium-substituted NYAB: $Y_{1-x}Nd_x(Al_{1-y}Ga_y)_3(BO_3)_4$." *J. Mater. Chem.* 5 (2) 265-271 (1995).
- (4) Jung, S. T., Choi, D. Y., and Chung, S. J. "Crystal growth of neodymium yttrium aluminum borate with several neodymium contents." *Materials Research Bulletin* 31 8 1007-1012 (1996).
- (5) Wang, Pu; Dawes, Judith M.; Dekker, Peter; Knowles, David S.; and Piper, James A. "Growth and evaluation of ytterbium-doped yttrium aluminum borate as a potential self-doubling laser crystal." *J. Opt. Soc. Am. B* 16 1 63-69 (1999).
- (6) Jung, S. T., Choi, D. Y., Kang, J. K., Chung, S. J. "Top-seeded growth of Nd:YAl₃(BO₃)₄ from high temperature solution." *Journal of Crystal Growth* 148 207-210 (1995).
- (7) Wang, Pu; Dawes, Judith M.; Dekker, Peter; Piper, James A. "Highly efficient diode-pumped ytterbium-doped yttrium aluminum borate laser." *Optics Communications* 174 467-470 (2000).
- (8) Wang, Guofu; Han, T. P. J.; Gallagher, H. G.; and Henderson, B. "Crystal growth and optical properties of Ti³⁺:YAl₃(BO₃)₄ and Ti³⁺:GdAl₃(BO₃)₄." *Journal of Crystal Growth* 181 48-54 (1997).
- (9) Nikolov, V., Peshev, P. "A new solvent for the growth of Y_{1-x}Nd_xAl₃(BO₃)₄ single crystals from high-temperature solutions." *Journal of Crystal Growth* 144 187-192 (1994).
- (10) Belokoneva, E. L., Azizov, A. V., Leonjuk, N. I., Simonov, M. A., Belov, N. V., "The crystal structure of YAl₃(BO₃)₄." *Zhurnal Strukturnoi Khimii* 22 196-198 (1981).

(11) Leonyuk, N. I., Leonyuk, L. I. "Growth and Characterization of $RM_3(BO_3)_4$ Crystals." *Prog. Crystal Growth and Charact.* 31 179-278 (1995).

(12) Peterson, Gregory A., Keszler, Douglas A., Reynolds, Thomas A. "Stoichiometric, trigonal huntite borate $CeSc_3(BO_3)_4$." *International Journal of Inorganic Materials* 2 101-106 (2000).

(13) Chani, Valery I.; Shimamura, Kiyoshi; Inoue, Keiji; and Fukuda, Tsuguo "Huntite-borate crystallization in stoichiometric melts." *Journal of Crystal Growth* 133 181-184 (1993).

(14) Chani, Valery I.; Shimamura, Kiyoshi; Inoue, Keiji; and Fukuda, Tsuguo "Synthesis and search for equilibrium compositions of borates with the huntite structure." *Journal of Crystal Growth* 132 173-178 (1993).

(15) Wang, Guofu; He, Meiyun; Chen, Wenzhi; Lin, Zhonbin; Lu, Shaofang; and Wu, Qiangjin "Structure of low temperature phase γ - $LaSc_3(BO_3)_4$ crystal." *Mat. Res. Innovat.* 2 341-344 (1999).

(16) Jung, S. T., Yoon, J. T., and Chung, S. J. "Phase Transition of Neodymium Yttrium Aluminum Borate with Composition." *Materials Research Bulletin* 31 8 1021-1027 (1996).

(17) DIFABS: Walker, N. & Stuart, *Acta Cryst.* A39, 158-166 (1983). An empirical absorption correction program.

(18) SIR92: Altomare, A., Cascarano, M., Giacovazzo, C., Guagliardi, A. (1993). *J. Appl. Cryst.*, 26, 343.

(19) DIRDIF94: Beurskens, P.T., Admiraal, G., Beurskens, G., Bosman, W.P., de Gelder, R., Israel, R. and Smits, J.M.M.(1994). The DIRDIF-94 program system, Technical Report of the Crystallography Laboratory, University of Nijmegen, The Netherlands.

(20) Least Squares function minimized:

$\sum w(|F_o| - |F_c|)^2$ where

$$w = 1/[\sigma^2(F_o)] = [\sigma^2_c(F_o) + \rho^2 F_o^2/4]^{-1}$$

$\sigma_c(F_o)$ = e.s.d. based on counting statistics

ρ = p-factor

(21) Standard deviation of an observation of unit weight:

$$[\sum w(|F_o| - |F_c|)^2 / (N_o - N_v)]^{1/2}$$

where

N_o = number of observations

N_v = number of variables

- (22) Cromer, D. T. & Waber, J. T.; "International Tables for X-ray Crystallography", Vol. IV, The Kynoch Press, Birmingham, England, Table 2.2 A (1974).
- (23) Ibers, J. A. & Hamilton, W. C.; *Acta Crystallogr.*, 17, 781 (1964).
- (24) Creagh, D. C. & McAuley, W.J. ; "International Tables for Crystallography", Vol C, (A.J.C. Wilson, ed.), Kluwer Academic Publishers, Boston, Table 4.2.6.8, pages 219-222 (1992).
- (25) Creagh, D. C. & Hubbell, J.H.; "International Tables for Crystallography", Vol C, (A.J.C. Wilson, ed.), Kluwer Academic Publishers, Boston, Table 4.2.4.3, pages 200-206 (1992).
- (26) teXsan for Windows: Crystal Structure Analysis Package, Molecular Structure Corporation (1997).
- (27) Shannon, R. D. "Revised Effective Ionic Radii and Systematic Studies of Interatomic Distances in Halides and Chalcogenides." *Acta Cryst. A* 32 751-767 (1976).
- (28) Kurtz, S. K., and Perry, T. T. "A Powder Technique for the Evaluation of Nonlinear Optical Materials." *Journal of Applied Physics* 39 8 3798-3813 (1968).
- (29) Kathleen I. Schaffers, Ph.D. dissertation, Oregon State University, 1992.
- (30) C.T. Chen, *Development of new nonlinear optical crystals in the borate series*, Harwood Academic Publishers, Langhorne, PA, 1993.
- (31) D.A. Keszler, "NLO materials for deep UV generation," American Conference on Crystal Growth and Epitaxy, Vail, CO, USA, August 2000; D.A. Keszler, "New materials for high-power laser systems," National Meeting of the Materials Research Society, Boston, MA, USA, December 2000.

CHAPTER 3

LaCa₄O(BO₃)₃ (LaCOB): OPTICAL SECOND-
HARMONIC GENERATION FROM TRIANGULAR OXOANIONS

Jennifer L. Stone-Sundberg and Douglas A. Keszler

To be submitted to Acta Crystallographica C (2001).

Abstract

$\text{LaCa}_4\text{O}(\text{BO}_3)_3$ (LaCOB) has been synthesized and structurally characterized. This material is isostructural with $\text{GdCa}_4\text{O}(\text{BO}_3)_3$ (1) and its optical properties have been described by Adams et. al. (2). This material is predicted to be a critically phase-matchable material for converting 1064 nm light to 532 nm light.

Introduction

The $\text{LnCa}_4\text{O}(\text{BO}_3)_3$ (LnCOB where Ln = lanthanide) family of nonlinear optical crystals incorporates materials that can be critically phase-matched for converting near-infrared light to frequency-doubled visible light. Recent interest in $\text{LaCa}_4\text{O}(\text{BO}_3)_3$ (LaCOB) (2) stems from the ease of crystal growth, high transparency, high damage threshold, high borate nonlinear optical susceptibility, and desirable phase-matching conditions similar to those of other LnCOB crystals (2-7). This contribution demonstrates the ease of crystal growth and reports the structure demonstrating the similarities between LaCOB and GdCOB (1).

Experimental

Crystals were grown for X-ray study analysis by mixing stoichiometric amounts of La_2O_3 (Stanford, 99.999%), CaCO_3 (Cerac, 99.95%), and B_2O_3 (Alfa AESAR, 99.98%), placing the ground mixture in a platinum crucible, heating the mixture to 1673 K and slowly cooling at a rate of 10 K/h to room temperature. Numerous, colorless rod-like crystals were observed, radiating from the center of the crucible. A transparent, blunt rod of approximate dimensions 0.2 x 0.2 x 0.4 mm was selected and mounted on a glass fiber with epoxy for structure determination. The noncentrosymmetric nature of the mounted crystal was confirmed by observing the production of green, 532 nm light following irradiation with a Q-switched, Nd:YAG laser producing 1064-nm light. All measurements were made on a single-crystal, rotating-anode Rigaku AFC6R diffractometer with graphite-monochromated Mo $K\alpha$ radiation. Cell constants and an orientation matrix for data collection were obtained from a least-squares refinement, using the setting angles of 25 carefully centered reflections in the range $25 \leq 2\theta \leq 35^\circ$. The cell constants corresponded to a C-centered monoclinic cell with parameters $a = 8.159(3)$, $b = 16.077(5)$, $c = 3.6286(5)\text{\AA}$, $\beta = 101.39(2)^\circ$, $V = 466.6(2)\text{\AA}^3$, and $Z = 2$. Intensity data were collected over the range of indices $-11 \leq h \leq 11$, $0 \leq k \leq 22$, $-5 \leq l \leq 5$ by using the ω - 2θ scan technique to a maximum 2θ value of 60° . Of the 2831 reflections collected, 1426 were unique, and 701 had $F_o^2 \geq 3\sigma(F_o^2)$. The intensity of three standard reflections measured

after every set of 150 reflections varied by an average of 1.2% during the collection.

The structure was solved using programs from the TEXSAN crystallographic software package (8). On the basis of the systematic absence of hkl : $h+k = 2n+1$, the statistical analysis of the intensity distribution, packing considerations, and the successful solution and refinement of the structure, the crystal was found to form in the noncentrosymmetric space group Cm (#8). The La and Ca positions were derived from the direct methods program SIR92 (9), and the remaining atom positions were determined from difference electron density maps generated by Fourier techniques (10). After a full-matrix refinement of the model, an empirical absorption correction with the program DIFABS (11) was applied with isotropic displacement coefficients on each atom, which resulted in transmission factors ranging from 0.63 to 0.91. The data were averaged ($R_{int} = 0.034$), and then the model was refined with anisotropic displacement coefficients on each atom other than O(2) – O(6). The final cycle of full-matrix, least-squares refinement (12) was based on 701 observed reflections ($I > 3.00\sigma(I)$) and 66 variable parameters; it converged (largest parameter shift was 2.50 times its esd) with unweighted and weighted agreement factors $R = 0.022$ and $R_w = 0.027$. The standard deviation of an observation of unit weight (13) was 0.87. The maximum and minimum peaks on the final difference electron-density map corresponded to 0.47 and 0.26% of the La atom, respectively. Neutral atom scattering factors were taken from Cromer and Waber (14). Anomalous dispersion effects were included in F_{calc} (15); the values for $\Delta f'$

and $\Delta f''$ were those of Creagh and McAuley (16). The values for the mass attenuation coefficients are those of Creagh and Hubbell (17). Crystal data are outlined in Table 3.1, and atomic positional parameters and equivalent isotropic displacement coefficients are listed in Table 3.2. Anisotropic displacement coefficients are listed in Table 3.3, and selected interatomic distances and angles are given in Table 3.4.

Table 3.1. Crystallographic data for LaCOB.

Formula Weight, amu	491.65
Crystal System	Monoclinic
Space Group	Cm [8]
a , Å	8.159(3)
b , Å	16.077(5)
c , Å	3.6286(5)
β°	101.39(2)
V , Å ³	466.6(2)
Z	2
D_{calc} , g cm ⁻³	3.499
$F(000)$	464
Diffractometer	Rigaku AFC6R
Radiation	Mo K α ($\lambda=0.71069$) graphite-monochromated
Data Collection	$\pm h, k, \pm l$
No. Observations (total, unique) ($F_o^2 \geq 3\sigma(F_o^2)$)	2831, 1426 701
R	0.022
R_w	0.027
Maximum Shift in Final Cycle	2.50

$$R = \frac{\sum ||F_o| - |F_c||}{\sum |F_o|} = 0.022$$

$$R_w = \left[\frac{\sum w (|F_o| - |F_c|)^2}{\sum w F_o^2} \right]^{1/2} = 0.027$$

Table 3.2. Positional and thermal parameters (B_{eq}) for LaCOB.

Atom	Wyckoff	x	y	z	B_{eq}^*
La(1)	2a	0	0	0	0.7763
Ca(1)	4b	0.2721	0.1804	-0.3325	0.7055
Ca(2)	4b	0.3530	0.1142	0.3349	0.7321
O(1)	2a	0.2156(8)	0	-0.384(2)	1.2(1)
O(2)	2a	-0.1764(7)	0	0.417(2)	0.37(9)
O(3)	4b	0.1021(5)	0.1480(3)	0.096(1)	0.65(5)
O(4)	4b	-0.1926(5)	0.1691(3)	0.894(1)	0.95(6)
O(5)	4b	0.4747(5)	0.0742(3)	-0.241(1)	0.73(6)
O(6)	4b	-0.0287(5)	0.2696(3)	0.283(1)	0.93(6)
B(1)	2a	0.3889(9)	0	-0.290(2)	0.4(1)
B(2)	4b	-0.0405(7)	0.1960(4)	0.091(2)	0.52(8)

$$*B_{eq} = (8\pi/3)^2 \sum_i \sum_j U_{ij} a_i^* a_j^* a_i a_j$$

Table 3.3. Anisotropic displacement parameters for LaCOB.

Atom	U_{11}	U_{22}	U_{33}	U_{12}	U_{13}	U_{23}
La(1)	0.0098	0.0098	0.0098	0	0.0018	0
Ca(1)	0.0089	0.0089	0.0089	0	0.0018	0
Ca(2)	0.0093	0.0093	0.0093	0	0.0018	0
B(1)	0.004(2)	0.004(2)	0.004(2)	0	0	0
B(2)	0.005(2)	0.005(2)	0.005(2)	-0.001(2)	0	0.006(2)

Table 3.4. Selected interatomic distances (Å) and angles (°) for LaCOB.

La(1) - O(1)	2.439(8)	O(1) - La(1) - O(1)	93.0(2)
La(1) - O(1)	2.562(6)	O(1) - La(1) - O(2)	82.9(2)
		O(1) - La(1) - O(2)	173.6(2)
		O(1) - La(1) - O(2)	175.9(2)
		O(1) - La(1) - O(2)	80.6(2)
		O(1) - La(1) - O(3)	80.1(1)
		O(1) - La(1) - O(3)	80.1(1)
		O(1) - La(1) - O(3)	74.64(9)
La(1) - O(2)	2.303(7)	O(2) - La(1) - O(2)	103.5(2)
La(1) - O(2)	2.318(5)	O(2) - La(1) - O(3)	98.0(1)
		O(2) - La(1) - O(3)	98.0(1)
		O(2) - La(1) - O(3)	104.54(9)
		O(2) - La(1) - O(3)	104.54(9)
La(1) - O(3)	2.520(4)	O(3) - La(1) - O(3)	142.3(2)
La(1) - O(3)	2.520(4)		
Ca(1) - O(1)	2.938(2)	O(1) - Ca(1) - O(3)	73.4(2)
		O(1) - Ca(1) - O(3)	70.5(2)
		O(1) - Ca(1) - O(4)	164.0(2)
		O(1) - Ca(1) - O(5)	52.4(2)
		O(1) - Ca(1) - O(6)	114.7(2)
		O(1) - Ca(1) - O(6)	110.1(2)

Table 3.4 (cont.)

		O(1) - Ca(1) - O(6)	113.6(2)
Ca(1) - O(3)	2.347(5)	O(3) - Ca(1) - O(3)	101.8(2)
Ca(1) - O(3)	2.328(4)	O(3) - Ca(1) - O(4)	92.2(2)
		O(3) - Ca(1) - O(5)	104.0(2)
		O(3) - Ca(1) - O(6)	81.5(1)
		O(3) - Ca(1) - O(6)	82.2(1)
		O(3) - Ca(1) - O(6)	171.8(1)
		O(3) - Ca(1) - O(4)	120.3(1)
		O(3) - Ca(1) - O(5)	104.4(2)
		O(3) - Ca(1) - O(6)	174.6(2)
		O(3) - Ca(1) - O(6)	52.0(1)
		O(3) - Ca(1) - O(6)	85.1(2)
Ca(1) - O(4)	2.553(5)	O(4) - Ca(1) - O(5)	128.0(1)
		O(4) - Ca(1) - O(6)	54.9(1)
		O(4) - Ca(1) - O(6)	73.6(1)
		O(4) - Ca(1) - O(6)	80.3(2)
Ca(1) - O(5)	2.343(4)	O(5) - Ca(1) - O(6)	78.7(1)
		O(5) - Ca(1) - O(6)	156.4(1)
		O(5) - Ca(1) - O(6)	78.4(2)
Ca(1) - O(6)	2.609(4)	O(6) - Ca(1) - O(6)	124.9(1)
Ca(1) - O(6)	2.956(4)	O(6) - Ca(1) - O(6)	91.3(2)

Table 3.4 (cont.)

Ca(1) - O(6)	2.464(5)	O(6) - Ca(1) - O(6)	98.8(1)
Ca(2) - O(2)	2.304(4)	O(2) - Ca(2) - O(4)	88.0(2)
		O(2) - Ca(2) - O(4)	88.9(2)
		O(2) - Ca(2) - O(5)	98.5(2)
		O(2) - Ca(2) - O(5)	97.7(2)
		O(2) - Ca(2) - O(6)	177.1(2)
Ca(2) - O(4)	2.348(4)	O(4) - Ca(2) - O(4)	99.2(2)
Ca(2) - O(4)	2.417(5)	O(4) - Ca(2) - O(5)	173.3(2)
		O(4) - Ca(2) - O(5)	80.7(2)
		O(4) - Ca(2) - O(6)	89.8(2)
		O(4) - Ca(2) - O(5)	79.5(2)
		O(4) - Ca(2) - O(5)	173.4(2)
		O(4) - Ca(2) - O(6)	93.4(2)
Ca(2) - O(5)	2.367(4)	O(5) - Ca(2) - O(5)	99.8(2)
Ca(2) - O(5)	2.375(5)	O(5) - Ca(2) - O(6)	83.7(2)
		O(5) - Ca(2) - O(6)	80.0(2)
Ca(2) - O(6)	2.349(5)		
B(1) - O(1)	1.37(1)	O(1) - B(1) - O(5)	120.3(4)
		O(1) - B(1) - O(5)	120.3(4)
B(1) - O(5)	1.390(6)	O(5) - B(1) - O(5)	119.4(7)

Table 3.4 (cont.)

B(2) - O(3)	1.378(8)	O(3) - B(2) - O(4)	120.1(5)
		O(3) - B(2) - O(6)	120.1(5)
B(2) - O(4)	1.377(7)	O(4) - B(2) - O(6)	119.8(5)
B(2) - O(6)	1.375(7)		

Results and Discussion

The structure of LaCOB is illustrated in Figures 3.1 and 3.2 and selected bond lengths and angles are given in Table 3.4. This structure consists of six-coordinate La atoms binding to six O atoms to form distorted octahedra (O – La – O long angles of 142.3 to 175.9° and short angles ranging between 74.64 and 104.54°), seven-coordinate Ca atoms, and three-coordinate B atoms occupying triangular positions (O – B – O angles ranging from 119.4 to 120.3°).

Interatomic distances in this borate are normal. The interatomic distances for La – O were found to range over 2.303 to 2.562 Å which compares favorably with the value calculated using crystal radii (18) of 2.392 Å. The Ca-O distances reported range from 2.304 to 2.639 Å compared to the crystal radii value of 2.42 Å. The B-O distances reported range from 1.370 to 1.390 Å compared to the crystal radii value of 1.37 Å. These values are also similar to those found in γ -LaSc₃(BO₃)₄ (La-O distances range from 2.424 to 2.521 Å) (19) and GdCOB (Ca-O distances range from 2.3319 to 2.9324 Å, and B-O distances range from 1.3698 to 1.3822 Å) (1).

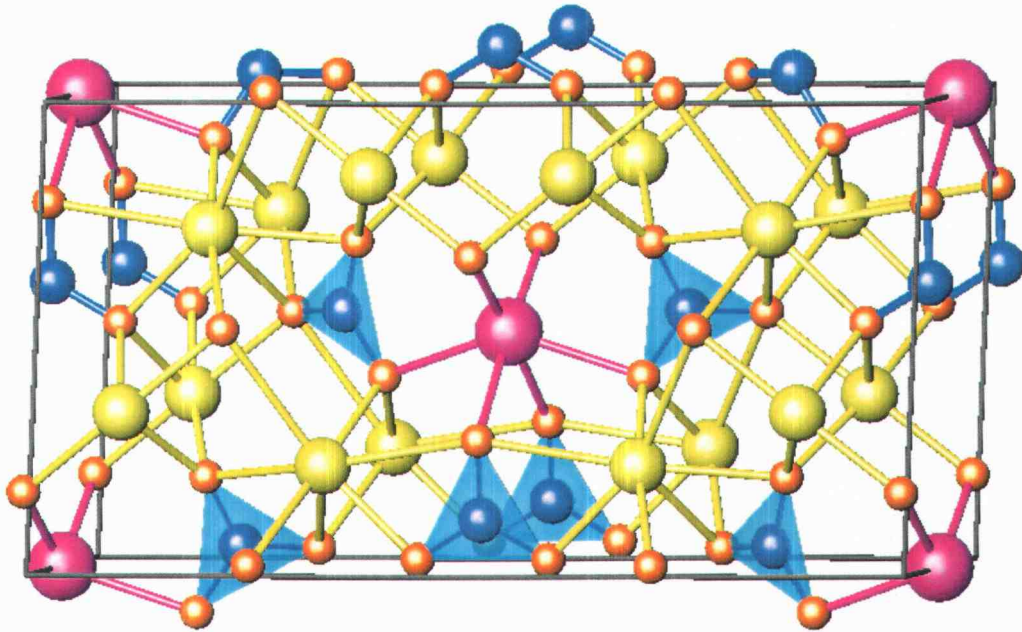


Figure 3.1. LaCOB viewed down the c -axis. La atoms are pink, Ca atoms are yellow, B atoms are blue, and O atoms are orange.

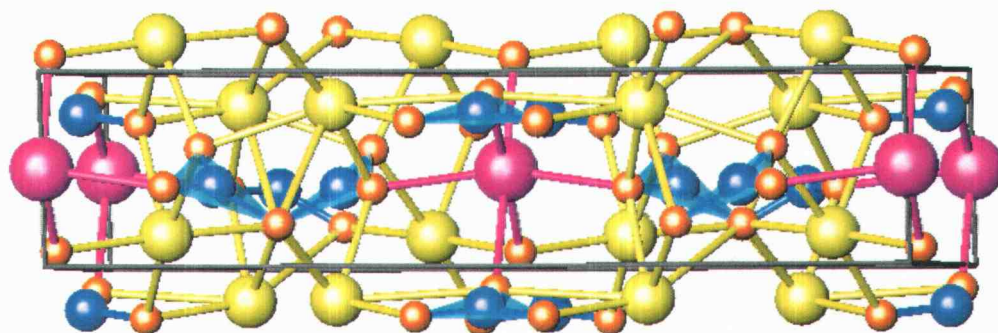


Figure 3.2. LaCOB viewed down the a -axis.

Acknowledgment

NSF is gratefully acknowledged for supporting the work.

References

- (1) Ilyukhin A. B., Dzhurinskii B. F. "Crystal structures of double oxoborates $\text{LnCa}_4\text{O}(\text{BO}_3)_3$ (Ln=Gd, Tb, Lu) and $\text{Eu}_2\text{CaO}(\text{BO}_3)_2$ " *Zhurnal Neorganicheskoi Khimii* 38 917-920 (1993).
- (2) Adams, J. J., Ebberts, C. A., Schaffers, K. I., and Payne, S. A. "Nonlinear optical properties of $\text{LaCa}_4\text{O}(\text{BO}_3)_3$ " *Optics Letters* 26 (4) 217-219 (2001).
- (3) Chai, Bruce H. T. "Advances in bulk inorganic nonlinear optical materials." *Optics & Photonics News* January 31-38 (1999).
- (4) Shao, Zongshu; Lu, Junhua; Wang, Zhengping; Wang, Jiyang; and Jiang, Minhua. "Anisotropic properties of Nd:ReCOB (Re=Y, Gd): A low symmetry self-frequency doubling crystal." *Process in Crystal Growth and Characterization of Materials* 40 63-73 (2000).
- (5) Wang, Jiyang; Shao, Zongsu; Wei, Jingqian; Hu, Xiaobo; Liu, Yaogang; Gong, Bo; Li, Guangming; Lu, Junhua; Guo, Ming; and Jiang, Minhua. "Research on Growth and Self-Frequency Doubling of Nd:ReCOB (Re=Y or Gd) Crystals." *Progress in Crystal Growth and Characterization of Materials* 40 17-31 (2000).
- (6) Zhang, Shujun; Cheng, Zhenxiang; Zhou, Guangyong; Sun, Yuming; Hou, Xueyan; Liu, Xuesong; Han, Jianru; Shao, Zongshu; and Chen, Huanchu. "Growth and Properties of (Cr^{3+} , Nd^{3+}) Doped $\text{GdCa}_4\text{O}(\text{BO}_3)_3$ Crystals." *Progress in Crystal Growth and Characterization of Materials* 40 81-88 (2000).
- (7) Mougel, F., Aka, G., Kahn-Harari, A., Hubert, H., Benitez, J. M., and Vivien, D. "Infrared laser performance and self-frequency doubling of $\text{Nd}^{3+}:\text{Ca}_4\text{GdO}(\text{BO}_3)_3$ (Nd:GdCOB)." *Optical Materials* 8 161-173 (1997).
- (8) teXsan for Windows: Crystal Structure Analysis Package, Molecular Structure Corporation (1997).
- (9) SIR92: Altomare, A., Cascarano, M., Giacovazzo, C., Guagliardi, A. (1993). *J. Appl. Cryst.*, 26, 343.
- (10) DIRDIF94: Beurskens, P.T., Admiraal, G., Beurskens, G., Bosman, W.P., de Gelder, R., Israel, R. and Smits, J.M.M.(1994). The DIRDIF-94 program system, Technical Report of the Crystallography Laboratory, University of Nijmegen, The Netherlands.

(11) DIFABS: Walker, N. & Stuart, Acta Cryst. A39, 158-166 (1983). An empirical absorption correction program.

(12) Least Squares function minimized:

$$\sum w(|F_o| - |F_c|)^2 \text{ where}$$

$$w = 1/[\sigma^2(F_o)] = [\sigma_c^2(F_o) + p^2 F_o^2/4]^{-1}$$

$$\sigma_c(F_o) = \text{e.s.d. based on counting statistics}$$

$$p = \text{p-factor}$$

(13) Standard deviation of an observation of unit weight:

$$[\sum w(|F_o| - |F_c|)^2 / (N_o - N_v)]^{1/2}$$

$$\text{where } N_o = \text{number of observations}$$

$$N_v = \text{number of variables}$$

(14) Cromer, D. T. & Waber, J. T.; "International Tables for X-ray Crystallography", Vol. IV, The Kynoch Press, Birmingham, England, Table 2.2 A (1974).

(15) Ibers, J. A. & Hamilton, W. C.; Acta Crystallogr., 17, 781 (1964).

(16) Creagh, D. C. & McAuley, W.J. ; "International Tables for Crystallography", Vol C, (A.J.C. Wilson, ed.), Kluwer Academic Publishers, Boston, Table 4.2.6.8, pages 219-222 (1992).

(17) Creagh, D. C. & Hubbell, J.H.; "International Tables for Crystallography", Vol C, (A.J.C. Wilson, ed.), Kluwer Academic Publishers, Boston, Table 4.2.4.3, pages 200-206 (1992).

(18) Shannon, R. D. "Revised Effective Ionic Radii and Systematic Studies of Interatomic Distances in Halides and Chalcogenides." Acta Cryst. A 32 5 (751-767 (767).

(19) Wang, Guofu; He, Meiyun; Chen, Wenzhi; Lin, Zhonbin; Lu, Shaofang; and Wu, Qiangjin "Structure of low temperature phase γ -LaSc₃(BO₃)₄ crystal." Mat. Res. Innovat. 2 341-344 (1999).

CHAPTER 4

BPO₄: OPTICAL SECOND-HARMONIC GENERATION FROM WIDE BAND-GAP TETRAHEADRAL GROUPS

Jennifer L. Stone-Sundberg and Douglas A. Keszler

To be submitted to Chemistry of Materials (2001).

Abstract

Crystals of BPO_4 have been grown and structurally characterized. The compound crystallizes with two formula units in the tetragonal space group I-4 with cell parameters $a = 4.334(1)$, $c = 6.643(2)\text{\AA}$, and $V = 124.8(3)\text{\AA}^3$. The B and P atoms occupy distorted tetrahedral environments with B-O and P-O bond vectors that are slightly misaligned. Optical second-harmonic generation from powders and a calculation of d_{eff} are described, and comparisons are made among the structures and optical nonlinearities of BPO_4 and α -quartz.

Introduction

We have recently been investigating (1) the contribution of tetrahedral BO_4 groups to the second-order optical nonlinearity of complex polyborates such as LiB_3O_5 (2) and $\text{CsLiB}_6\text{O}_{10}$ (3). As an extension of this work, we became interested in the nonlinearity of the simple material BPO_4 . As noted from the powder diffraction work of Schulze (4), this compound crystallizes in a simple noncentrosymmetric structure comprised of vertex-sharing BO_4 and PO_4 tetrahedra, a connectivity reminiscent of the condensation of SiO_4 tetrahedra in α -quartz, SiO_2 , the first reported example of a nonlinear optical material (5).

Cursory examination of the reported BPO_4 structure reveals that the BO_4 and PO_4 tetrahedra are only slightly canted one relative to the other. This alignment is favorable for summation of the microscopic hyperpolarizability coefficients of the tetrahedral groups and observation of a significant macroscopic nonlinearity. In this contribution, we describe the crystal growth and single-crystal structural characterization of BPO_4 . These results are then used to assess the structural origins of the observed optical nonlinearity, providing a simple accounting that can be extended to the properties of α -quartz.

Experimental

Synthesis and powder characterization

Powder synthesis

A powder sample of BPO_4 was formed by heating in a Pt crucible stoichiometric amounts of H_3BO_3 (Alfa AESAR, 99.99%) and $(\text{NH}_4)_2\text{HPO}_4$ (Mallinckrodt, reagent grade). After grinding, the sample was heated at 673 K for 17 h, 1273 K for 20 h, and 1373 K for 19 h. A powder diffraction pattern of the product was obtained on a Siemens D-5000 diffractometer.

Powder SHG measurements

The experimental method of Kurtz and Perry (11) was followed to measure the powder SHG signals of the title compound relative to that of the known frequency converter α -quartz by using a 1064-nm fundamental beam. The samples were ground and sieved to produce 11 equally distributed particle size ranges from 25 to 250+ μm . The samples were pressed between glass microscope cover slides and secured with tape in 1-mm thick aluminum holders containing a 5-mm diameter hole. The samples were then placed in a light-tight box and excited with 20-mJ pulses from a Q-switched Nd:YAG laser (New Wave Research Minlase-20). The laser beam was passed through a long-pass filter to eliminate flash-lamp light and then directed onto the sample. The second-harmonic signal was collected through an interference filter ($530 \pm 10 \text{ nm}$) with a

photomultiplier attached to a Tektronix SC 504 80-MHz oscilloscope. A null reading was established by measuring the signal for the centrosymmetric material Al_2O_3 (Stanford Materials 99.999%).

Single crystal growth

Single crystals were grown from a melt of composition 0.7 LiPO_3 : 0.3 BPO_4 molar ratio. Stoichiometric amounts of Li_2CO_3 (Cerac, 99.999%), B_2O_3 (Alfa AESAR, 99.98%), and $(\text{NH}_4)_2\text{HPO}_4$ (Mallinckrodt, reagent grade) were ground together, placed in a platinum crucible and heated to 823 K for one h, reground, heated to 1323 K for one h, and then cooled to 1073 K at a rate of 5 K/h. This heating and cooling regiment resulted in the production of colorless, transparent, block-shaped crystals having edge lengths in the range of 0.1 – 0.6 mm.

X-ray studies

Unit-cell determination and data collection

A colorless tetrahedral crystal having a height of 0.25(2) mm was mounted with epoxy on a glass fiber. All measurements were made on a Rigaku AFC6R diffractometer with graphite monochromated Mo-K α radiation from a rotating-anode generator. Cell constants and an orientation matrix for data collection were obtained from a least-squares refinement by using the setting angles of 16 carefully centered reflections in the 2θ range 21.97-37.75°, leading to an I-centered tetragonal cell (Laue group: 4/m) with dimensions $a = 4.334(1)$, $c =$

6.643(1) Å, and $V = 124.80(3) \text{ \AA}^3$. Intensity data were collected over the range of indices $-8 \leq h \leq 8$, $0 \leq k \leq 8$, $-13 \leq l \leq 13$ by using the ω - 2θ scan technique to a maximum 2θ value of 90° . Of the 1110 reflections collected, 275 were unique and 264 had $F_o^2 \geq 3\sigma(F_o^2)$. The intensity of three standard reflections measured after every 500 reflections varied by an average of 0.5% during the collection, therefore no decay correction was applied. Azimuthal scans of several reflections indicated no need for an absorption correction and therefore none was applied.

Structure refinement

The structure was solved by using programs from the TEXSAN crystallographic software package (5). On the basis of the systematic absence $h+k+l = 2n+1$, packing considerations, a statistical analysis of the intensity distribution, and the successful solution and refinement of the structure, the space group was determined to be I-4 [#82]. The structure was solved by placing the B and P atoms at the previously reported 2a and 2d positions (4), respectively, and then determining the O position from a difference electron-density map. After a full-matrix isotropic refinement of the model, the data were averaged ($R_{\text{int}} = 0.032$) and then refined with anisotropic thermal displacement coefficients on each atom. The final cycle of full-matrix least-squares refinement (6) with 264 observed reflections ($I > 3.00\sigma(I)$) and 15 variable parameters (secondary extinction coefficient = 8.52×10^{-5}) converged to agreement factors of $R = 0.021$ and $R_w = 0.033$. Plots of $\sum w (|F_o| - |F_c|)^2$ versus $|F_o|$, reflection order in data collection, $\sin \theta/\lambda$, and various classes of indices showed no unusual trends. The

maximum and minimum peaks on the final electron density map corresponded to 2.19 and 1.30% of the P atom, respectively. Neutral atom scattering factors were taken from Cromer and Waber (7). Anomalous dispersion effects were included in F_{calc} (8); and the values for $\Delta f'$ and $\Delta f''$ were those of Creagh and McAuley (9). The values for the mass attenuation coefficients are those of Creagh and Hubbell (10). Crystal data are outlined in Table 4.1; atomic parameters are listed in Table 4.2; and anisotropic displacement coefficients are summarized in Table 4.3.

Table 4.1. Experimental details for the structure solution of BPO₄.

Formula Weight, amu	105.78
Crystal System	Tetragonal
Space Group	I-4 [#82]
a , Å	4.334(1)
c , Å	6.643(2)
V , Å ³	124.8(3)
Z	2
D_{calc} , g cm ⁻³	2.815
F(000)	104
Diffractometer	Rigaku AFC6R
Radiation	Mo K α ($\lambda=0.71069$) graphite-monochromated
Data Collection	$\pm h, k, \pm l$
No. Observations. total, unique ($F_o^2 \geq 3\sigma(F_o^2)$)	1110, 275 264
R	0.021
R_w	0.033
Maximum Shift in Final Cycle	0.00
GOF	0.60

$$R = \Sigma ||F_o| - |F_c|| / \Sigma |F_o| = 0.021$$

$$R_w = [(\Sigma w (|F_o| - |F_c|)^2 / \Sigma w F_o^2)]^{1/2} = 0.033$$

Table 4.2. Positional and isotropic displacement coefficients (B_{eq}) for BPO_4 .

Atom	Wyckoff	x	y	z	B_{eq}^*
B	2d	0	0	0	0.36(1)
P	2a	0	½	¾	0.273(3)
O	8g	0.1401(2)	0.2421(2)	0.1232(1)	0.47(1)

*

$$*B_{eq} = (8\pi/3)^2 \sum_i \sum_j U_{ij} a_i^* a_j^* a_i a_j$$

Table 4.3. Anisotropic displacement parameters for BPO_4 .

Atom	$U_{11} = U_{22} = U_{33}$	U_{12}	U_{13}	U_{23}
B	0.0043(4)	0	0	0
P	0.00352(9)	0	0	0
O	0.0060(3)	-0.0002(2)	0.0034(3)	0.0002

Results and Discussion

Structure

As seen in Figure 4.1, BPO_4 adopts a structure characterized by a condensation of distorted BO_4 and PO_4 tetrahedra. Like the common structures of SiO_2 (12, 13), the tetrahedra share vertices to produce two-coordinate O atoms.

Since the B and P atoms occupy special positions 2a and 2d, respectively, the only variable positional parameters are those associated with the O atom (Table 4.2). From refinement with powder X-ray diffraction data, Schulze (2) reported for the O parameter: $x = 0.138$, $y = 0.26$, $z = 0.131$. These values differ only slightly from those reported here (Table 4.2). A comparison of our experimental powder diffraction pattern to those calculated from the single-crystal structure refinement and Schulze's parameters is presented in Figure 4.2.

Interatomic distances and angles are listed in Table 4.4. Both B-O and P-O distances, 1.4626(9) and 1.5258(9) Å, respectively, are consistent with the corresponding lengths, 1.46 and 1.52 Å, predicted on the basis of crystal radii (14). The results are statistically different from those of Schulze: 1.436 Å for B-O and 1.544 Å for P-O. The BO_4 and PO_4 groups are slightly distorted – point group S_4 – so the O-B-O and O-P-O angles deviate from the ideal tetrahedral angle (Table 4.4). The B-O-P angle, $132.02(6)^\circ$, is more acute than the Si-O-Si angles, typically $\sim 145^\circ$, in quartz (12) and silicates (13).

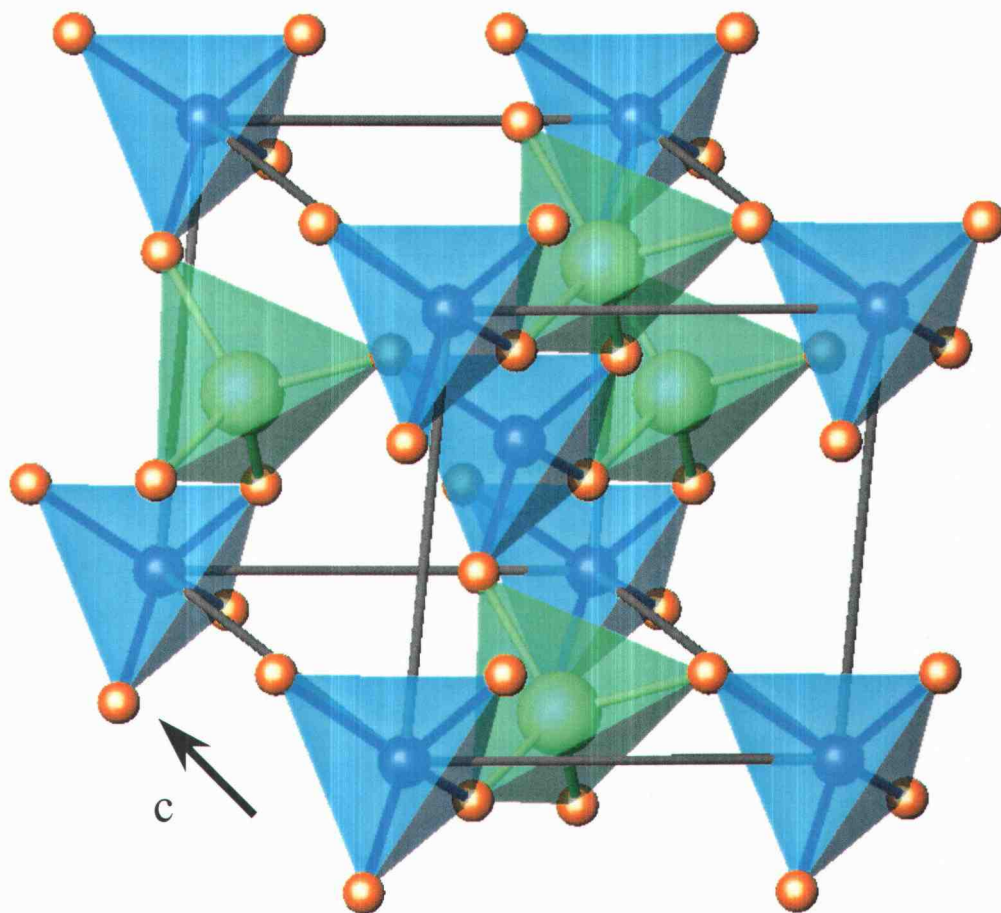


Figure 4.1. Unit-cell drawing of BPO₄. Tetrahedra shaded blue represent BO₄ groups, and tetrahedra shaded green represent PO₄ groups.

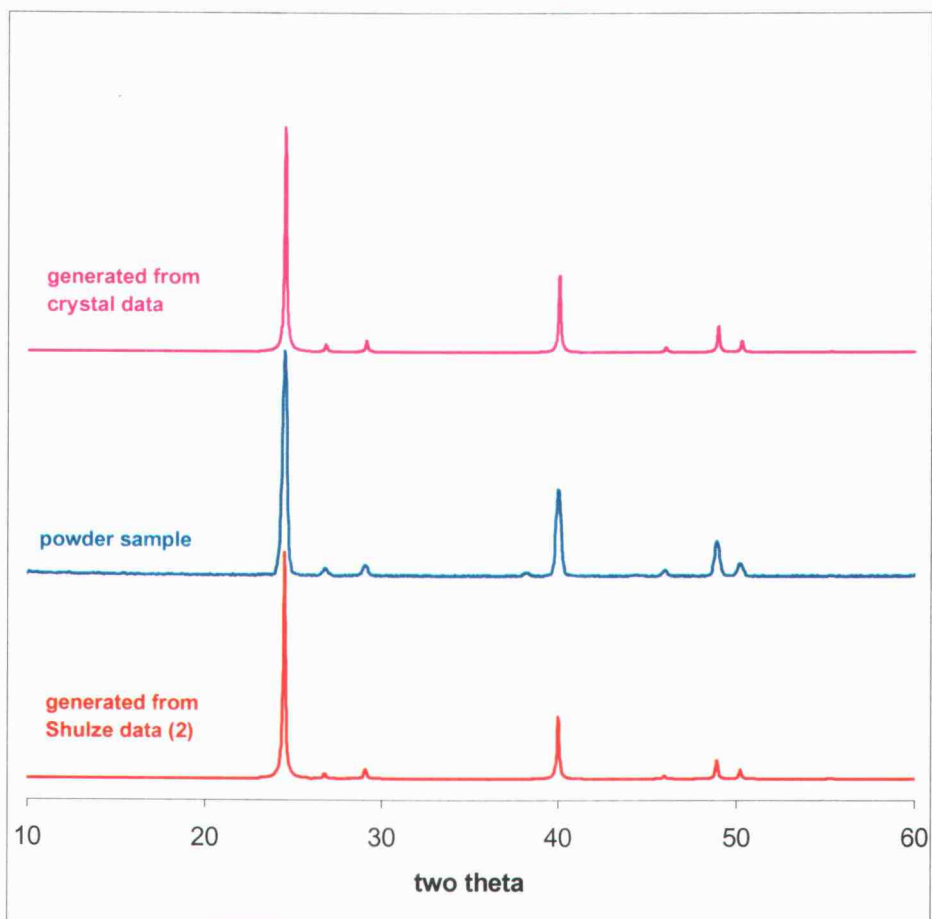


Figure 4.2: Powder diffraction patterns for BPO_4 .

Table 4.4. Interatomic distances(Å) and angles(°) for BPO₄.

B - O (x 4)	1.4626(9)	O - B - O	108.24(4)
		O - B - O	111.97(7)
P - O (x 4)	1.5258(9)	O - P - O	107.76(3)
		O - P - O	112.95(7)
		B - O - P	132.02(6)

SHG properties

Because BPO_4 crystallizes in a noncentrosymmetric structure, a second-harmonic signal is observed when a sample is placed in the path of a high-intensity laser beam. This signal can be correlated to the nonlinear susceptibility coefficients d_{jk} , which can be approximated on the basis of an oriented-gas model (15, 16). In this model, the nonlinearity is associated primarily with the relative orientations of the individual BO_4 and PO_4 groups.

The method has been applied with considerable success to a wide range of borates containing exclusively BO_3 groups (16), but it has only recently been successfully extended to the analysis of complex polyborates containing both BO_3 and BO_4 groups (1). By using equation (4.1),

$$d_{ijk} = \frac{1}{V} \sum_1^N \sum_{lmn} R_{il} R_{jm} R_{kn} \beta_{lmn} \quad (4.1)$$

the components of the hyperpolarizability tensor components (β_{lmn}) are summed according to the directional cosines or orientation functions (R) of the individual groups and weighted by their number densities ($1/V$). For polyborates, hyperpolarizabilities have generally been derived on the basis of various quantum-mechanical methods by using molecular fragments of three-dimensional structures. (16, 17). These results have to date provided rather poor agreement with experimental results. We note, however, that first-principle calculations including translational symmetry have recently provided an effective means for calculation of both linear and nonlinear optical properties of the compound β -

BaB₂O₄ (18). To provide an effective and simple predictive tool for estimating nonlinearities, we have employed equation 4.1 to derive simple functional forms of β for different types of groups (1) and to assign a self-consistent set of β values to these groups on the basis of reported d coefficients (1).

The magnitude of d_{ijk} for BPO₄ from equation 4.1 depends significantly on the relative orientations of the BO₄ and PO₄ tetrahedra as given by the direction cosines R . In a *hypothetical* BPO₄ structure, containing fully aligned tetrahedra and a collinear arrangement of B-O and P-O bonds, each tetrahedron would make a unit contribution to d through R and a maximum nonlinearity would ensue. As shown in Figure 4.3, however, the BO₄ and PO₄ tetrahedra are tilted one relative to the other, producing a misalignment of the B-O and P-O bonds and their associated tetrahedra. The angular misalignment can be deduced by using equations 4.2 – 4.4:

$$\mathbf{B} \cdot \mathbf{P} \equiv x_B * x_P + y_B * y_P + z_B * z_P \quad (4.2)$$

$$\mathbf{B} \cdot \mathbf{P} = BP \cos \theta \quad (4.3)$$

$$\theta = \cos^{-1} \frac{\mathbf{B} \cdot \mathbf{P}}{BP} \quad (4.4)$$

where \mathbf{B} and \mathbf{P} are the vectors describing the selected B-O and P-O bonds, respectively; x, y, z are the Cartesian coordinates of the O atoms of the selected B-O and P-O bonds relative to a common origin; B and P are the bond lengths of the selected bonds; and θ is the resulting alignment angle. For BPO₄, this angle is $\theta = 25^\circ$ (Figure 4.4).

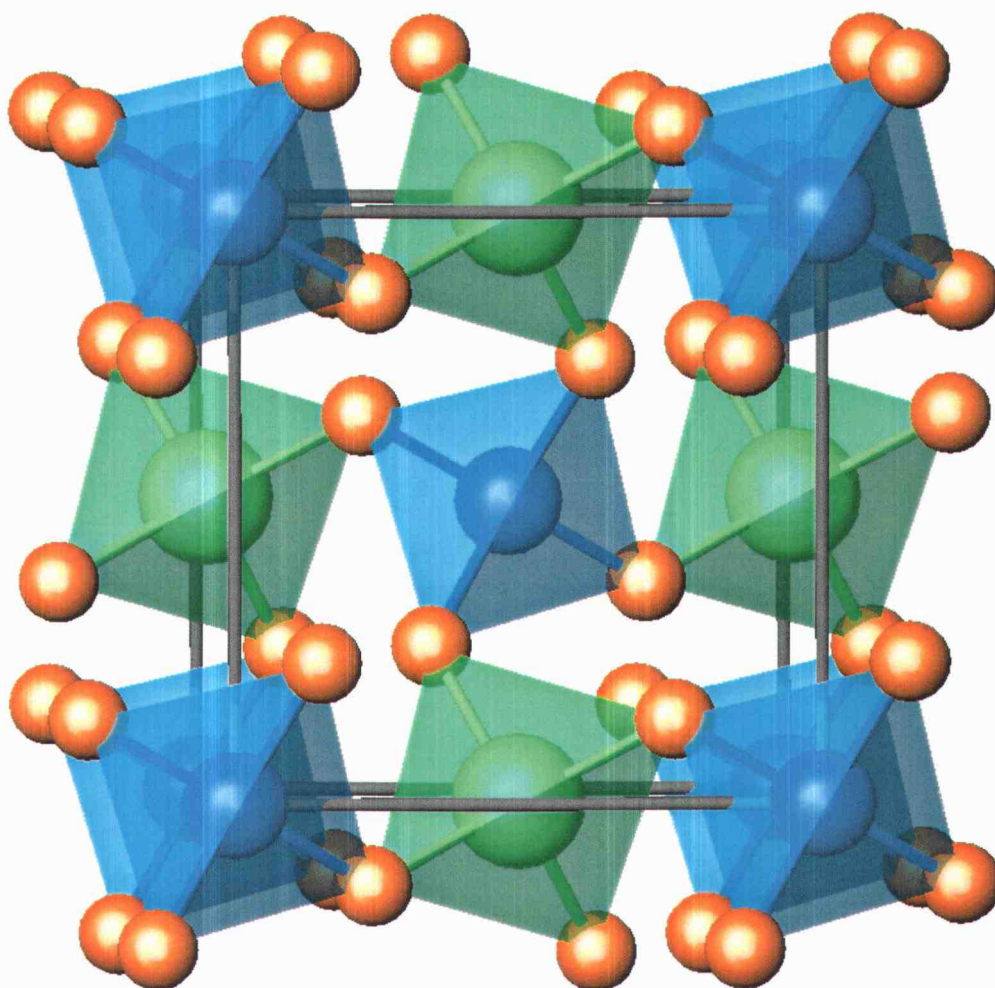


Figure 4.3. BPO₄ viewed down the *c* axis.

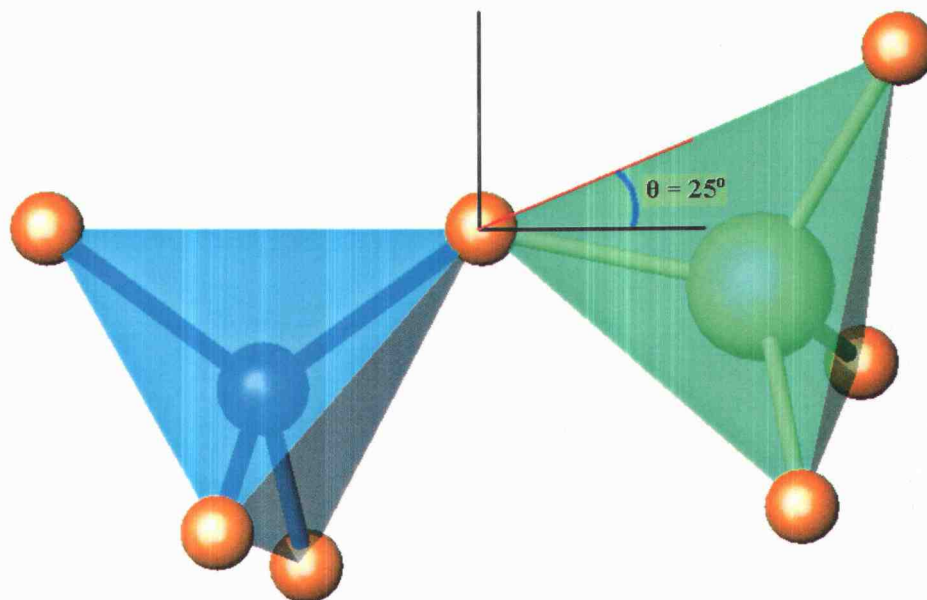


Figure 4.4. Illustration of tetrahedra orientation in BPO_4 .

In BPO_4 (point group -4), the relevant second-order coefficient is d_{14} , $\chi(1,2,3)$, and this coefficient correlates directly to the hyperpolarizability coefficient, $\beta_{1,2,3}$, for an isolated tetrahedral group. As seen from Figure 4.5, rotation of a tetrahedral group by 90° about one of the Cartesian axes produces an orientation that is centrosymmetrically related to the original. In this case, the sum of the β values for the two orientations must equal zero, so $\beta(1,2,3) = -\beta'(1,2,3)$ (Figure 4.5). As a result, $\beta(1,2,3)$ follows a $\cos 2\theta$ functional dependence. In BPO_4 , the misalignment angle of 25° between the BO_4 and PO_4 tetrahedra corresponds to a Cartesian-axis rotation, so the structural contribution

to the nonlinear coefficient is $(\beta(1,2,3) + \beta(1,2,3) * \cos(2 * 25^\circ))/2 = 0.8$, i.e., the orientation of the tetrahedra is 80% of optimum.

These results can be directly compared to those of α -quartz, SiO_2 (19). In this compound (Figure 4.6), the three SiO_4 tetrahedra in each unit cell are related by a 3_1 screw axis along c . Inspection of Figure 4.6 reveals that two of the SiO_4 groups (A and B) are related by an approximate center of symmetry, leaving the third group to contribute to the nonlinearity and a structural contribution that is approximately 33% of optimum. Application of equation 4.1 reveals a calculated structural contribution of 38%.

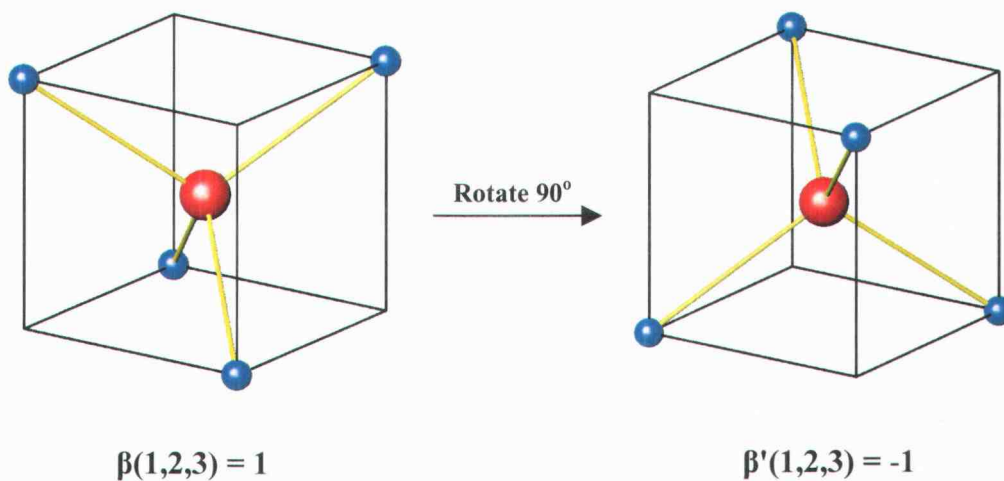


Figure 4.5. Rotation of a tetrahedral group by 90° about one of the Cartesian axes produces an orientation that is centrosymmetrically related to the original resulting in the sum of the β values for the two orientations equaling zero, or $\beta(1,2,3) = -\beta'(1,2,3)$.

Because energy gaps differ only slightly for BO_4 , PO_4 , and SiO_4 tetrahedra, we can assume that their hyperpolarizability coefficients, e.g., β_{123} , are equivalent. Any differences in the nonlinearities of BPO_4 and SiO_2 must then derive from the relative number densities and structural orientations of the tetrahedral groups. The relevant tetrahedral number densities for BPO_4 and SiO_2

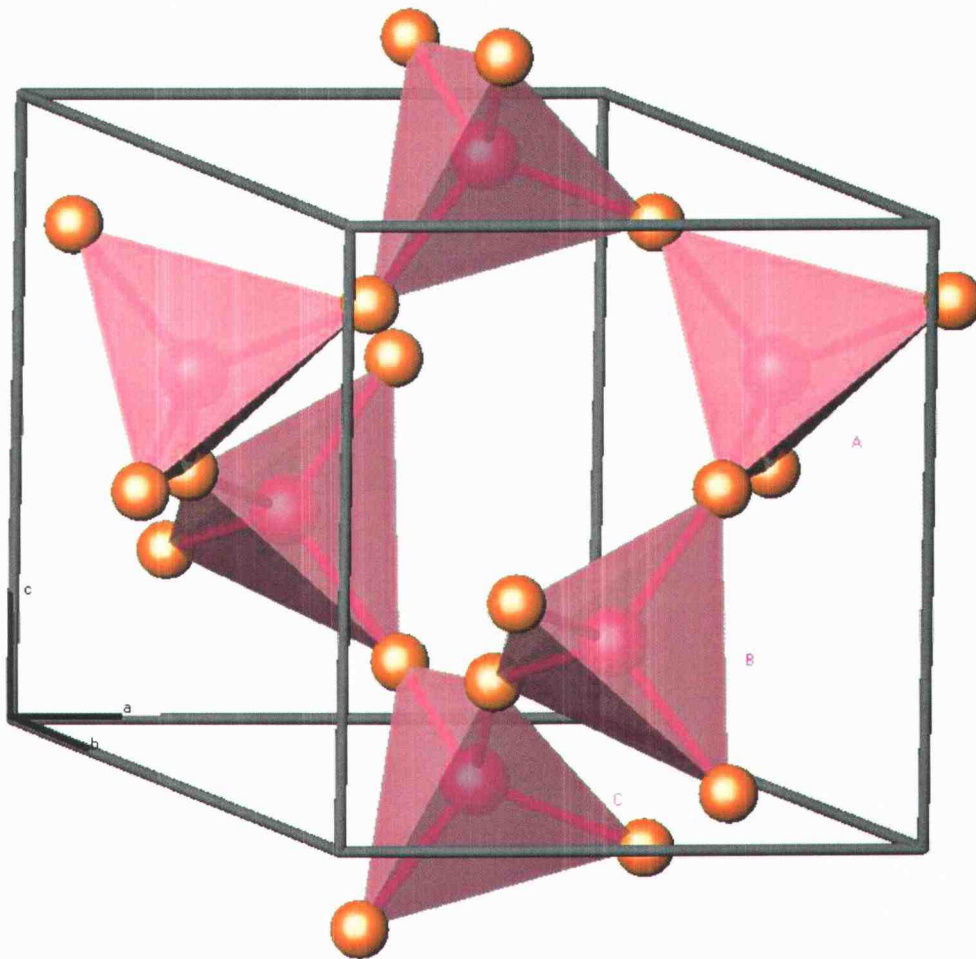


Figure 4.6. Drawing of a unit cell of α -quartz.

are 3.2×10^{22} and $2.9 \times 10^{22} \text{ cm}^{-3}$, respectively, a difference of approximately 10%, so the predominant factor contributing to the difference in the nonlinearities must be the unique structural arrangements of the tetrahedral groups. Considering the number densities and orientation contributions, from equation 4.1 the ratio $d_{calc}(BPO_4)/d_{calc}(SiO_2) = 2.3$. From equation 4.5 (11),

$$\frac{I^{2\omega}(A)}{I^{2\omega}(B)} = \frac{\langle d_{ijk}^{2\omega}(A) \rangle^2}{\langle d_{ijk}^{2\omega}(B) \rangle^2} \quad (4.5)$$

we see that the ratio of second-harmonic intensities of two compounds A and B varies as the square of the ratio of the nonlinear coefficients for the two materials, assuming their phase matching lengths are comparable. From measurements of second-harmonic generation signals, we find $I^{2\omega}(BPO_4)/I^{2\omega}(SiO_2) = 4$, a result that corresponds to a ratio $d_{obs}(BPO_4)/d_{obs}(SiO_2) = 2$, a value in general agreement with the very simple orientation model and the importance of the structural contribution to the observed nonlinearity. We also note that the magnitude of the signal for BPO_4 corresponds to a value of $d_{14} \sim 0.8 \text{ pm/V}$, a value that is comparable to those of the commercial frequency converters LiB_3O_5 (19) and $CsLiB_6O_{10}$ (19).

From the variation of the second-harmonic signals of the BPO_4 samples with particle size, we find no evidence for angular phase matching from the Kurtz-Perry tests (11). This result is consistent with the relatively small refractive indexes associated with wide band-gap materials of this type and the absence of any anisotropic structural element, e.g., a planar BO_3 group, which could produce a significant birefringence.

Summary

The O positional parameters in the structure of BPO₄ have been refined from single-crystal X-ray data to provide a precise description of the relative orientations of the BO₄ and PO₄ tetrahedra for a calculation of its nonlinear d_{14} coefficient. This coefficient was found to be approximately two times greater than that of α quartz, which is consistent with the orientations of the relevant B-, P-, and Si-centered tetrahedra. The present analysis represents the application of a very simple model to an estimation of the nonlinearity of α -quartz. Insofar as we know, this is the only explanation produced for the nonlinearity of α -quartz.

Acknowledgements

The authors wish to thank the US National Science Foundation (Grant #0114017) for funding the work.

References

- (1) Keszler, D.A. "NLO materials for deep UV generation," American Conference on Crystal Growth and Epitaxy, Vail, CO, USA, August 2000; D.A. Keszler, "New materials for high-power laser systems," National Meeting of the Materials Research Society, Boston, MA, USA, December 2000.
- (2) Shulze, Gustav E. R.; "Die Kristallstruktur von BPO₄ und BasO₄." Z. Physik. Chem. B 24 215-240 (1933).
- (3) Franken, P. A.; Hill, A. E.; Peters, C. W.; and Weinreich, G. "Generation of optical harmonics." Physical Review Letters 7 (4) 118-119 (1961).
- (4) Xue, D., Betzler, K., and Hesse, H. "Structural characteristics and second order nonlinear optical properties of borate crystals." OSA Trends Opt. Photonics Ser. (Advanced Solid State Lasers) 34 542-547 (2000).
- (5) teXsan for Windows: Crystal Structure Analysis Package, Molecular Structure Corporation (1997).
- (6) Least Squares function minimized:
 $\Sigma w(|F_o| - |F_c|)^2$ where
 $w = 1/[\sigma^2(F_o)] = [\sigma^2 c(F_o) + p^2 F_o^2/4]^{-1}$
 $\sigma c(F_o) = \text{e.s.d. based on counting statistics}$
 $p = \text{p-factor}$
 Standard deviation of an observation of unit weight:
 $[\Sigma w(|F_o| - |F_c|)^2 / (N_o - N_v)]^{1/2}$
 where $N_o = \text{number of observations}$
 $N_v = \text{number of variables}$
- (7) Cromer, D. T. & Waber, J. T.; "International Tables for X-ray Crystallography", Vol. IV, The Kynoch Press, Birmingham, England, Table 2.2 A (1974).
- (8) Ibers, J. A. & Hamilton, W. C.; Acta Crystallogr., 17, 781 (1964).
- (9) Creagh, D. C. & McAuley, W.J. ; "International Tables for Crystallography", Vol C, (A.J.C. Wilson, ed.), Kluwer Academic Publishers, Boston, Table 4.2.6.8, pages 219-222 (1992).
- (10) Creagh, D. C. & Hubbell, J.H.; "International Tables for Crystallography", Vol C, (A.J.C. Wilson, ed.), Kluwer Academic Publishers, Boston, Table 4.2.4.3, pages 200-206 (1992).

- (11) Kurtz, S. K., and Perry, T. T. "A Powder Technique for the Evaluation of Nonlinear Optical Materials." *Journal of Applied Physics* 39 8 3798-3813 (1968).
- (12) Zachariassen, W. H.; and Plettinger, H. A. *Acta Crystallographica* 18, 710 (1965).
- (13) O'Keeffe, M. O.; and Hyde, B. G. *Acta Crystallographica, Section B* 34, 27 (1978).
- (14) Shannon, R. D. "Revised Effective Ionic Radii and Systematic Studies of Interatomic Distances in Halides and Chalcogenides." *Acta Cryst. A* 32 751-767 (1976).
- (15) Kathleen I. Schaffers, Ph.D. dissertation, Oregon State University, 1992.
- (16) C.T. Chen, *Development of new nonlinear optical crystals in the borate series*, Harwood Academic Publishers, Langhorne, PA, 1993.
- (17) W.D. Cheng, J.T. Chen, Q.W. Lin, Q.E. Zhang, J.X. Lu, "Cluster modeling of electronic structure and nonlinear properties for the optical materials MB_6O_{10} ($M=Cs_2, Li_2, CsLi$)," *Phys. Rev. B: Condens. Matter Mater. Phys.* **60**, pp. 11747-11754, 1999.
- (18) Lin, M.-H. Lee, Z.-P. Liu, C. Chen, C. J. Pickard, "Mechanism for linear and nonlinear optical effects in β - BaB_2O_4 crystals," *Phys. Rev. B: Condens. Matter Mater. Phys.* **60**, pp. 13380-13389, 1999; Z. Lin, J. Lin, Z. Wang, C. Chen, M.-H. Lee, "Mechanism for linear and nonlinear optical effects in LiB_3O_5 , CsB_3O_5 , and $CsLiB_6O_{10}$ crystals," *Phys. Rev. B: Condens. Matter Mater. Phys.* **62**, 1757-1764, 2000.
- (19) Smith, A. V. "How to select nonlinear crystals and model their performance using SNLO software," <http://www.sandia.gov/imrl/XWEB1128/xxxtal.htm> (2000).

CHAPTER 5

STRUCTURE AND SECOND-HARMONIC GENERATION FOR NaAlO_2

Jennifer L. Stone-Sundberg and Douglas A. Keszler

To be submitted to Acta Crystallographica, Section C (2001).

Abstract

Single crystals of NaAlO_2 have been grown and structurally characterized. The material crystallizes with four formula units in the orthorhombic space group $\text{Pna}2_1$ with unit-cell parameters $a = 5.370(2)$, $b = 7.019(1)$, $c = 5.207(2)$ Å, and $V = 196.27$ Å³. The compound adopts a distorted structure related to chalcopyrite with all of the atoms located in distorted tetrahedral environments. The metal-centered tetrahedra can be considered to be slightly canted from the c axis, leading to an optical second-harmonic signal that is approximately twice that of α -quartz.

Introduction

During investigations into the crystal growth of new, complex aluminum borates, we have on different occasions isolated crystals of the simple compound NaAlO_2 . This material is known to form in a low pressure α form (1) and a high-pressure β form (2) The α form can be considered to be a distorted version of the chalcopyrite structure, while the β form is isostructural to NaFeO_2 . Low sodium-content β aluminas have long been of interest for their ion-conductivity properties, and such interest has recently been extended to the properties of NaAlO_2 derivatives (3).

As part of our continuing interest in the optical nonlinearities of wide band-gap oxides containing only tetrahedral groups, we have elected to refine from single-crystal X-ray data the noncentrosymmetric structure of NaAlO_2 and to correlate this structure to the relatively strong second-harmonic response that is observed for the conversion of 1064 to 532-nm laser light.

Experimental

Synthesis and powder characterization

Powder synthesis

A powder sample of NaAlO₂ was formed by heating in a Pt crucible stoichiometric amounts of Na₂CO₃ (Cerac, 99.995%), and Al₂O₃ (Stanford, 99.998%). After grinding, the sample was heated at 1628 K for 50 h. A powder diffraction pattern of the product was obtained on a Siemens D-5000 diffractometer.

Powder SHG measurements

The experimental method of Kurtz and Perry (4) was followed to measure the powder SHG signals of the title compound relative to that of the known frequency converter α -quartz by using a 1064-nm fundamental beam. The samples were ground and sieved to produce 11 equally distributed particle size ranges from 25 to 250+ μm . The samples were pressed between glass microscope cover slides and secured with tape in 1-mm thick aluminum holders containing a 5-mm diameter hole. The samples were then placed in a light-tight box and excited with 20-mJ pulses from a Q-switched Nd:YAG laser (New Wave Research Minlase-20). The laser beam was passed through a long-pass filter to eliminate flash-lamp light and then directed onto the sample. The second-harmonic signal was collected through an interference filter (530 ± 10 nm) with a

photomultiplier attached to a Tektronix SC 504 80-MHz oscilloscope. A null reading was established by measuring the signal for the centrosymmetric material Al_2O_3 (Stanford Materials 99.999%).

Crystal growth

Crystals of NaAlO_2 were grown from a melt of composition NaAlO_2 by using Na_2CO_3 (Cerac, 99.995%), and Al_2O_3 (Stanford, 99.998%). The mixture was heated to 1723 K and cooled at 10 K/h to 1223 K and then rapidly cooled to room temperature.

X-ray studies

A crystalline block with edge lengths near 0.30 mm was physically extracted from the melt and mounted on a glass fiber with epoxy for X-ray analysis. Measurements were made on a single-crystal, rotating-anode Rigaku AFC6R diffractometer with graphite-monochromated $\text{Mo K}\alpha$ radiation. Cell constants and an orientation matrix for data collection were obtained from a least-squares refinement with 17 automatically-centered reflections in the range $10 \leq 2\theta \leq 23^\circ$. The cell constants, $a = 5.370(2)$, $b = 7.019(1)$, $c = 5.207(2)$ Å, $V = 196.27$ Å³, correspond to a primitive orthorhombic cell; Laue symmetry mmm was determined on the diffractometer. Intensity data were collected over the range of indices $-7 \leq h \leq 7$, $0 \leq k \leq 8$, $0 \leq l \leq 10$ by using the ω - 2θ scan technique to a maximum 2θ value of 65° . Of the 831 reflections collected, 454 were unique,

and 221 had $F_o^2 \geq 3\sigma(F_o^2)$. The intensity of three standard reflections measured after every set of 500 reflections varied by an average of 0.5% during the collection.

The structure was solved by using programs from the TEXSAN crystallographic software package (5). On the basis of the systematic absences of $0kl: k + l = 2n+1$, and $h0l: h = 2n+1$, the statistical analysis of the intensity distribution, packing considerations, and the successful solution and refinement of the structure, the crystal was found to form in the noncentrosymmetric space group $Pna2_1$ [#33]. All atom positions were derived from the direct methods program SIR92 (6). After convergence of full-matrix refinement of the model with isotropic displacement coefficients on each atom, the data were averaged ($R_{int} = 0.057$) and then refined with anisotropic displacement coefficients on all atoms. A correction for secondary extinction was applied (coefficient =). The final cycle of full-matrix least-squares refinement (7) with 221 reflections ($I > 3.00\sigma(I)$) and 38 variable parameters, including the secondary extinction coefficient = 5.16×10^{-6} , converged to the agreement factors of $R = 0.031$ and $R_w = 0.029$. The weighting scheme was based on counting statistics and included a factor ($p = 0.010$) to downweight the intense reflections. Plots of $\sum w (|Fo| - |Fc|)^2$ versus $|Fo|$, reflection order in data collection, $\sin \theta/\lambda$ and various classes of indices showed no unusual trends. The maximum and minimum peaks on the final difference electron-density map corresponded to 0.64 and 0.58% for the Al atom, respectively. Neutral atom scattering factors were taken from Cromer and Waber (8). Anomalous dispersion effects were included in F_{calc} ; the values for

$\Delta f''$ and $\Delta f'''$ were those of Creagh and McAuley (9). The values for the mass attenuation coefficients are those of Creagh and Hubbel (10). Crystal data are outlined in Table 5.1, atomic positional and isotropic thermal parameters are listed in Table 5.2, and atomic anisotropic thermal parameters are listed in Table 5.3.

Table 5.1. Crystallographic data for NaAlO₂.

Formula Weight, amu	81.97
Crystal System	Orthorhombic
Space Group	Pna2 ₁ [33]
<i>a</i> , Å	5.370(2)
<i>b</i> , Å	7.019(1)
<i>c</i> , Å	5.207(2)
<i>V</i> , Å ³	196.27(8)
<i>Z</i>	4
<i>D</i> _{calc} , g cm ⁻³	2.774
F(000)	160
Diffractometer	Rigaku AFC6R
Radiation	Mo Kα (λ=0.71069) graphite monochromated
Data Collection	± <i>h</i> , <i>k</i> , <i>l</i>
No. Observations, total, unique (<i>F</i> _o ² ≥ 3σ(<i>F</i> _o ²))	831, 454 221
<i>R</i>	0.031
<i>R</i> _w	0.029
Maximum Shift in Final Cycle	0.04
GOF	1.19

$$R = \frac{\sum ||F_o| - |F_c||}{\sum |F_o|} = 0.031$$

$$R_w = \left[\frac{\sum w (|F_o| - |F_c|)^2}{\sum w F_o^2} \right]^{1/2} = 0.029$$

Table 5.2. Positional and isotropic displacement parameters (B_{eq}) for NaAlO_2 .

Atom	Wy	x	y	z	B_{eq}^*
Na	4a	-0.0660	0.3768	0.2052	1.0288
Al	4a	0.0605	0.1257	0.6868	0.4287
O(1)	4a	0.3747(7)	0.1753(5)	0.7538(7)	0.69(5)
O(2)	4a	0.0337(7)	0.0755(5)	0.3559(8)	0.78(6)

$$*B_{eq} = (8\pi/3)^2 \sum_i \sum_j U_{ij} a_i^* a_j^* a_i a_j$$

Table 5.3. Anisotropic displacement parameters for NaAlO_2 .

Atom	U_{11}	U_{22}	U_{33}	U_{12}	U_{13}	U_{23}
Na	0.0130	= U_{11}	= U_{11}	0	0	0
Al	0.0054	= U_{11}	= U_{11}	0	0	0
O(1)	0.009(1)	= U_{11}	= U_{11}	0	-0.004(1)	0
O(2)	0.011(2)	= U_{11}	= U_{11}	-0.003(1)	-0.003(2)	0

Results and Discussion

Structure

Three views, each along one of the crystallographic axes, of the structure are given in Figures 5.1 - 5.3. The structure exhibits distorted tetrahedral coordination of each of the atoms with a three-dimensional arrangement that is similar to that of chalcopyrite, CuFeS_2 . As seen in Figure 5.1, this arrangement produces M-O (M = Na, Al) bond vectors that are generally aligned along the c axis.

A summary of interatomic distances and angles is given in Table 5.4. The average Na-O distance, 2.34(4) Å, is comparable to the value, 2.37 Å, calculated from crystal radii (11). Likewise, the average Al-O distance, 1.75(1) Å, is consistent with the value, 1.77 Å, from crystal radii. The M-centered angles are fairly regular with O-Na-O angles ranging from 102.8 to 107.5° and O-Al-O angles covering the range 107.8 to 112.3°.

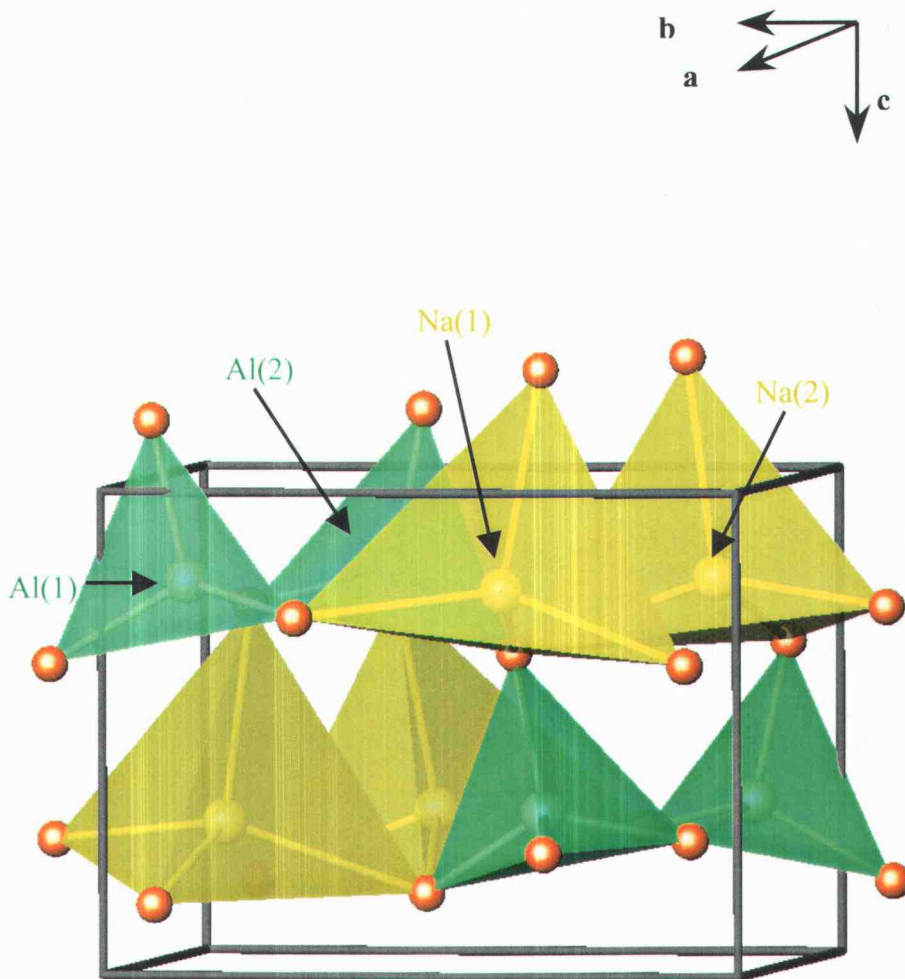


Figure 5.1. Structure of NaAlO₂ viewed approximately down the *a* axis. Yellow tetrahedra are centered by Na atoms, and green tetrahedra are centered by Al atoms.

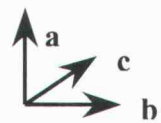
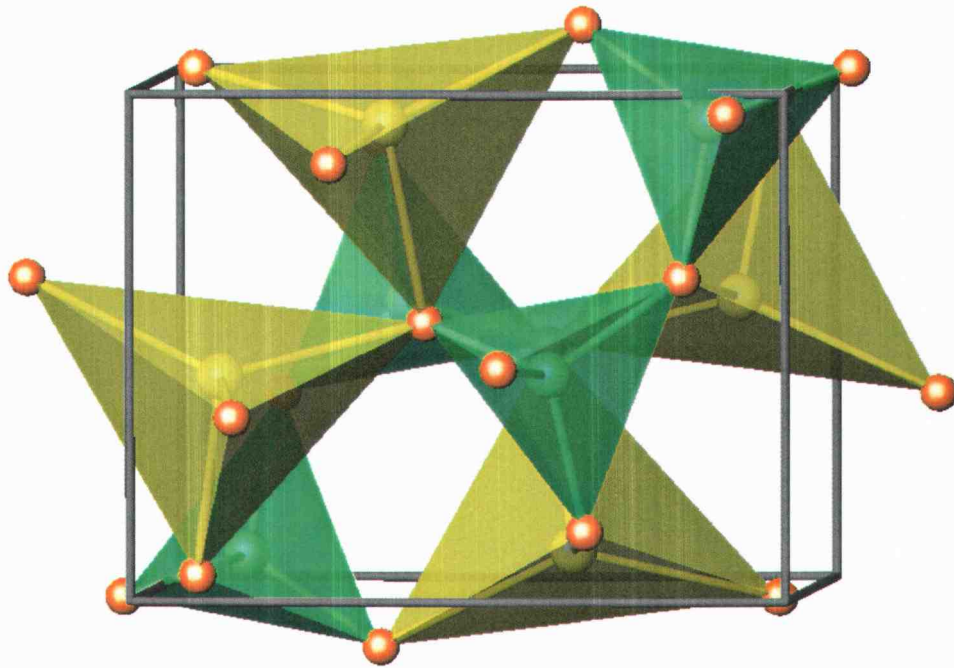


Figure 5.2. NaAlO₂ viewed down the *c* axis.

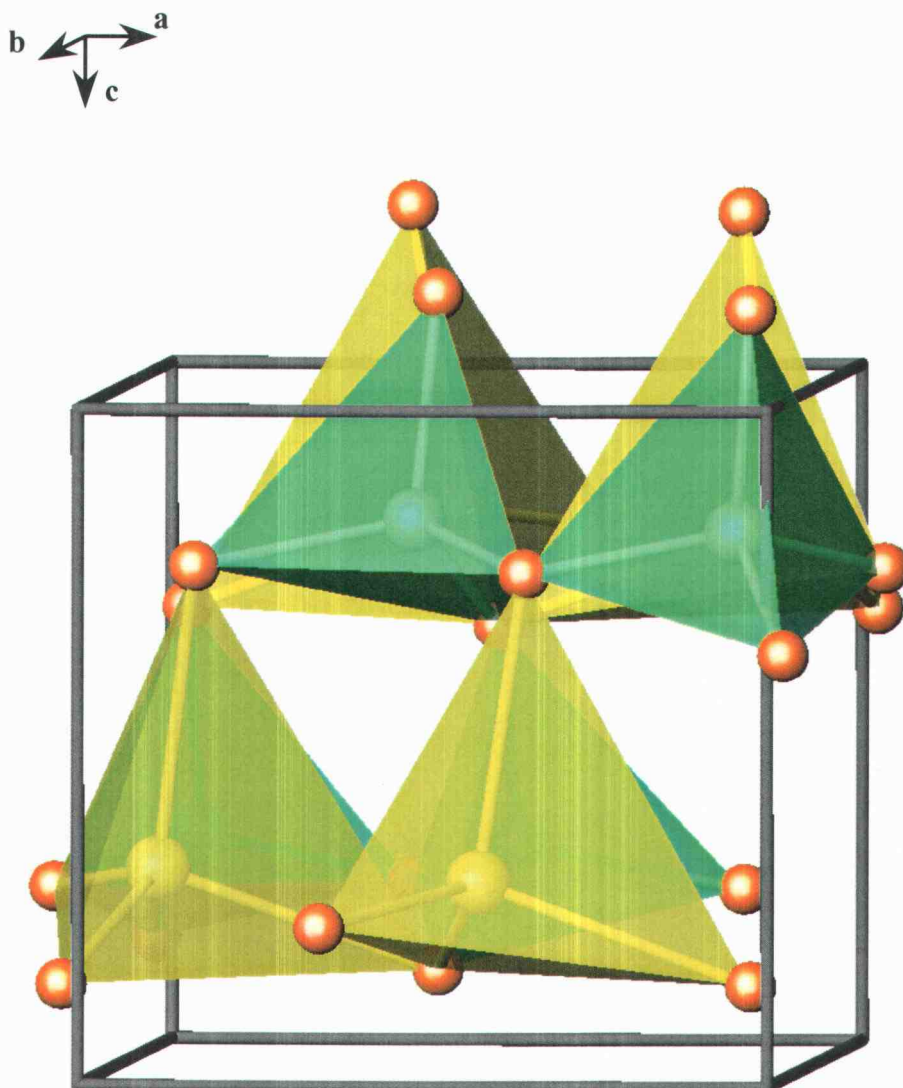


Figure 5.3. NaAlO_2 viewed approximately down the b axis.

Table 5.4. Selected Interatomic Distances (Å) and Angles (°) for NaAlO₂.

Na - O(1)	2.402(7)	O(1) - Na - O(1)	107.5(4)
Na - O(1)	2.343(4)	O(1) - Na - O(2)	102.8(3)
Na - O(2)	2.320(5)	O(1) - Na - O(2)	103.2(9)
Na - O(2)	2.31(1)	O(1) - Na - O(2)	104.1(2)
		O(2) - Na - O(2)	103.3(3)
Al - O(1)	1.756(7)	O(1) - Al - O(1)	110.5(2)
Al - O(1)	1.753(5)	O(1) - Al - O(2)	108.2(9)
Al - O(2)	1.764(5)	O(1) - Al - O(2)	109.9(5)
Al - O(2)	1.740(6)	O(1) - Al - O(2)	107.8(6)
		O(1) - Al - O(2)	112.3(5)
		O(2) - Al - O(2)	108.0(3)

SHG properties

Powder SHG measurements

NaAlO₂ is an extremely hygroscopic material; hence the results from the complete Kurtz-Perry powder SHG measurement were not reliable and are being repeated by mounting the powders in epoxy. As time went by on the measurements, the SHG signal decreased tremendously for all samples. However, initially the samples showed SHG intensity comparable to twice that of α - quartz.

Calculation of d_{ijk}

Because NaAlO₂ crystallizes in a noncentrosymmetric structure, a second-harmonic signal is observed when a sample is placed in the path of a high-intensity laser beam. This signal can be correlated to the nonlinear susceptibility coefficients d_{ijk} , which can be approximated on the basis of an oriented-gas model (12, 13). In this model, the nonlinearity is associated primarily with the relative orientations of the individual NaO₄ and AlO₄ groups.

The method has been applied with considerable success to a wide range of borates containing exclusively BO₃ groups (13), but it has only recently been successfully extended to the analysis of complex polyborates containing both BO₃ and BO₄ groups (14). By using equation (5.1),

$$d_{ijk} = \frac{1}{V} \sum_1^N \sum_{lmn} R_{il} R_{jm} R_{kn} \beta_{lmn} \quad (5.1)$$

the components of the hyperpolarizability tensor components (β_{lmn}) are summed according to the directional cosines or orientation functions (R) of the individual groups and weighted by their number densities ($1/V$). For polyborates, hyperpolarizabilities have generally been derived on the basis of various quantum-mechanical methods by using molecular fragments of three-dimensional structures. (13, 14). These results have to date provided rather poor agreement with experimental results. We note, however, that first-principle calculations including translational symmetry have recently provided an effective means for calculation of both linear and nonlinear optical properties of the compound β -BaB₂O₄ (15). To provide an effective and simple predictive tool for estimating nonlinearities, we have employed equation 5.1 to derive simple functional forms of β for different types of groups (14) and to assign a self-consistent set of β values to these groups on the basis of reported d coefficients (14).

The magnitude of d_{ijk} for NaAlO₂ from equation 5.1 depends significantly on the relative orientations of the NaO₄ and AlO₄ tetrahedra as given by the direction cosines R . In a *hypothetical* NaAlO₂ structure, containing fully aligned tetrahedra and a collinear arrangement of Na-O and Al-O bonds, each tetrahedron would make a unit contribution to d through R and a maximum nonlinearity would ensue. As shown in Figure 5.1, however, the NaO₄ and AlO₄ tetrahedra are tilted one relative to the other, producing a misalignment of the Na-O and Al-O

bonds and their associated tetrahedra. The angular misalignment can be deduced by using equations 5.2 – 5.4:

$$\mathbf{N} \cdot \mathbf{A} \equiv x_N * x_A + y_N * y_A + z_N * z_A \quad (5.2)$$

$$\mathbf{N} \cdot \mathbf{A} = NA \cos \theta \quad (5.3)$$

$$\theta = \cos^{-1} \frac{\mathbf{N} \cdot \mathbf{A}}{NA} \quad (5.4)$$

where \mathbf{N} and \mathbf{A} are the vectors describing the selected Na-O and Al-O bonds, respectively; x , y , z are the Cartesian coordinates of the O atoms of the selected Na-O and Al-O bonds relative to a common origin; N and A are the bond lengths of the selected bonds; and θ is the resulting alignment angle. For NaAlO₂, there are three unique angles (between two corner sharing NaO₄ tetrahedra, between two corner sharing AlO₄ tetrahedra, and between a corner sharing NaO₄ tetrahedron and an AlO₄ tetrahedron). Between the two alumina tetrahedra, this angle is $\theta = 23.1^\circ$; between Al(1) and Na(1) $\theta = 23.8^\circ$ (Figure 5.4); and between Al(1) and Na(2) $\theta = 12.7^\circ$. Refer to Figure 5.1 for atom labels.

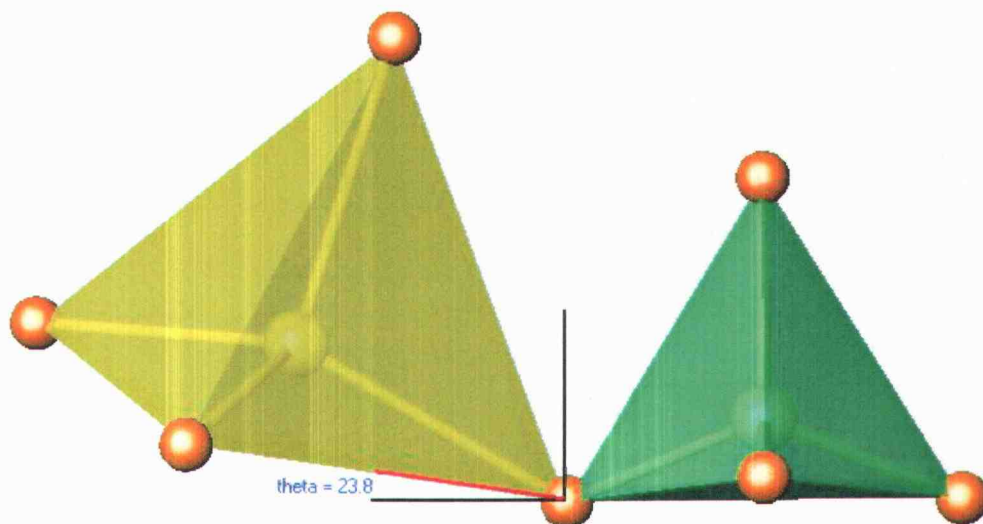


Figure 5.4. Illustration of tetrahedra orientation in NaAlO_2 .

In NaAlO_2 (point group $\text{mm}2$), the relevant second-order coefficients are d_{31} , $\chi(3,1,1)$, and d_{32} , $\chi(3,2,2)$. These coefficients correlate directly to the hyperpolarizability coefficients, $\beta_{3,1,1}$, and $\beta_{3,2,2}$ for an isolated tetrahedral group. As seen from Figure 5.5, rotation of a tetrahedral group by 90° about one of the Cartesian axes produces an orientation that is centrosymmetrically related to the original. In this case, the sum of the β values for the two orientations must equal zero, so $\beta(l,m,n) = -\beta'(l,m,n)$. As a result, $\beta(l,m,n)$ follows a $\cos 2\theta$ functional dependence. In NaAlO_2 , the three misalignment angles of 23.1° , 23.8° , and 12.7° between the $\text{Al}(1)\text{O}_4$ tetrahedra and the $\text{Al}(2)\text{O}_4$, $\text{Na}(1)\text{O}_4$, and $\text{Na}(2)\text{O}_4$ tetrahedra respectively, correspond to Cartesian-axis rotations, so the structural contribution to the nonlinear coefficient is

$$\frac{\beta_{Al1} + \beta_{Al1-Al2}(\cos 2(23.1)) + \beta_{Al1-Na1}(\cos 2(23.8)) + \beta_{Al1-Na2}(\cos 2(12.7))}{4} = 0.817$$

i.e., the orientation of the tetrahedra is 81.7% of optimum.

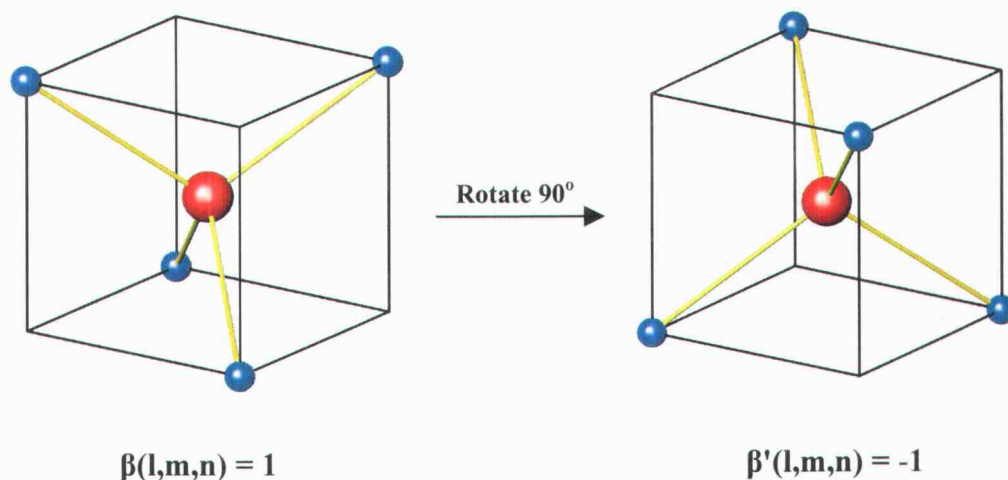


Figure 5.5. Rotation of a tetrahedral group by 90° about one of the Cartesian axes produces an orientation that is centrosymmetrically related to the original resulting in the sum of the β values for the two orientations equaling zero, or $\beta(l,m,n) = -\beta'(l,m,n)$.

We predict no phase-matching for NaAlO_2 , this would be consistent with the relatively small refractive indexes associated with wide band-gap materials of this type and the absence of any anisotropic structural element such as a trigonal planar group, which could produce a significant birefringence.

Acknowledgement

The authors wish to thank the US National Science Foundation for funding.

References

- (1) Kaduk, James A., Pei, Shiyou. "The Crystal Structure of Hydrated Sodium Aluminate, $\text{NaAlO}_2 \cdot \frac{1}{4}\text{H}_2\text{O}$, and Its Dehydration Product" *Journal of Solid State Chemistry* 115, 126-139 (1995).
- (2) Reid, A. F.; Ringwood, A. E. *Inorganic Chemistry* 7 443-5 (1968).
- (3) Smirnov, N.B.; Burmakin, E. I.; Shekhtman, G. Sh.; Stepanov, A. P. *Russ. J. Electrochem.* 36 408-412 (2000).
- (4) Kurtz, S. K., and Perry, T. T. "A Powder Technique for the Evaluation of Nonlinear Optical Materials." *Journal of Applied Physics* 39 8 3798-3813 (1968).
- (5) teXsan for Windows: Crystal Structure Analysis Package, Molecular Structure Corporation (1997).
- (6) DIRDIF94: Beurskens, P.T., Admiraal, G., Beurskens, G., Bosman, W.P., de Gelder, R., Israel, R. and Smits, J.M.M.(1994). The DIRDIF-94 program system, Technical Report of the Crystallography Laboratory, University of Nijmegen, The Netherlands.
- (7) Least Squares function minimized:

$$\Sigma w(|F_o| - |F_c|)^2$$
 where

$$w = 1/[\sigma^2(F_o)] = [\sigma_c^2(F_o) + p^2 F_o^2/4]^{-1}$$

$$\sigma_c(F_o) = \text{e.s.d. based on counting statistics}$$

$$p = \text{p-factor}$$
 Standard deviation of an observation of unit weight:

$$[\Sigma w(|F_o| - |F_c|)^2 / (N_o - N_v)]^{1/2}$$
 where N_o = number of observations
 N_v = number of variables
- (8) Cromer, D. T. & Waber, J. T.; "International Tables for X-ray Crystallography", Vol. IV, The Kynoch Press, Birmingham, England, Table 2.2 A (1974).
- (9) Creagh, D. C. & McAuley, W.J. ; "International Tables for Crystallography", Vol C, (A.J.C. Wilson, ed.), Kluwer Academic Publishers, Boston, Table 4.2.6.8, pages 219-222 (1992).
- (10) Creagh, D. C. & Hubbell, J.H.; "International Tables for Crystallography", Vol C, (A.J.C. Wilson, ed.), Kluwer Academic Publishers, Boston, Table 4.2.4.3, pages 200-206 (1992).

- (11) Shannon, R. D. "Revised Effective Ionic Radii and systematic Studies of Interatomic Distances in Halides and Chalcogenides." *Acta Cryst. A* 32 5 751-767 (1976).
- (12) Kathleen I. Schaffers, Ph.D. dissertation, Oregon State University, 1992.
- (13) C.T. Chen, *Development of new nonlinear optical crystals in the borate series*, Harwood Academic Publishers, Langhorne, PA, 1993.
- (14) Keszler, D.A. "NLO materials for deep UV generation," American Conference on Crystal Growth and Epitaxy, Vail, CO, USA, August 2000; D.A. Keszler, "New materials for high-power laser systems," National Meeting of the Materials Research Society, Boston, MA, USA, December 2000.
- (15) Lin, M.-H. Lee, Z.-P. Liu, C. Chen, C. J. Pickard, "Mechanism for linear and nonlinear optical effects in β -BaB₂O₄ crystals," *Phys. Rev. B: Condens. Matter Mater. Phys.* **60**, pp. 13380-13389, 1999; Z. Lin, J. Lin, Z. Wang, C. Chen, M.-H. Lee, "Mechanism for linear and nonlinear optical effects in LiB₃O₅, CsB₃O₅, and CsLiB₆O₁₀ crystals," *Phys. Rev. B: Condens. Matter Mater. Phys.* **62**, 1757-1764, 2000.

CHAPTER 6

TOURMALINE: STRUCTURE, COMPOSITION, AND OPTICAL
SECOND-HARMONIC GENERATION

Jennifer L. Stone-Sundberg, Jeffrey Barber, Joseph W. Nibler, Erwin Schutfort,
and Douglas A. Keszler

To be submitted to the Journal of Solid State Chemistry (2001).

Abstract

The mineral tourmaline, long recognized as a piezoelectric and pyroelectric material, crystallizes in a noncentrosymmetric space group and is studied as a nonlinear optical (NLO) material in this paper. A nearly colorless tourmaline crystal of African origin has been structurally and chemically characterized and studied as a new nonlinear optical material. The composition has been examined by means of electron-microprobe methods, ICP, and X-ray structure refinement. Type I phase-matched, second-harmonic generation from a 1064 nm input beam has been observed, and data on the phase-matching angle, nonlinear susceptibility, and damage threshold of this acid insoluble material are presented.

Introduction

The complex cyclosilicate tourmaline, $WX_3Y_6(BO_3)_3(Si_6O_{18})Z_4$, has a variable composition where the variable positions contain combinations of the elements: $W = Na, Ca, K$; $X = Mg, Al, Fe, Li, Mn$; $Y = Al, Fe, Cr, V$; and $Z = O, OH, F$. Tourmaline has long been known as a piezoelectric and pyroelectric material. These properties stem from the lack of a center of symmetry and the presence of a unique, polar axis in the crystal. In 1880, the brothers Pierre and Jacques Curie first noted and studied the piezoelectric effect in a variety of crystals including tourmaline and quartz (1). Tourmaline piezoelectric gauges made by cutting plates of the crystal normal to the polar c axis have been used by the United States to record blast pressures for every atomic explosion performed to date (2, 3).

The complex nature of the composition has resulted in an elusive absolute structure for tourmaline. The material is reported to crystallize in the noncentrosymmetric trigonal space group $R3m$ [#160] with a number of characteristic structural features. An illustration of the basic structure is given in Figure 6.1. Si_6O_{18} rings are present with some combination of the cations $Na, Ca, K, Mg, Sr, or B$ and anions $O, OH, or F$ alternating above and below the centers of the rings. Sheets of aligned BO_3 triangles lie between the layers of Si_6O_{18} rings. The distorted octahedral X site rests interior, and the distorted octahedral Y site rests exterior to the silicate rings, linking the borate groups and silicate rings (4-7).

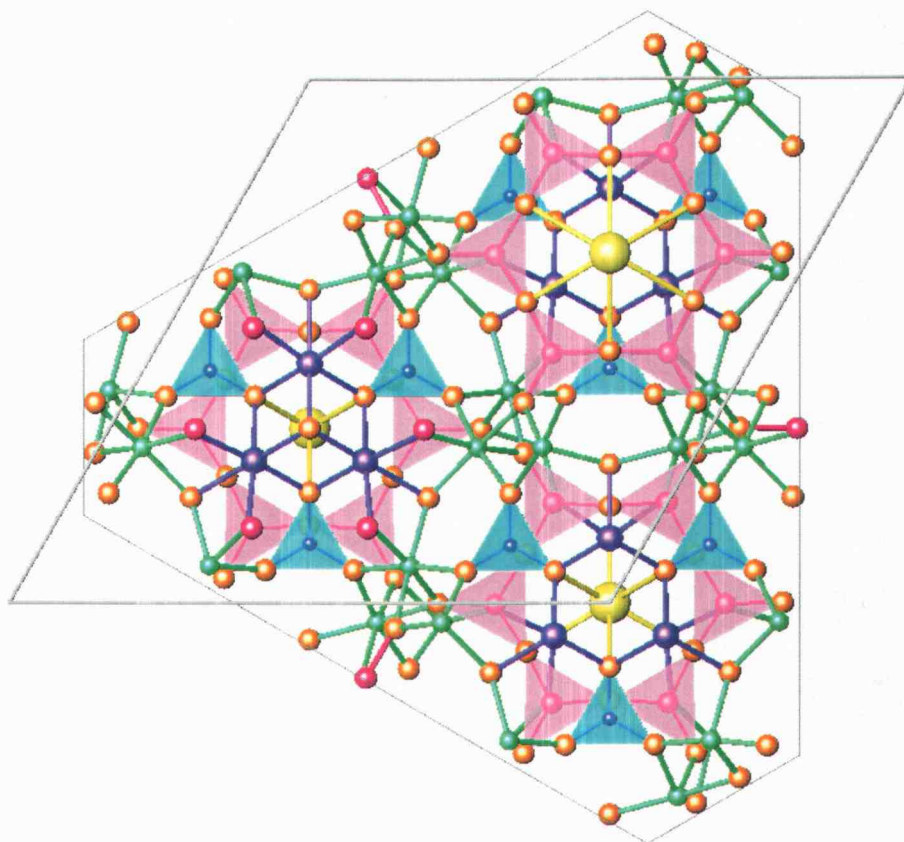


Figure 6.1. Tourmaline structure viewed down the c axis. The yellow spheres correspond to the cation(s) occupying site W, the violet spheres the cation(s) occupying site X, the green spheres the cations at site Y, the pink spheres Si, the blue spheres B, and the orange spheres O.

Our investigations of the frequency-doubling characteristics of noncentrosymmetric borates and related oxides has included materials containing both triangular and tetrahedral oxoanions. The influence of these groups on the second-harmonic generation (SHG) conversion efficiency is recognized. Many factors affect the role of these groups in this process, including their packing

density and relative orientation within a given material and the identity of the central atom, which contributes to the hyperpolarizability of the group. We have been prompted to examine tourmaline because it has an ideal structural arrangement of both the trigonal planar BO_3 groups and the tetrahedral SiO_4 groups for efficient SHG.

The lack of development of high-quality synthetic crystals and widespread use of this material compared to the piezoelectric mineral quartz are three-fold: quartz is a better radio frequency oscillator; quartz is much more naturally abundant and therefore historically a cheaper and more readily available material; and finally the complex composition of tourmaline versus quartz indicates a much more complicated synthetic crystal growth, in fact no high quality tourmaline crystals of any appreciable size have been grown to date to the knowledge of the authors (3, 8-16). However, large crystals are available in nature, although clear, nearly colorless examples are rare. The crystals utilized in this work were represented as African in origin and were purchased from Thaigems.com. One of the crystals has been structurally characterized via X-ray diffraction methods and was found to form in the normal tourmaline arrangement. The nonlinear optical properties of this same crystal has been examined, and numerous techniques have been applied to determine the chemical composition.

Experimental

X-Ray analysis

Unit cell and intensity data collection

A small block of approximate dimensions 0.2 x 0.2 x 0.2 mm was fractured from a larger 2 x 1 x 1 cm hexagonal columnar crystal and mounted on a glass fiber with epoxy. All measurements were made on a Rigaku AFC6R diffractometer with graphite monochromated Mo-K α radiation from a rotating-anode generator. Cell constants and an orientation matrix for data collection were obtained from a least-squares refinement of 23 centered reflections in the 2θ range 26.94-34.88°. The cell was determined to be trigonal (Laue group $-3m$) with dimensions $a = 15.817(3)$, $c = 7.101(4)$ Å, and $V = 1538.6(5)$ Å³. Intensity data were collected over the range of indices -27 to +27 in h , 0 to +27 in k , and -12 to +12 in l by using the ω - 2θ scan technique to a maximum 2θ value of 75°. Of the 5591 reflections collected, 990 were unique and 969 had an $F_o^2 \geq 3\sigma(F_o^2)$. The intensity of three standard reflections measured after every 500 reflections varied by an average of 1.2% during the collection.

Refinement

The structure was solved by using programs from the TEXSAN crystallographic software package (17). On the basis of the systematic condition

hkil: $-h+k+l = 3n$, packing considerations, a statistical analysis of the intensity distribution, and a successful solution and refinement of the structure, the space group was determined to be R3m [#160]. The structure was solved by using direct methods (18) and expanded by using Fourier techniques (19). Isotropic displacement coefficients were included on each atom in the refinement, and a correction for secondary extinction was applied (coefficient = 2.23×10^{-5}). The final cycle of full-matrix least-squares refinement (20) of the current model was based on 969 observed reflections ($I > 3.00\sigma(I)$) and 44 variable parameters. These variables included the occupancy factors for the Ca(X) site and the Al(Y) site. This refinement solution produced agreement factors of $R = 0.049$ and $R_w = 0.060$. The maximum and minimum peaks in the final electron-density map corresponded to 2.83 and 1.83% of the Si atom, respectively. Neutral atom scattering factors were taken from Cromer and Waber (21). Anomalous dispersion effects were included in F_{calc} (22); and the values for Δf and $\Delta f'$ were those of Creagh and McAuley (23). The values for the mass attenuation coefficients are those of Creagh and Hubbell (24). Crystal data are outlined in Table 6.1, and atomic parameters are listed in Table 6.2.

Table 6.1. Crystallographic data for tourmaline crystal.

Formula	$(\text{Ca}_{0.47}\text{Na}_{0.53})(\text{Li}_{1.65}\text{Al}_{1.35})\text{Al}_6(\text{BO}_3)_3(\text{Si}_6\text{O}_{18})(\text{OH})_4$
Formula Weight, amu	941.75
Crystal System	Trigonal (hexagonal setting)
Space Group	R3m [#160]
a , Å	15.817(3)
c , Å	7.101(4)
V , Å ³	1538.6(5)
Z	3
D_{calc} , g cm ⁻³	3.05
F(000)	1401
Diffractometer	Rigaku AFC6R
Radiation	Mo K α ($\lambda=0.71069$) graphite-monochromated
Data Collection	$\pm h, k, \pm l$
No. Observations. total, unique	5591, 990
$(F_o^2 \geq 3\sigma(F_o^2))$	969
R	0.049
R_w	0.060
Maximum Shift in Final Cycle	19.63
GOF	6.34

$$R = \frac{\sum ||F_o| - |F_c||}{\sum |F_o|} = 0.049$$

$$R_w = \left[\frac{\sum w (|F_o| - |F_c|)^2}{\sum w F_o^2} \right]^{1/2} = 0.060$$

Table 6.2. Positional and isotropic displacement coefficients (B_{eq}).

Atom	Wyckoff	x	y	z	B_{eq}^a
Ca ^b	3a	0	0	0.1202(3)	1.34(4)
Si	18c	0.00197(5)	0.19208(5)	0.3578	0.36(1)
Al(1) ^c	9b	0.06196(8)	-0.0620	-0.2785(3)	0.61(5)
Al(2)	18c	0.03703(6)	0.29676(6)	0.7464	0.45(2)
O(1)	3a	0	0	-0.4271(8)	2.7(1)
O(2)	9b	0.1990	0.595	-0.1239(3)	1.21(4)
O(3)	9b	0.1845	0.0922	0.2833(3)	0.68(3)
O(4)	9b	0.13395(8)	0.2679	0.8497(3)	0.77(3)
O(5)	9b	0.09265(8)	-0.0926	0.2619(3)	0.59(3)
O(6)	18c	-0.0611(1)	0.2090(1)	0.9164	0.53(2)
O(7)	18c	-0.0001(1)	0.2859(1)	0.2780	0.48(2)
O(8)	18c	0.0100(1)	0.1954(1)	0.5822	0.62(2)
B(1)	9b	-0.1089(1)	0.1089	-0.0989(4)	0.34(3)

$$^a B_{eq} = (8\pi/3)^2 \sum_i \sum_j U_{ij} a_i^* a_j^* a_i a_j$$

$$^b \text{occupancy} = 0.76$$

$$^c \text{occupancy} = 0.58$$

Elemental analyses

Electron microprobe

An electron microprobe analysis (CAMECA SX-50 electron microprobe) was performed on a sample from the same tourmaline crystal that was structurally characterized. Six sets of qualitative and quantitative elemental analyses were collected and averaged using standards. A summary of that data is given in Table 6.3.

Table 6.3. Electron-microprobe analysis of studied tourmaline crystal.

Oxide or element	Average weight %	Cations per formula unit*
CaO	2.70(3)	0.44(0)
Na ₂ O	1.02(2)	0.30(1)
Al ₂ O ₃	38.53(25)	6.92(3)
SiO ₂	37.24(22)	5.68(1)
MnO	0.17(1)	0.02(0)
MgO	trace	trace
K ₂ O	trace	trace
TiO ₂	trace	trace
F	1.45(6)	0.70(3)

Inductively coupled plasma spectroscopy (ICP)

We wished to verify the presence of Li in our studied tourmaline crystal and to come up with another independent analytical technique to verify the ratio of various cations. A Liberty 100 ICP Emission Spectrometer was used to

perform an analysis on 15.52 mg of a sample that was ground, fused in K_2CO_3 , and subsequently dissolved in a 2% nitric acid solution. A tabulation of the data is presented in Table 6.4.

Table 6.4. ICP data for studied tourmaline crystal.

Element	Concentration (ppm)	Weight%	# Cations per formula unit assuming full occupancy of W site
Ca	1.115	1.80	0.416
Na	0.449	1.45	0.584
Al	5.983	19.30	6.617
Li	0.295	0.90	1.200
Fe	0.101	0.33	0.055
Mn	0.067	0.22	0.037
Mg	0.012	0.00	0

FTIR study to determine the presence of OH

A Nicolet 5PC FTIR was used to collect an absorption spectrum from 500 to 4000 cm^{-1} of a polished 2.5 cm thick plate of the tourmaline crystal. A broad, strong absorption corresponding to the presence of OH was observed centered at 3550 cm^{-1} . A plot of the percent transmittance as a function of wavenumber is presented in Figure 6.2.

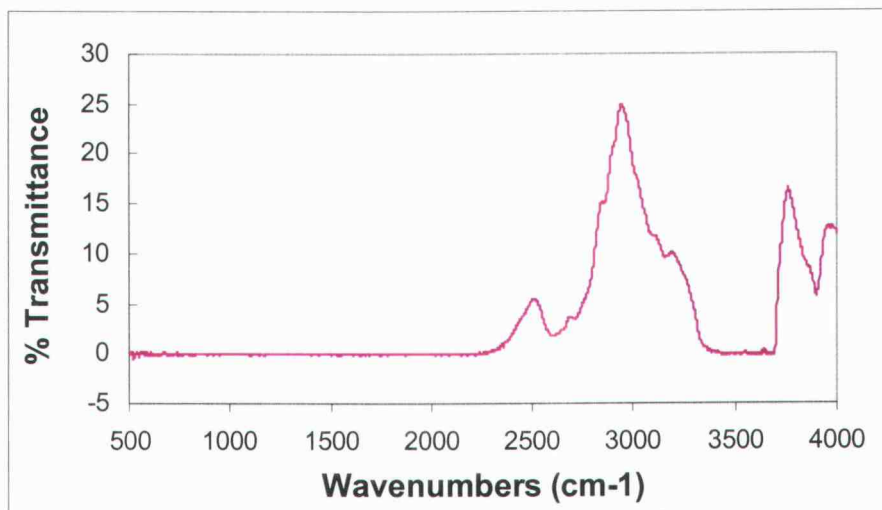


Figure 6.2. FTIR of tourmaline crystal

SHG characterization

The structurally and compositionally characterized tourmaline crystal was optically characterized in our ongoing survey of SHG borate materials. Parameters determined include the phase-matching angle, type of phase-matching, the SHG conversion efficiency relative to KDP, and the surface-damage threshold. All of these measurements were performed by using a Nd:YAG flashlamp pumped laser operating at 1064 nm (Cooper MY series laser), and power meters (molelectron).

Determination of the phase-matching angle

This measurement is made by cutting and polishing parallel faces perpendicular to the optic axis of the crystal, placing the crystal on a calibrated rotating plate in the path of a laser beam of frequency ω with the beam traveling down the optic axis, rotating the crystal 360° about the optic axis, and recording the four angles at which bright spots of produced light of frequency 2ω are seen. The angular difference between 0° and spots 3 and 4 and the angular difference between 180° and spots 2 and 3 will give four values for the phase-matching angle.

Determination of types of phase-matching

This determination is made by placing the phase-matched crystal in the laser beam, determining the polarization direction of the fundamental and SHG frequencies, and seeing if the input light has one polarization orthogonal to the SHG (Type I) or if the input light has two orthogonal polarizations one matching that of the SHG (Type II).

Determination of conversion efficiency (d_{eff})

The experimental method of Kurtz and Perry (25) was used to measure powder SHG signals with a 1064-nm laser. The sample was ground and sieved by using a stack of mesh sizes 25, 45, 53, 63, 75, 106, 125, 150, 212, and 250 μm . Samples of KH_2PO_4 (KDP), $\beta\text{-BaB}_2\text{O}_4$ (BBO), and $\alpha\text{-quartz}$ were prepared as reference materials in an identical fashion. The samples were pressed between

glass microscope cover slides and secured with tape in 1-mm thick aluminum holders containing a 5-mm diameter hole. The samples were then placed in a light-tight box and excited with 20-mJ, 1064-nm pulses from a Q-switched New Wave Research Minilase-20 Nd:YAG laser. A cutoff filter was used to limit background flash-lamp light on the sample, and an interference filter (530 ± 10 nm) was used to select the second harmonic prior to detection with a photomultiplier tube attached to a Tektronix SC 504 80-MHz oscilloscope. Samples of Al_2O_3 (Stanford Materials, 99.999%) and α quartz were used to monitor and calibrate the instrumental setup. .

Determination of surface-damage threshold

The surface-damage threshold was measured by placing the phase-matched crystal in the beam at the phase-matched angle and monitoring both the incident 1064 nm radiation and the produced 532 nm radiation. The power per area of the incident radiation was slowly increased and when the intensity of the produced radiation suddenly dropped, that value of power per area was taken as the surface-damage threshold intensity. The pulsewidth in ns is also reported.

Results and Discussion

Structure and elemental composition

The structure adopts a normal tourmaline arrangement. Interatomic distances and angles (4-7) are summarized in Table 6.6. From crystal radii (26), the various interatomic distances were calculated to be: Ca-O 2.54 Å; Na-O 2.60 Å; Al-O 1.895 Å; Li-O 2.12 Å; Si-O 1.62 Å; and B-O 1.37 Å. This structure refinement resulted in distances Ca-O of 2.384(2) Å; Al(1)-O of 1.996(2), 1.998(2), 2.174(1), and 1.961 Å; Al(2)-O of 1.951(2), 1.907(2), 1.889(2), 1.887(2), 1.949(2), and 1.850(2) Å; Si-O of 1.6234(8), 1.634(1), and 1.605(2) Å; and B-O of 1.366(2) and 1.375(1) Å. The SiO₄ tetrahedral angles range from 102.32(6) to 111.93(8)^o; the AlO₆ octahedral angles range from 76.04 to 108.32^o and 170.52 to 175.59^o; and the BO₃ trigonal planar angles are 116.6(2) and 121.70(7)^o.

Table 6.5. Interatomic distances (Å) and angles (°) for tourmaline.

Ca -	O(2) (x 3)	2.384(2)	O(2) - Ca - O(2)	72.62(8)
			O(2) - Ca - O(3)	71.35(6)
				127.85(3)
			O(2) - Ca - O(5)	87.09(4)
				154.63(8)
	O(3) (x 3)	2.777(1)	O(3) - Ca - O(3)	104.02(6)
			O(3) - Ca - O(5)	54.88(2)
				134.01(8)
	O(5) (x 3)	2.728(1)	O(5) - Ca - O(5)	107.37(5)
Si -	O(3)	1.6234(8)	O(3) - Si - O(5)	102.32(6)
			O(3) - Si - O(7)	110.58(7)
			O(3) - Si - O(8)	111.93(8)
	O(5)	1.634(1)	O(5) - Si - O(7)	109.87(8)
			O(5) - Si - O(8)	111.0(1)
	O(7)	1.605(2)	O(7) - Si - O(8)	110.82(9)
	O(8)	1.602(2)		

Table 6.5. (cont.)

Al(1) - O(1)	1.996(2)	O(1) - Al(1) - O(2)	85.1(1)
		O(1) - Al(1) - O(4)	173.2(2)
		O(1) - Al(1) - O(8)	99.3(1)
O(2) (x 2)	1.998(2)	O(2) - Al(1) - O(2)	89.91(9)
		O(2) - Al(1) - O(4)	99.65(8)
		O(2) - Al(1) - O(8)	89.87(6)
			175.59(9)
O(4)	2.174(1)	O(4) - Al(1) - O(8)	76.04(7)
O(8) (x 2)	1.961(2)	O(8) - Al(1) - O(8)	90.0(1)
Al(2) - O(4)	1.951(2)	O(4) - Al(2) - O(6)	92.23(8)
			95.35(6)
		O(4) - Al(2) - O(7)	94.55(7)
			171.66(8)
		O(4) - Al(2) - O(8)	84.34(8)
O(6)	1.907(2)	O(6) - Al(2) - O(6)	170.52(7)

Table 6.5. (cont.)

			O(6) - Al(2) - O(7)	78.02(8)
				95.77(8)
				95.68(8)
				76.94(7)
			O(6) - Al(2) - O(8)	91.00(7)
				95.40(8)
		1.889(2)		
	O(7)	1.887(2)	O(7) - Al(2) - O(7)	89.45(4)
			O(7) - Al(2) - O(8)	108.32(7)
				93.13(8)
		1.949(2)		
	O(8)	1.850(2)		
B -	O(2)	1.366(2)	O(2) - B(1) - O(6)	121.70(7)
	O(6)	1.375(1)	O(6) - B(1) - O(6)	116.6(2)

Determining the absolute stoichiometry of a particular tourmaline crystal is challenging due to the wide range of elements, limitations of the analytical techniques in detecting certain types of elements, and debates in the literature on the treatment of occupancies for many of the sites. In the present study, we have employed a greater variety of methods than has been previously utilized for the analysis of the tourmaline problem.

From electron-microprobe analysis, the following charge-balanced stoichiometry can be derived.



This formula was determined assuming full occupancy of the B site and charge balancing with O and H. It should be noted that the microprobe is blind to the Li and B atoms, and determination of O and F concentrations is rather precarious. Hence, the formula was established using ratios of the heavy elements from microprobe data and simultaneously assuming full occupancy of the B site. Charge balance is achieved by adding an appropriate quantity of O and H. It is quite common for electron-microprobe analyses to reveal a Si deficiency in tourmalines (4,5,27-29). Traditionally, the mineralogical community has compensated this Si deficiency through substitution of B on the Si site. From a crystal-chemical viewpoint, such a substitution is highly improbable. It certainly is not favored by the dissimilar crystal radii (26) of the B ($r = 0.25 \text{ \AA}$) and Si ($r = 0.40 \text{ \AA}$) atoms. Indeed, we are aware of no synthetic crystal containing such a disorder. For example, in borosilicate glasses, the borate and silicate extended matrices are intertwined, but chemically separated. In any event, the Si

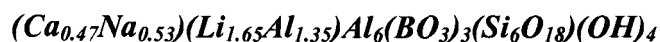
deficiency appears to be an artifact of the microprobe analysis, as the ICP and X-ray measurements (*vide infra*) do not reveal a deficiency.

On the basis of the ICP data the following stoichiometry can be derived.



In the ICP analysis, the concentrations of each of the elements except H, O, and F are directly determined. The formula is deduced by assuming complete occupation of the W, B, and Si sites and then charge compensating with appropriate numbers of O and H atoms.

The single-crystal refinement of included refining the occupancies of the Ca site and Al(1) site, producing values of 0.127 and 0.289 respectively. After elemental analyses were obtained, it was determined that the Ca site is shared with Na and the Al(1) site is shared with Li. Calculations were made based on this elemental information and the refined values to produce the following charge-balanced stoichiometry.



In the X-ray analysis, the primary compositional uncertainties are associated with the X and Z sites. From refinement of occupancies, effective average atomic numbers of the elements in these sites can be deduced. The Ca:Na ratio in the W site agrees quite well with the ICP analysis. There remains considerable uncertainty in the occupation of the X site as the formulation deduced in the occupation of the X site from the ICP analysis does not sufficiently account for the electron density in the X-ray study. FTIR was performed on the crystal to verify the presence of H to justify using it to charge balance the formulas. To

more fully describe the stoichiometry of this particular tourmaline, additional absolute ratios of the elements Ca, Na, Al, Li, Si, B, F, Mn, and Fe will be determined. An additional ICP measurement is being done with an improved Li standard to establish a better Li/Al ratio. To garner additional information, qualitative/quantitative elemental analysis is currently underway by using instrumental neutron activation analysis (INAA).

Optical characterization

The high orientation of the BO_3 groups with respect to each other and the SiO_4 groups with respect to each other indicated to us that tourmaline has potential as a reasonable frequency-doubling material with a sufficient second-order NLO susceptibility. The approximately planar layers of BO_3 groups should yield a birefringence large enough to allow phase-matching. The organization of the silica tetrahedra and borate triangles can be seen in Figures 6.3 and 6.4.

Determination of the phase-matching angle

The bulk of the hexagonal crystal described previously was polished along the (0001) and (000-1) faces and six faces perpendicular to the {0001} faces. The crystal was mounted on a calibrated rotating plate. This mount was placed on a laser table with the (0001) crystal face centered and perpendicular to the 1064 nm laser beam. The crystal was rotated in the laser beam 360° in a direction around the optic axis with 0 and 360° lying along the z axis and 90 and 180° lying

orthogonal to the z axis. Four bright spots of SHG intensity (corresponding to phase-matching) were observed. The phase-matching occurred at centered angles of rotation of 74.56, 106.31, 252.91, and 286.23°. This corresponds to an average phase-matching angle of $\theta_{\text{pm}} = 73.7(4)^\circ$.

Determination of types of phase-matching

Tourmaline, which crystallizes in the trigonal space group R3m, belongs to the point group 3m and therefore is a uniaxial crystal. Since tourmaline's ordinary refractive index is greater than its extraordinary refractive index at a given wavelength, it is a negative uniaxial crystal. This limits the types of phase-matching possible to Type I (ooe) and Type II (oee or eoe). Rotation about an identified θ_{pm} direction \mathbf{k} will reveal which type of phase-matching is occurring: Rotation about a Type I \mathbf{k} will result in two maxima separated by 180° whereas rotation about a Type II \mathbf{k} will result in four maxima separated by 90°. Monitoring the polarization of light entering the crystal versus the polarization of light produced by the crystal will also give you the same information. If the input light and SHG light give a maximum when the polarizations are orthogonal, the phase matching is Type I. If no SHG light is produced when the input light is polarized perpendicular to the produced light, yet an SHG light maximum is observed when the input and SHG polarizations are at a 45° angle to each other, the phase-matching is Type II. This experiment was tested on a KDP crystal then our tourmaline crystal. Type II phase-matching was clearly observed for the KDP crystal at an angle of 58.7° by monitoring the polarizations of the input and SHG

lights. The tourmaline crystal distinctly showed orthogonal polarizations of input and produced SHG light, a clear indication of Type I phase-matching.

Determination of conversion efficiency (d_{eff})

The intensity of SHG of tourmaline was found to be 0.34 times that of KDP. Using equation 6.1, the d_{eff} of tourmaline was calculated to be 0.58 times KDP.

$$\frac{I^{2\omega}(tour)}{I^{2\omega}(KDP)} = \frac{\langle d_{ijk}^{2\omega}(tour) \rangle^2}{\langle d_{ijk}^{2\omega}(KDP) \rangle^2} \quad (6.1)$$

Determination of surface-damage threshold

The intensity of the produced SHG dropped suddenly at an energy of 19(1) J/cm² and a pulse-width (τ_p) of 10 ns – a value that falls between those of KDP at 10 J/cm² and CLBO at 25 J/cm², both for 10 ns pulsewidths..

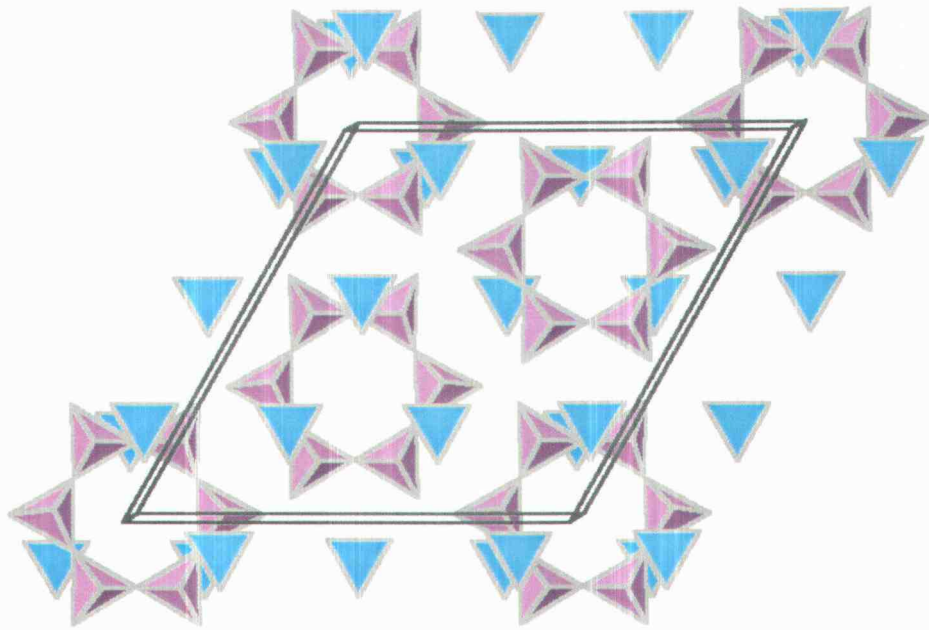


Figure 6.3. View down the optic axis of tourmaline viewing only the SiO_4 tetrahedra (purple) and BO_3 triangles (blue).

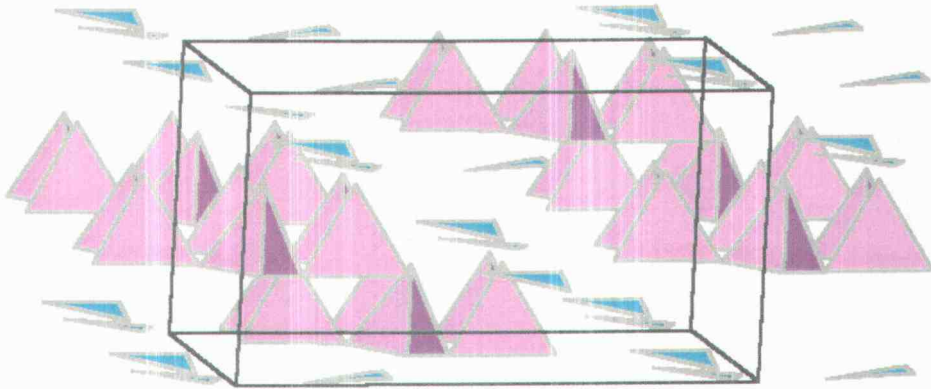


Figure 6.4. View orthogonal to the optic axis of tourmaline.

Summary

The negative uniaxial tourmaline crystal studied demonstrated suitable properties for producing 532 nm light via SHG conversion. This acid-insoluble material with a hardness of 7.5 on the Moh's scale was determined to have at a fundamental wavelength of 1064 nm Type I phase-matching at a θ_{pm} of $73.7(4)^\circ$ with a d_{eff} of approximately 0.58 times d_{eff} KDP and a surface-damage threshold of $19(1) \text{ J/cm}^2$ for 10 ns pulses.

Acknowledgements

The authors wish to thank NSF for funding and Professor Roger Neilson of the Department of Geosciences at Oregon State University for the electron microprobe analysis. Jennifer Stone Sundberg would like to thank ICDD for the Ludo Frevel Crystallography Scholarship, 2001.

References

- (1) Piezo Systems, Inc. "History of Piezoelectricity." <http://www.piezo.com/history.html> (2001).
- (2) Klein, Cornelis; Hurlbut, Cornelius S. "Manual of Mineralogy, 21st Edition." John Wiley & Sons, Inc. (1993).
- (3) Webster, Robert. "Gems: Their Sources, Descriptions, and Identification, 5th Edition." Butterworth Heinemann (1994).
- (4) Foit, Franklin F., Jr.; Rosenberg, Philip E. "The structure of vanadium-bearing tourmaline and its implications regarding tourmaline solid solutions." *American Mineralogist* 64 7-8 788-798 (1979).
- (5) Foit, Franklin F., Jr. "Crystal chemistry of alkali-deficient schorl and tourmaline structural relationships." *American Mineralogist* 74 (3-4) 422-431 (1989).
- (6) Pieczka, Adam. "Statistical interpretation of structural parameters of tourmalines. The ordering of ions in the octahedral sites." *Eur. J. Mineral.* 11 2 243-251 (1999).
- (7) Hawthorne, Frank C.; Henry, Darrell J. "Classification of the minerals of the tourmaline group." *Eur. J. Mineral.* 11 2 201-215 (1999).
- (8) Goerne, G. V., Franz, G., Heinrich, W. "Synthesis of tourmaline solid solutions in the system Na₂O-MgO-Al₂O₃-SiO₂-B₂O₃-H₂O-HCl and the distribution of Na between tourmaline and fluid at 300 to 700°C and 200 Mpa." *Contributions to Mineralogy and Petrology* 141 2 160-173 (2001).
- (9) Schreyer, Werner; Wodara, Ulrich; Marler, Bernd; VanAken, Peter A.; Seifert, Friedrich; Robert, Jean-Louis. "Synthetic tourmaline (olenite) with excess boron replacing silicon in the tetrahedral site: I. Synthesis conditions, chemical and spectroscopic evidence." *Eur. J. Mineral.* 12 3 529-541 (2000).
- (10) Mashkovtsev, R. I. "Optical absorption in synthetic tourmalines containing Mn, Fe, Ni, and Cu." *Geol. Geofiz.* 36 4 122-126 (1995).
- (11) Rosenberg, Philip E.; Foit, Franklin F., Jr.; Ekambaram, Vanavan. "Synthesis and characterization of tourmaline in the system Na₂O-Al₂O₃-SiO₂-B₂O₃-H₂O." *American Mineralogist* 71 7-8 971-976 (1986).

(12) Philip E. Rosenberg; and Foit, Franklin F., Jr.; "Tourmaline solid solutions in the system MgO-Al₂O₃-SiO₂-B₂O₃-H₂O." *American Mineralogist* 70 11-12 1217-1223 (1985).

(13) Kargaltsev, S. V. "Study of characteristics of growth of synthetic tourmaline crystals." Conference proceedings Fiz.-Khim. Issled. Sulfidnykh silik. Sist. Publisher Akad. Nauk, SSSR. 73-79 (1984).

(14) Suwa Seikosha Co., Ltd., Japan. "Growth of synthetic tourmaline single crystals." Japanese patent JP 59152286 A2 19840830. Jpn. Kokai tokkyo Koho (1984).

(15) Rosenberg, Philip E.; Foit, Franklin F.; "Synthesis and characterization of alkali-free tourmaline." *American Mineralogist* 64 1-2 180-186 (1979).

(16) Emelyanova, E. N., Zigareve, T. A. "Tourmaline growth in hydrothermal conditions." *Kristallografiya* 5 955-957 (1960).

(17) teXsan for Windows: Crystal Structure Analysis Package, Molecular Structure Corporation (1997).

(18) SIR92: Altomare, A., Cascarano, M., Giacovazzo, C., Guagliardi, A. (1993). *J. Appl. Cryst.*, 26, 343.

(19) DIRDIF94: Beurskens, P.T., Admiraal, G., Beurskens, G., Bosman, W.P., de Gelder, R., Israel, R. and Smits, J.M.M. (1994). The DIRDIF-94 program system, Technical Report of the Crystallography Laboratory, University of Nijmegen, The Netherlands.

(20) Least Squares function minimized:

$\sum w(|F_o| - |F_c|)^2$ where

$$w = 1/[\sigma^2(F_o)] = [\sigma^2 c(F_o) + \rho^2 F_o^2/4]^{-1}$$

$\sigma c(F_o)$ = e.s.d. based on counting statistics

ρ = p-factor

Standard deviation of an observation of unit weight:

$$[\sum w(|F_o| - |F_c|)^2 / (N_o - N_v)]^{1/2}$$

where N_o = number of observations

N_v = number of variables

(21) Cromer, D. T. & Waber, J. T.; "International Tables for X-ray Crystallography", Vol. IV, The Kynoch Press, Birmingham, England, Table 2.2 A (1974).

(22) Ibers, J. A. & Hamilton, W. C.; *Acta Crystallogr.*, 17, 781 (1964).

- (23) Creagh, D. C. & McAuley, W.J. ; "International Tables for Crystallography", Vol C, (A.J.C. Wilson, ed.), Kluwer Academic Publishers, Boston, Table 4.2.6.8, pages 219-222 (1992).
- (24) Creagh, D. C. & Hubbell, J.H.; "International Tables for Crystallography", Vol C, (A.J.C. Wilson, ed.), Kluwer Academic Publishers, Boston, Table 4.2.4.3, pages 200-206 (1992).
- (25) Kurtz, S. K., and Perry, T. T. "A Powder Technique for the Evaluation of Nonlinear Optical Materials." *Journal of Applied Physics* 39 8 3798-3813 (1968).
- (26) Shannon, R. D. "Revised effective ionic radii and systematic studies of interatomic distances in halides and chalcogenides." *Acta Crystallographica A* 32 5 751-767 (1976).
- (27) Foit, Franklin F., Jr.; Fuchs, Yves; Myers, Paul E. "Chemistry of alkali-deficient schorls from two tourmaline-dumortierite deposits." *American Mineralogist* 74 1317-1324 (1989).
- (28) MacDonald, Daniel J.; Hawthorne, Frank C. "The crystal chemistry of Si \leftrightarrow Al substitution in tourmaline." *The Canadian Mineralogist* 33 849-858 (1995).
- (29) Ertl, A.; Pertlik, F.; and Bernhardt, H.-J. "Investigations on olenite with excess boron from the Koralpe, Styria, Austria." *Anzeiger Abt. I* 134 3-10 (1995).

CHAPTER 7

NONLINEAR OPTICAL BORATE CRYSTAL $\text{Ba}_2\text{B}_{10}\text{O}_{17}$

Jennifer L. Stone, Douglas A. Keszler, Gérard Aka, Andrée Kahn-Harari,
Thomas A. Reynolds

Published in Proc. SPIE-Int. Soc. Opt. Eng. (2001).

Abstract

Single crystals of the noncentrosymmetric barium borate, $\text{Ba}_2\text{B}_{10}\text{O}_{17}$, have been grown by slowly cooling a stoichiometric melt. The material crystallizes in the triclinic space group P1 with cell parameters $a = 9.858(1)$, $b = 9.990(1)$, $c = 6.706(1)$ Å, $\alpha = 96.79(1)$, $\beta = 106.64(1)$, and $\gamma = 76.89(1)^\circ$. The structure is a new type characterized by a condensation of B_3O_8 rings and BO_3 triangles. A calculation of the second-order nonlinear susceptibility coefficients on the basis of the orientations of the tetrahedral and triangular borate groups in the rings and triangles has yielded a maximum coefficient of $d_{11} = 0.2$ pm/V. This result is consistent with the measured second-harmonic signal – 0.5*KDP. Partial solid solubility of Sr in the host – $\text{Ba}_{2-x}\text{Sr}_x\text{B}_{10}\text{O}_{17}$ ($0 < x \leq 0.25$) – has also been observed.

Introduction

With their superb high-energy transparencies, suitable nonlinearities and birefringence, low impurity contents (1), and consequent high optical-damage thresholds, polyborates find widespread application for optical frequency conversion of high-power, short-wavelength light. LiB_3O_5 (LBO,) (2) for example, is commonly employed in high-power applications for second-harmonic generation of 1- μm laser light. While the material is transparent to 170 nm, its birefringence is insufficient for efficient direct second-harmonic generation to UV wavelengths near 266 nm by angular phasematching. For this reason, BaB_2O_4 (BBO) (3) with its higher birefringence has been commonly employed for UV generation. More recently, improved performance in direct UV generation has been reported by using the borate crystals $\text{CsLiB}_6\text{O}_{10}$ (CLBO) (4) and $\text{Li}_2\text{B}_4\text{O}_7$ (L2BO) (5); these crystals exhibit optical damage thresholds (26 GW/cm^2 for CLBO and 40 GW/cm^2 for L2BO) that are more than three times greater than that of BBO. As a result, the average UV power from CLBO can be an order of magnitude greater than that of BBO. While CLBO has been commercialized, its hygroscopic nature and poor mechanical properties are hindering its widespread adoption. L2BO exhibits a modest nonlinearity ($d_{15} = 0.1 \text{ pm}/\text{V}$,) (6) but reasonable conversion efficiencies have been observed in UV generation (5).

The crystals CLBO and L2BO clearly demonstrate that enhanced UV laser performance can be achieved in polyborates relative to the more commonly employed material BBO. To circumvent the problems associated with CLBO and

L2BO, we have been investigating the crystal growth and optical properties of several new polyborate crystals. In this contribution, we describe some of the characteristics of the noncentrosymmetric compound $\text{Ba}_2\text{B}_{10}\text{O}_{17}$ (7).

Experimental

Powder samples of $\text{Ba}_{2-x}\text{Sr}_x\text{B}_{10}\text{O}_{17}$ ($0 \leq x \leq 0.75$) were prepared by heating pressed tablets of stoichiometric mixtures of BaCO_3 , SrCO_3 , and H_3BO_3 . The tablets were placed on Pt foil in covered alumina crucibles and heated at 973 K for 24 h, ground, repressed into tablets, and then heated at 1023 K for 62 hours. A Siemens D5000 powder diffractometer with $\text{Co K}\alpha$ radiation was used to determine the products of the reactions. Several glass pellets were formed by heating and melting a stoichiometric sample of $\text{Ba}_2\text{B}_{10}\text{O}_{17}$ in a Pt crucible at 1273 K for one hour; the resulting viscous liquid was poured directly into different wells of an iron mold at room temperature. The glass pellets were then annealed at selected temperatures and analyzed by differential thermal analysis (DTA) to determine the crystallization temperature.

DTA measurements were made on both powders and the glass samples with a computer-controlled Netzsch STA 409 instrument. The experiments were conducted with the sample and reference material ($\alpha\text{-Al}_2\text{O}_3$) contained in separate Pt crucibles with heating rates of 5 and 10 K/min.

For crystal growth, approximately 200 g of $\text{Ba}_2\text{B}_{10}\text{O}_{17}$ was melted at 1173 K. A Pt wire attached to an alumina rod was dipped into the melt. The temperature of the melt was adjusted to approximately 10 K above the melting point followed by cooling at a rate of $2 \frac{1}{2}$ K per day.

A single crystal of approximate dimensions 0.3mm x 0.2mm x 0.2mm was isolated and mounted on a glass fiber for structure determination on a Rigaku AFC6R X-ray diffractometer. Least squares refinement of 23 automatically

centered reflections in the range $27 \leq 2\theta \leq 32^\circ$ gave a triclinic unit cell of dimensions $a = 9.858(1)$, $b = 9.990(1)$, $c = 6.706(1)$ Å, $\alpha = 96.79(1)$, $\beta = 106.64(1)$, and $\gamma = 76.89(1)^\circ$. Intensity data were collected at room temperature by using the ω -scan technique with a rate = $16.0^\circ \omega \text{ min}^{-1}$. The structure was solved by using the computer program SHELXS⁸ and refined by using the TEXSAN software package.⁹ The structure refines to $R = 0.038$ with 2978 reflections having $I > 3\sigma(I)$. The largest peak in the final difference electron density map corresponds to 0.5% of a Ba atom.

The second-order nonlinearity of $\text{Ba}_2\text{B}_{10}\text{O}_{17}$ has been examined by using a 1064-nm fundamental beam. The sample was ground and sieved to produce particle sizes in the range of 44 to 200 μm . Samples of KDP and GdCOB for reference were prepared in an identical fashion. The samples were pressed between thin mica windows and secured with tape in 1-mm thick plastic holders containing a 5-mm diameter hole. The samples were then placed in a light-tight box and excited with 350-mJ, 1064-nm pulses from a Nd:YAG laser. The filtered 532-nm light was detected with a photomultiplier tube attached to an oscilloscope. A set of 50 pulses over five-second intervals were averaged for each voltage measurement and each sample; the measurements were done twice for each sample.

Results

As shown in Figure 7.1, the structure of $\text{Ba}_2\text{B}_{10}\text{O}_{17}$ is characterized by a unique polyborate framework that results from the condensation of B_3O_8 rings (Figure 11.2) and BO_3 triangles in a ratio of two to one, respectively. Because each of the terminal atoms in these groups is shared by two B atoms the observed stoichiometry is readily achieved by considering the whole-number equivalent of the connectivity formula $\text{B}_3\text{O}_3\text{O}_{5/2} + 2 (\text{BO}_{3/2}) \equiv \text{B}_{10}\text{O}_{17}$. The Ba atoms occupy 8- and 9-coordinate sites with distances ranging from 2.66(1) to 3.00(1) Å.

Powder samples of $\text{Ba}_2\text{B}_{10}\text{O}_{17}$ are readily prepared by standard heating procedures. Excellent agreement is observed between the experimental X-ray pattern and that calculated on the basis of the single-crystal analysis (Figure 7.3.) Peak positions are not altered after placing samples in H_2O at 373 K for five minutes, indicating the compound is not appreciably hygroscopic. The same powder pattern is observed after annealing the glass tablets at 973 K for 15 h.

On the basis of powder diffraction data (Figure 7.4,) only limited solubility of Sr in the material is observed. Because the Sr atom is smaller than the Ba atom, peaks are expected to shift to larger values of two theta as the unit-cell volume decreases. The only significant peak shifts that occur in the series $\text{Ba}_{2-x}\text{Sr}_x\text{B}_{10}\text{O}_{17}$ are observed between $x = 0$ and $x = 0.25$; hence, the solubility limit is at or below $x = 0.25$.

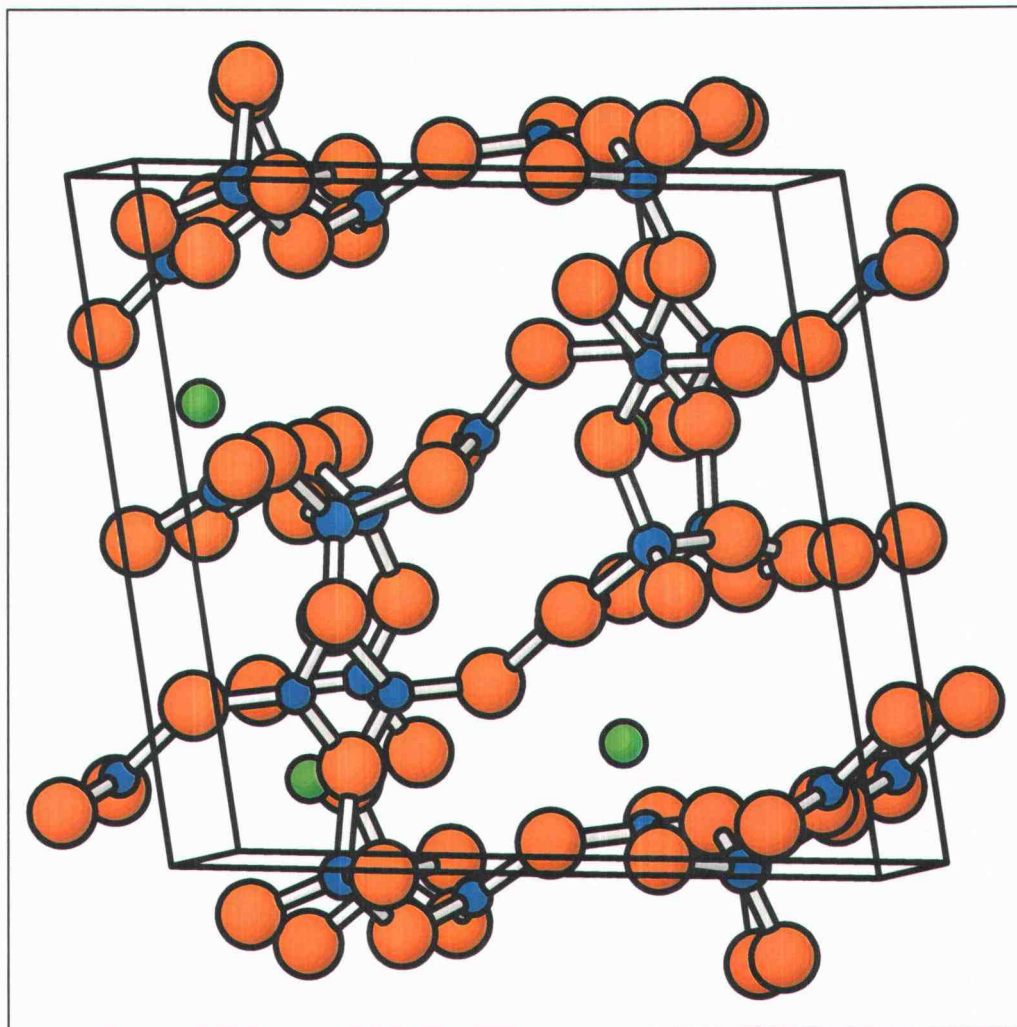


Figure 7.1. Structure of $\text{Ba}_2\text{B}_{10}\text{O}_{17}$ as viewed along c .

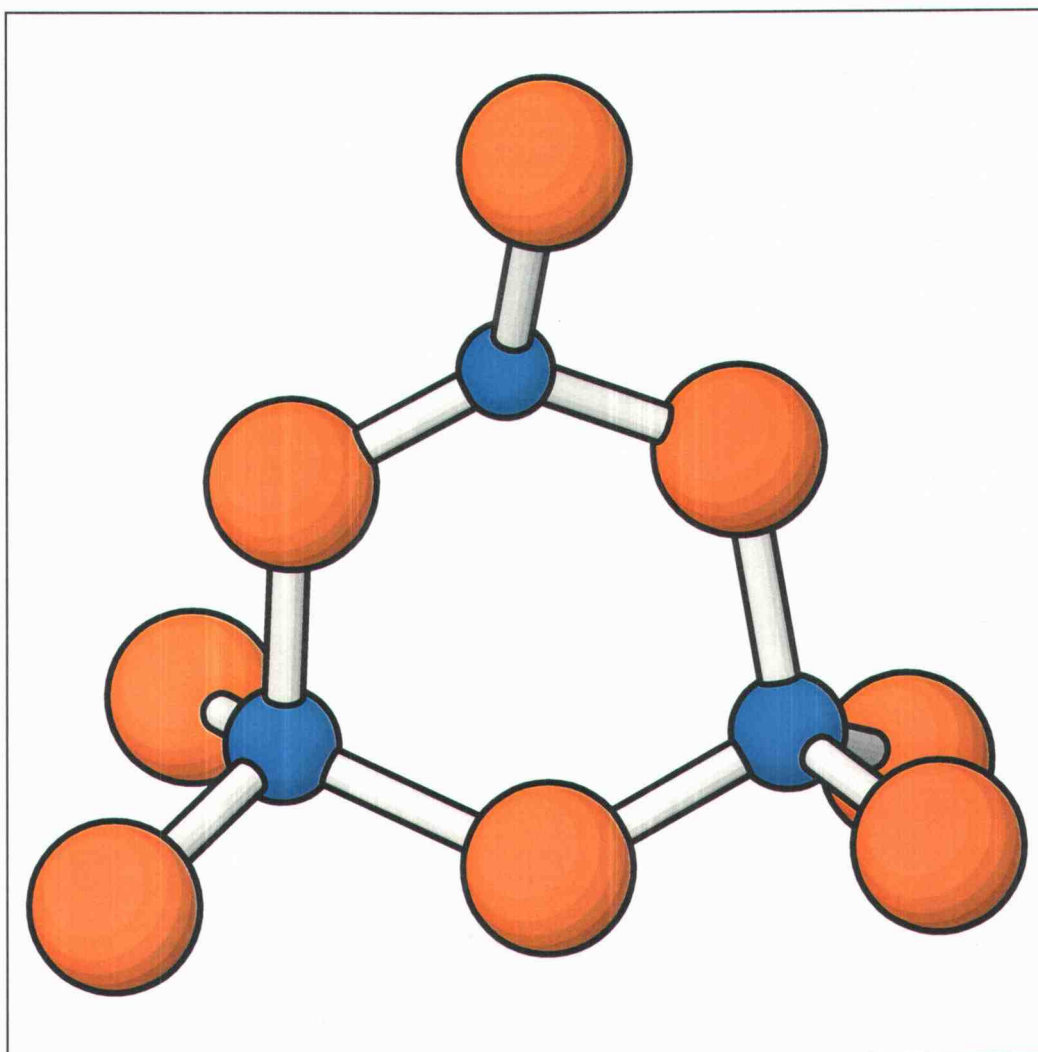


Figure 7.2. B₃O₈ ring.

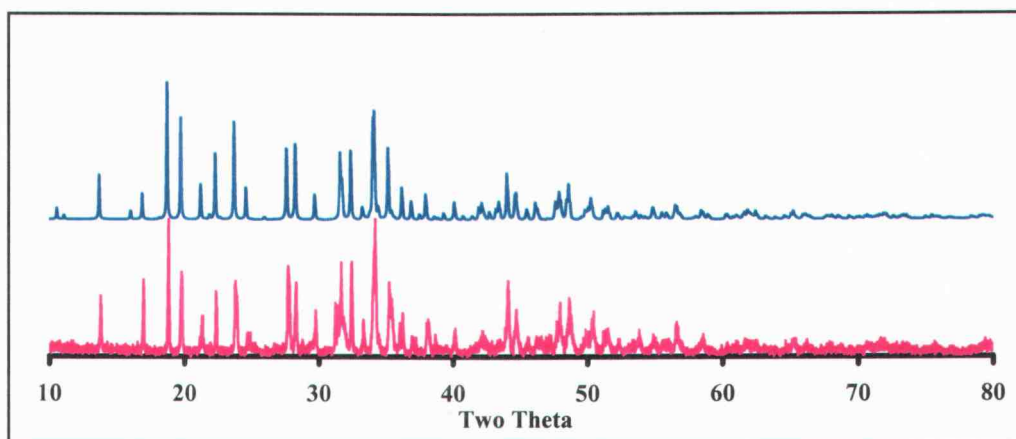


Figure 7.3. Calculated (top) and measured (bottom) X-ray powder patterns for $\text{Ba}_2\text{B}_{10}\text{O}_{17}$.

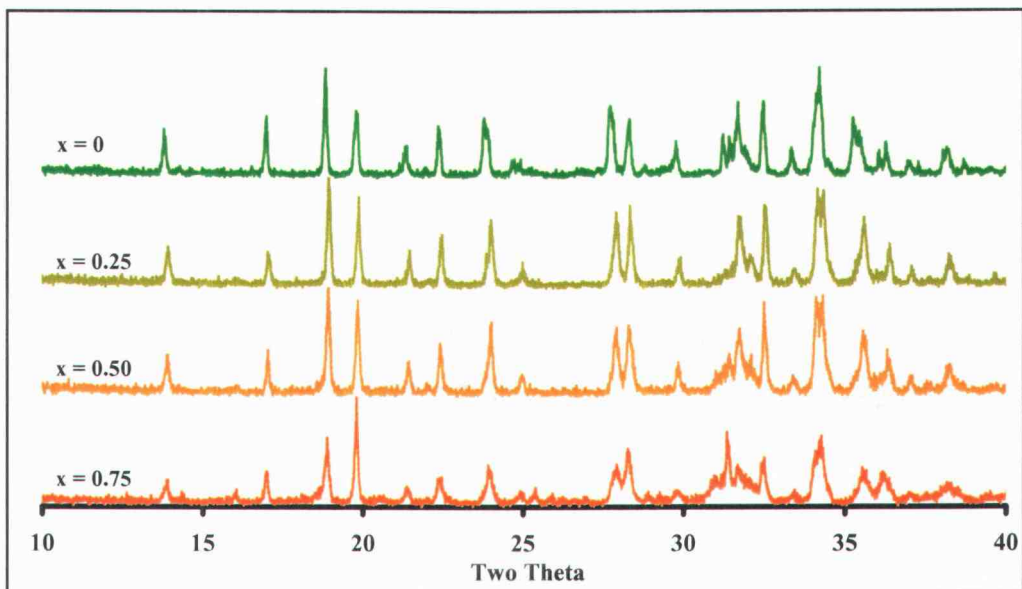


Figure 7.4. X-ray powder patterns for $\text{Ba}_{2-x}\text{Sr}_x\text{B}_{10}\text{O}_{17}$.

DTA data for glass and crystalline powder samples are given in Figures 7.5 and 7.6, respectively. For the glass on heating, a sharp exotherm corresponding to crystallization is observed at 700°C, and this is followed by a melting endotherm at 901°C; a corresponding recrystallization signal is not observed on cooling. The exotherm has been substantiated by visual and X-ray observation of large glass pellets which crystallize on annealing at 700°C. On heating a stoichiometric powder of $\text{Ba}_2\text{B}_{10}\text{O}_{17}$, a melting event is observed at 890°C. Following incorporation of Sr, a freezing point depression is noted, and the presence of two endotherms in the samples with $x = 0.50$ and 0.75 indicates phase separation. Considering these results in the context of the X-ray measurements, it is presumed that the solubility of Sr in $\text{Ba}_2\text{B}_{10}\text{O}_{17}$ does not extend beyond $x = 0.25$.

Transparent crystals of dimensions 1.0 x 1.0 x 0.4 cm were readily grown from a stoichiometric melt by utilizing a Pt wire as a nucleation source. X-ray patterns of these crystals were consistent with the triclinic structure of $\text{Ba}_2\text{B}_{10}\text{O}_{17}$, and second-harmonic generation with a 1064-nm source was confirmed. Additional work on crystal growth is in progress.

The second-harmonic signal for $\text{Ba}_2\text{B}_{10}\text{O}_{17}$ was measured to be $0.5 \cdot \text{KDP}$, which corresponds to $d_{\text{eff}} \sim 0.2 \text{ pm/V}$. The nonlinear d coefficients have been calculated on the basis of an oriented gas model (10, 11). In this model, the nonlinearity is associated primarily with the orientation of individual borate groups.

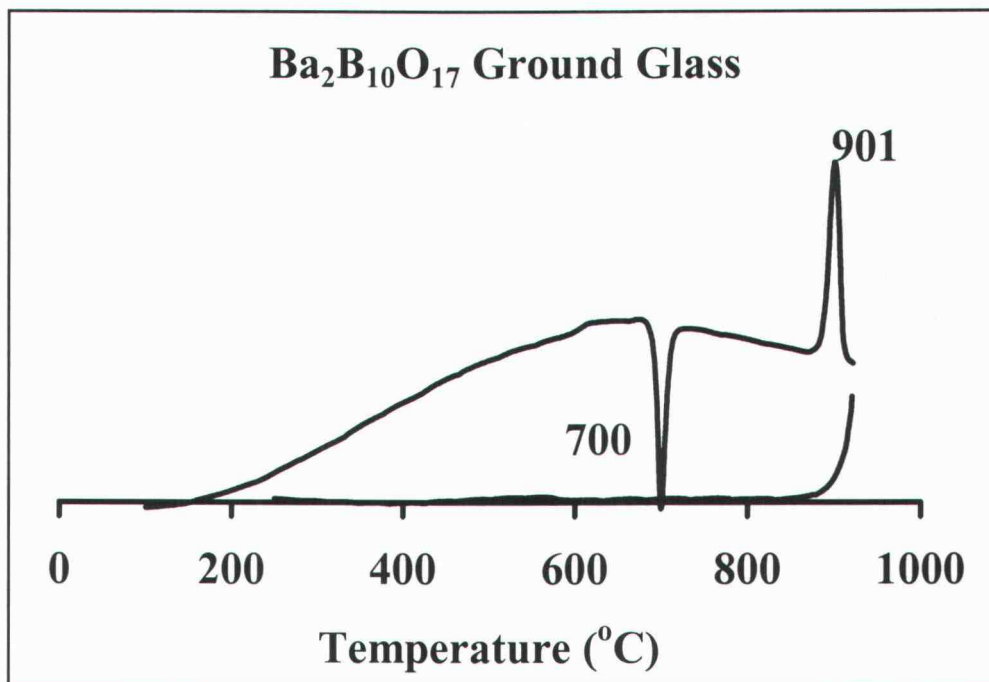


Figure 7.5. DTA of Ba₂B₁₀O₁₇ ground glass.

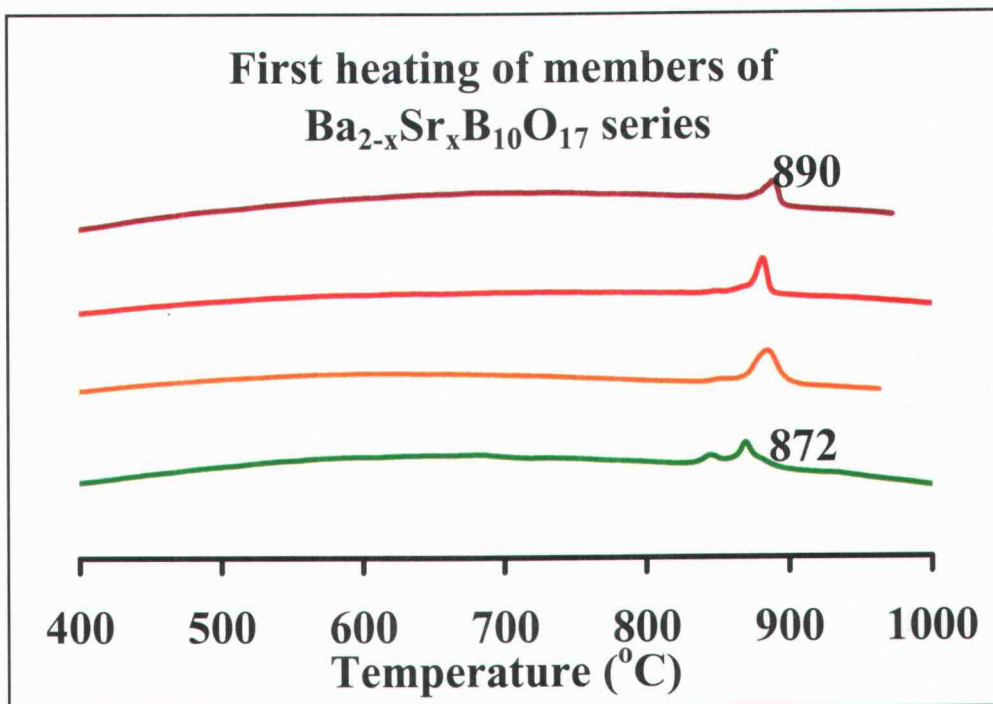


Figure 7.6. DTA of crystalline $\text{Ba}_{2-x}\text{Sr}_x\text{B}_{10}\text{O}_{17}$.

The method has been applied to a wide range of borates containing exclusively BO_3 groups, but it has only recently been successfully extended to the analysis of complex polyborates containing both BO_3 and BO_4 groups (12). By using eq. (7.1),

$$d_{ijk} = \frac{1}{V} \sum_1^N \sum_{lmn} R_{il} R_{jm} R_{kn} \beta_{lmn} \quad (7.1)$$

the components of the hyperpolarizability tensor components (β_{lmn}) are summed according to the direction cosines or orientation functions (R) of the individual groups and weighted by their number densities ($1/V$.) For polyborates, hyperpolarizabilities have generally been derived by various quantum-mechanical methods (11, 13). These results have to date provided rather poor agreement with experimental results from crystals. We note, however, that first-principle calculations have recently provided an effective means for calculation of both linear and nonlinear optical properties in various polyborate systems (14). To provide an effective, very simple predictive tool for estimating nonlinearities, we have derived values of β for BO_4 and BO_3 groups for use in polyborates from eq. 1 by using the reported crystal structure and d coefficients of LBO (12). Since transition moments and energy gaps for the BO_4 and BO_3 groups are expected to be similar, we assume $\beta(\text{BO}_4) = \beta(\text{BO}_3)$. With these simple assumptions, we readily calculate a value of $d_{11} = 0.2 \text{ pm/V}$ for $\text{Ba}_2\text{B}_{10}\text{O}_{17}$, a result that is entirely consistent with the SHG test.

Conclusions

The new, noncentrosymmetric borate $\text{Ba}_2\text{B}_{10}\text{O}_{17}$ has been structurally characterized, and some of its properties as a frequency-conversion crystal have been examined. Single crystals can be grown from a stoichiometric melt, and optical studies and modeling indicate a nonlinearity near 0.2 pm/V.

Acknowledgements

The authors gratefully acknowledge joint funding from CNRS and NSF.
We also thank Patrick Ascheoug for assistance with the SHG measurements.

References

- (1) P. A. Morris, "Defect chemistry of nonlinear optical oxide crystals," ACS Symp. Ser. (Mater. Nonlinear Opt.) **455**, pp. 380-393, 1991; P. A. Morris, "Impurities in nonlinear optical oxide crystals," *J. Cryst. Growth* **106**, pp. 76-78, 1990; P. A. Morris, "Defects in nonlinear optical oxide crystals," *Ceram. Trans. (Electro-Opt. Nonlinear Opt. Mater.)* **14**, pp. 1451-1465, 1990.
- (2) C. Chen, B. Wu, A. Jiang, G. You, R. Li, S. Lin, "New nonlinear-optical crystal: lithium borate (LiB_3O_5)," *J. Opt. Soc. Amer. B* **6**, pp. 616-621, 1988; S.P. Velsko, M. Webb, L. Davis, C. Huang, "Phase-matched harmonic generation in lithium triborate (LBO)," *IEEE J. Quant. Electron.* **27**, pp. 2182-2192 (1991).
- (3) C. Chen, B. Wu, A. Jiang, G. You, *Sci. Sin. Ser. B* **28**, pp. 235-240, 1985; D. Eimerl, L. Davis, S. Velsko, E.K. Graham, A. Zalkin, "Optical, mechanical, and thermal properties of barium borate," *J. Appl. Phys.* **62**, 1968-1983.
- (4) J.M. Tu, D.A. Keszler, "CsLiB₆O₁₀: A noncentrosymmetric polyborate" *Mater. Res. Bull.* **30**, pp. 209-214, 1995; Y. Mori, I Kuroda, S. Nakajima, T. Sasaki, S. Nakai, "Nonlinear optical properties of cesium lithium borate," *Appl. Phys. Lett.* **67**, pp. 1818-1820, 1995.
- (5) R. Komatsu, T. Sugawara, K. Sassa, N. Sarukura, Z. Liu, S. Izumida, Y. Segawa, S. Uda, T. Fukuda, K. Yamanouchi, "Growth and ultraviolet application of $\text{Li}_2\text{B}_4\text{O}_7$ crystals: Generation of the fourth and fifth harmonics of Nd:Y₃Al₅O₁₂ lasers," *Appl. Phys. Lett.* **70**, pp. 3492-3494, 1997.
- (6) S. Furusawa, O. Chikagawa, S. Tange, T. Ishidate, H. Orihara, Y. Ishibashi, K. Miwa, "Second harmonic generation in lithium diborate ($\text{Li}_2\text{B}_4\text{O}_7$)," *J. Phys. Soc. Japan* **60**, pp. 2691-2696, 1991; T.Y. Kwon, J.J. Ju, J.W. Cha, J.N. Kim, S.I. Yun, "Linear optical properties and characteristics of critically phase-matched second harmonic generation of a $\text{Li}_2\text{B}_4\text{O}_7$ crystal grown by the Czochralski method," *Mater. Lett.* **20**, pp. 211-216, 1994.
- (7) K. H. Huebner, "Borates $2\text{BaO} \cdot 5\text{B}_2\text{O}_3$, low- $\text{BaO} \cdot \text{B}_2\text{O}_3$, $2\text{BaO} \cdot \text{B}_2\text{O}_3$, and $4\text{BaO} \cdot \text{B}_2\text{O}_3$," *Neues Jahrb. Mineral. Monatsh.* **8**, pp. 335-342, 1969.
- (8) G.M. Sheldrick, "Phase annealing in SHELX-90: direct methods for larger structures," *Acta Crystallogr., Sect. A*, pp. 467-473, 1990.
- (9) TEXSAN, Structure Analysis Package, Molecular Structure Corporation, 900 New Trails Drive, Texas, USA, 77381-5209.
- (10) Kathleen I. Schaffers, Ph.D. dissertation, Oregon State University, 1992.

- (11) C.T. Chen, *Development of new nonlinear optical crystals in the borate series*, Harwood Academic Publishers, Langhorne, PA, 1993.
- (12) D.A. Keszler, "NLO materials for deep UV generation," American Conference on Crystal Growth and Epitaxy, Vail, CO, USA, August 2000; D.A. Keszler, "New materials for high-power laser systems," National Meeting of the Materials Research Society, Boston, MA, USA, December 2000.
- (13) W.D. Cheng, J.T. Chen, Q.W. Lin, Q.E. Zhang, J.X. Lu, "Cluster modeling of electronic structure and nonlinear properties for the optical materials MB_6O_{10} ($M=Cs_2, Li_2, CsLi$)," *Phys. Rev. B: Condens. Matter Mater. Phys.* **60**, pp. 11747-11754, 1999.
- (14) J. Lin, M.-H. Lee, Z.-P. Liu, C. Chen, C. J. Pickard, "Mechanism for linear and nonlinear optical effects in β - BaB_2O_4 crystals," *Phys. Rev. B: Condens. Matter Mater. Phys.* **60**, pp. 13380-13389, 1999; Z. Lin, J. Lin, Z. Wang, C. Chen, M.-H. Lee, "Mechanism for linear and nonlinear optical effects in LiB_3O_5 , CsB_3O_5 , and $CsLiB_6O_{10}$ crystals," *Phys. Rev. B: Condens. Matter Mater. Phys.* **62**, 1757-1764, 2000.

CHAPTER 8

 $\text{Sr}_3\text{Y}_{0.814}\text{Yb}_{0.186}(\text{BO}_3)_3$: STRUCTURE OF Yb-DOPED BORATE LASER MATERIAL

Jennifer L. Stone-Sundberg, Romain Gaumé, Paul-Henri Haumesser, Bruno Viana, Gérard Aka, Andrée Kahn-Harari, and Douglas A. Keszler

To be submitted to Solid State Science (2001).

Abstract

The structure of a new Yb-doped borate is reported. The compound $\text{Sr}_3\text{Y}_{0.814}\text{Yb}_{0.186}(\text{BO}_3)_3$ (Yb:BOYS) was found to crystallize in the trigonal space group R-3(h) [#148] with cell parameters of $a = 12.467(3)$, $c = 9.283(1)\text{\AA}$, $V = 1249.5(2)\text{\AA}^3$, and $Z = 6$. The occupancy of both Y atoms were refined and it was found that the Yb substitutes for only one of the two sites indicating a single luminescent center. The stoichiometry was confirmed by electron microprobe.

Introduction

When doped into certain hosts, the Yb^{3+} ion exhibits a broad emission band. This feature coupled with the small quantum defect and limited excited state absorption of Yb^{3+} provides a means to realize efficient, high-power, and short pulsewidth femtosecond lasers. Recently, the new Yb-doped borate crystal $\text{Sr}_3\text{Y}(\text{BO}_3)_3$ has been grown by using the Czochralski technique (1), and its optical properties have been characterized spectroscopically (2). The compound $\text{Sr}_3\text{Y}(\text{BO}_3)_3$ is isostructural to $\text{Sr}_3\text{Sc}(\text{BO}_3)_3$ (3), crystallizing as a member of the large STACK family of borates (4). This structure type is characterized by the presence of two crystallographically distinct, distorted octahedral sites that are occupied by the M^{3+} cations. In previous studies (4), crystallographic ordering has been observed between the two sites in mixed M^{3+} , M^{3+} systems on the basis of the sizes of the cations, but these studies did not include analysis of a system of cations of similar radii such as Y^{3+} ($r = 0.900 \text{ \AA}$) and Yb^{3+} ($r = 0.868 \text{ \AA}$). To examine this ordering and to assist in the continuing development of $\text{Yb}:\text{Sr}_3\text{Y}(\text{BO}_3)_3$ as a solid-state laser host, we describe herein the results of a crystal-structure analysis.

Experimental

Crystal growth

A crystal of $\text{Sr}_3\text{Y}_{0.85}\text{Yb}_{0.15}(\text{BO}_3)_3$ (Yb:BOYS) was Czochralski grown. The melt was prepared from a stoichiometric composition. The raw materials were alkaline earth carbonates and boron oxide with a purity of 99%, whereas the rare earth oxides were 99.99% pure. This growth was performed using a 50 mm diameter by 50 mm deep iridium crucible induction heated and embedded in ground zirconia surrounded by a calcia stabilized zirconia tube. The growth atmosphere was nitrogen, but the Czochralski apparatus was not well isolated from the ambient atmosphere. The rotation rate (from 10 to 50 rpm) always produces a convex crystallization interface. The crystallization rate was 1.2 mm/h. The process was automatically controlled by measuring the crystal weight to a sensitivity of 0.03 g with a Mettler PG802-S balance, and using a PI regulator to accurately control the crystal diameter. A typical boule size is 18 mm in diameter by 50-80 mm long. High temperature annealing is generally performed by maintaining the crystal at about 150 °C below its melting point for 36 h, and then cooling it down at a typical rate of 20 °C/h.

The Czochralski growth of Yb:BOYS is easy to control and leads to transparent boules when initiating the growth on an iridium rod. The spontaneous growth direction seems to be close to the unique optical axis of the structure. A

picture of the boule is given in Figure 8.1 and a summary of the growth parameters is presented in Table 8.1.



Figure 8.1. Boule of 15 at%-doped Yb:BOYS, grown on an iridium rod.

Table 8.1. Crystal growth parameters for Yb:BOYS.

Formula	$\text{Sr}_3\text{Y}_{0.85}\text{Yb}_{0.15}(\text{BO}_3)_3$
Space group	R-3 (uniaxial)
Z	6
a (Å)	12.48(8)
b (Å)	
c (Å)	9.27(5)
β (°)	
V (Å ³)	1252(1)
density	4.3
melting point (°C)	1400
seed orientation	no seed
diameter (mm)	18
useful length (cm)	4
growth rate (mm/h)	1.2
rotation rate (rpm)	10
cooling time (h)	43

X-Ray Analysis

Unit cell parameters and data collection

A small crystal (0.2 x 0.3 x 0.5 mm) was extracted from the Czochralski grown boule and mounted on a glass fiber with epoxy for X-ray analysis. All measurements were made on a Rigaku AFC6R diffractometer with graphite monochromated Mo-K α radiation from a rotating-anode generator.

Cell constants and an orientation matrix for data collection were obtained from a least-squares refinement by using the setting angles of 23 carefully centered reflections in the range $26.50 < 2\theta < 34.02^\circ$. The final cell is trigonal (hexagonal setting $-3m1$), having dimensions $a = 12.467(3)$, $c = 9.283(1)$ Å, and $V = 1249.5(2)$ Å³. On the basis of the systematic condition $hkl: -h+k+l = 3n$, packing considerations, a statistical analysis of intensity distribution, and the successful solution and refinement of the structure, the space group was determined to be R-3(h).

Data collection was performed by using the ω - 2θ scan technique to a maximum 2θ value of 65.2° . Scans of $(1.40 + 0.34 \tan \theta)^\circ$ were made at a speed of $16.0^\circ/\text{min}$ (in ω). The weak reflections ($I < 10.0\sigma(I)$) were rescanned a maximum of three times, and the counts were accumulated to ensure good counting statistics. Stationary background counts were recorded on each side of the reflection. The intensities of three representative reflections were measured after every block of 500 reflections; they had an average change of 0.05%; so no decay correction was applied.

Structure refinement

The structure was solved by direct methods (6) and expanded by using Fourier techniques (7). Refinement of the Y(1) and Y(2) occupancy parameters revealed that the Yb atom selectively occupied the Y(1) site. From the refined parameter, an approximate occupation of this site – 0.6 Y and 0.4 Yb – was deduced. The Yb atom was then added to the refinement with its occupancy parameter constrained to that of Y(1) to ensure unit occupancy. Following refinement with isotropic displacement parameters on each atom, the data were empirically corrected for absorption with the computer program DIFABS (5) and subsequently averaged ($R_{\text{int}} = 0.136$). Atoms Sr, Y(2), and B were then refined with anisotropic displacement coefficients. The final cycle of full-matrix least-squares refinement (8) with 510 observed reflections ($I > 3.00\sigma(I)$) and 37 variable parameters (secondary extinction coefficient = 4.18×10^{-7}) converged to the agreement factors $R = 0.051$ and $R_w = 0.050$.

Plots of $\sum w (|F_o| - |F_c|)^2$ versus $|F_o|$, reflection order in data collection, $\sin \theta/\lambda$ and various classes of indices showed no unusual trends. The maximum and minimum peaks on the final difference Fourier map corresponded to 1.1 and 0.9% of a Y atom, respectively.

Neutral atom scattering factors were taken from Cromer and Waber (10). Anomalous dispersion effects were included in F_{calc} (11); the values for $\Delta f'$ and $\Delta f''$ were those of Creagh and McAuley (12). The values for the mass attenuation coefficients are those of Creagh and Hubbel (13). All calculations were

performed by using the teXsan (14) crystallographic software package of Molecular Structure Corporation. A summary of experimental parameters is given in Table 8.2, positional and isotropic displacement parameters are presented in Table 8.3, anisotropic displacement parameters are listed in Table 8.4, and a tabulation of interatomic distance and angle is made in Table 8.5.

Table 8.2. Experimental details for the structure solution of Yb:BOYS.

Formula Weight, amu	545.02
Crystal System	Trigonal
Space Group	R-3 [#148]
a , Å	12.467(3)
c , Å	9.283(1)
V , Å ³	1249.5(2)
Z	6
D_{calc} , g cm ⁻³	4.345
$F(000)$	1477
Diffractometer	Rigaku AFC6R
Radiation	Mo K α ($\lambda=0.71069$) graphite-monochromated
Data Collection	$\pm h, k, \pm l$
No. Observations (total, unique) ($F_o^2 \geq 3\sigma(F_o^2)$)	3150, 1015 510
R	0.051
R_w	0.050
Maximum Shift in Final Cycle	0.03
GOF	1.35

$$R = \frac{\sum ||F_o| - |F_c||}{\sum |F_o|} = 0.051$$

$$R_w = \left[\frac{\sum w (|F_o| - |F_c|)^2}{\sum w F_o^2} \right]^{1/2} = 0.050$$

Table 8.3. Positional and isotropic displacement parameters (B_{eq}) for Yb:BOYS.

Atom	Wyc	x	y	z	Occ	B_{eq}^*
Yb(1)	3b	0	0	½	0.062	1.532
Y(1)	3b	0	0	½	0.105	1.532
Y(2)	3a	0	0	0	1/6	0.97(2)
Sr(1)	18f	0.5434	-0.0402	0.3101	1	2.026
O(1)	18f	0.7500(8)	0.0153(9)	0.198(1)	1	3.5(2)
O(2)	18f	0.1747(9)	0.0505(9)	0.6128(9)	1	3.9(2)
O(3)	18f	0.6154(9)	0.1574(9)	0.1751(9)	1	3.5(2)
B(1)	18f	0.200(1)	0.051(1)	0.751(1)	1	1.4(2)

$$*B_{eq} = (8\pi/3)^2 \sum_i \sum_j U_{ij} a_i^* a_j^* a_i a_j$$

Table 8.4. Anisotropic displacement parameters for Yb:BOYS.

Atom	U_{11}	U_{22}	U_{33}	U_{12}	U_{13}	U_{23}
Y(1)	0.044(1)	0.0436	0.044(6)	0.0218	0	0
Y(2)	0.0123(7)	0.0123	0.012(1)	0.0062	0	0
Sr(1)	0.0257	0.0257	0.0257	0.0128	0	0
B(1)	0.018(5)	0.018(5)	0.018(6)	0.009(4)	0	0

Table 8.5. Interatomic distances (Å) and angles (°) for Yb:BOYS.

Y(1) - O(2)	2.21(1) (x 6)	O(2) - Y(1) - O(2)	87.0(2)
Y(2) - O(3)	2.44(1) (x 6)	O(3) - Y(2) - O(3)	87.6(3)
			92.4(3)
			180.0000(2)
Sr(1) - O(1)	2.53(1)	O(1) - Sr(1) - O(1)	80.2(3)
	2.706(8)		
	2.45(1)		
O(2)	2.85(1)	O(2) - Sr(1) - O(2)	71.9(5)
	2.87(1)		
	2.730(9)		
O(3)	2.49(1)	O(1) - Sr(1) - O(3)	93.2(3)
	2.66(1)		
B(1) - O(1)	1.35(2)	O(1) - B(1) - O(2)	121(1)
O(2)	1.32(1)	O(2) - B(1) - O(3)	118(1)
O(3)	1.38(2)	O(1) - B(1) - O(3)	121(1)

Elemental analysis

A small sample of the crystal boule was coated with carbon, placed in an electron microprobe device (Cameca SX 50 WDS electron microprobe), and four sets of quantitative elemental analysis data were collected to determine the Y to Yb ratio. A summary of data is presented in Table 8.6.

Table 8.6. Microprobe analysis of Yb:BOYS crystal.

Element	Oxide Weight Percent	Cations per formula
Y	16.1(2)	0.814(4)
Yb	5.64(6)	0.186(4)

Results and Discussion

Structure

A picture of the structure of Yb:BOYS is given in Figure 8.2. The bond lengths and angles of the triangular BO₃ groups are regular with B – O bond lengths of 1.32(2), 1.35(1), and 1.38(1) Å, and O-B-O angles of 118(1) and 121(1)°. Both Y(1) and Y(2) atoms are slightly distorted octahedral and have Y – O bond lengths of 2.21(1) and 2.44 Å, and O-Y-O bond angles of 87.0(2), 87.6(3), 92.4(3), and 180.0000(2). The Sr atom is nine coordinate with Sr – O distances ranging from 2.45(1) to 2.87(1) Å. Calculated bond lengths from Shannon (15) crystal radii include B – O of 1.36 Å, Y – O of 2.26 Å, Yb – O of 2.228, and Sr – O of 2.66 Å.

Elemental Analysis

From the elemental analysis performed on the crystal, the ratio of Y to Yb was determined to be Y_{0.814(4)} and Yb_{0.186(4)}. This result is in excellent agreement with that determined by refinement of the occupancies during the single crystal structure refinement which also produced a Y to Yb ratio of Y_{0.814(4)} and Yb_{0.186(4)}.

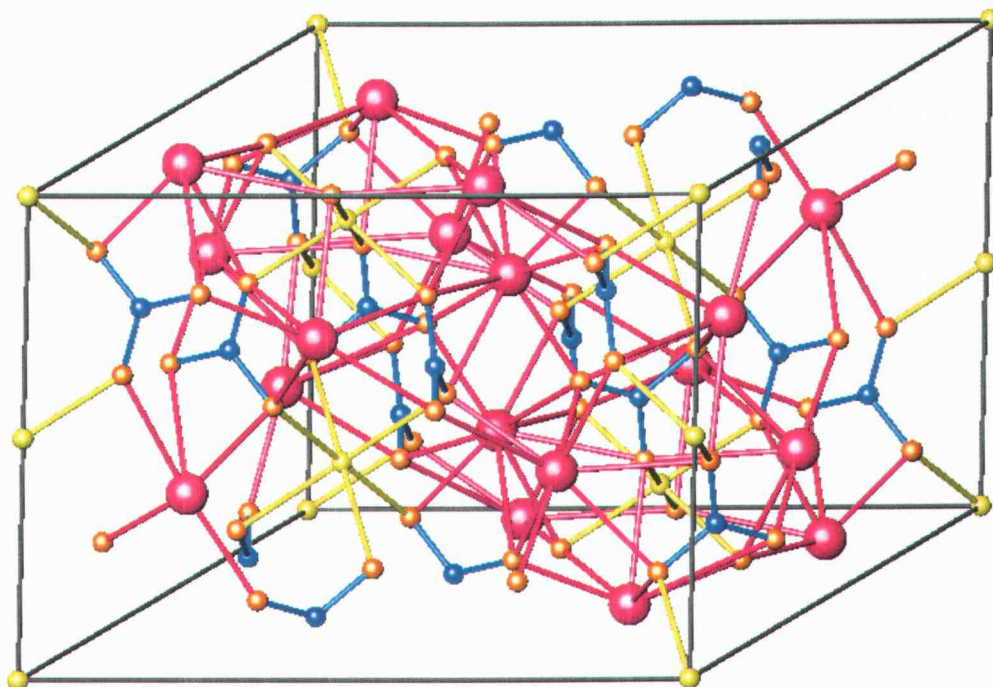


Figure 8.2. Structure of $\text{Sr}_3\text{Y}_{0.814}\text{Yb}_{0.186}(\text{BO}_3)_3$ viewed down the a axis. The c axis is vertical and the b axis is horizontal. Sr is pink, B is blue, Y is yellow, and O is gold.

Acknowledgements

The authors thank Professor Roger Nielsen for performing the microprobe elemental analysis. The authors gratefully acknowledge CNRS and NSF for funding.

References

- (1) Haumesser, Paul-Henri; Gaume, Romain; Viana, Bruno; Antic-Fidancev, Elisabeth; Vivien, Daniel. "Spectroscopic and crystal-field analysis of new Yb-doped laser materials." *J. Phys.: Condens. Matter* 13 23 5427-5447 (2001).
- (2) Haumesser, Paul-Henri; Gaume, Romain; Aka, Gerard; Viana, Bruno; Harari, Andree Kahn; Vivien, Daniel. "Elaboration and spectroscopic analysis of new Yb³⁺ doped double borates." *OSA Trends Opt. Photonics Ser.* 34 (Advanced Solid State Lasers) 555-560 (2000).
- (3) Thompson, P. D.; Keszler, D. A. "Structure of Sr₃Sc(BO₃)₃." *Chemistry of Materials* 6 2005-2007 (1994).
- (4) Schaffers, K. I.; Alekel, T.; Thompson, P. D.; Cox, J. R.; and Keszler, D. A. *Journal of the American Chemical Society* 112, 7068-xx (1990).
- (5) DIFABS: Walker, N. & Stuart, Acta Cryst. A39, 158-166 (1983). An empirical absorption correction program.
- (6) SIR92: Altomare, A., Casciarano, M., Giacovazzo, C., Guagliardi, A. (1993). *J. Appl. Cryst.*, 26, 343.
- (7) DIRDIF94: Beurskens, P.T., Admiraal, G., Beurskens, G., Bosman, W.P., de Gelder, R., Israel, R. and Smits, J.M.M.(1994). The DIRDIF-94 program system, Technical Report of the Crystallography Laboratory, University of Nijmegen, The Netherlands.
- (8) Least Squares function minimized:

$$\sum w(|F_o| - |F_c|)^2$$
 where

$$w = 1/[\sigma^2(F_o)] = [\sigma_c^2(F_o) + p^2 F_o^2/4]^{-1}$$

$$\sigma_c(F_o) = \text{e.s.d. based on counting statistics}$$

$$p = \text{p-factor}$$
- (9) Standard deviation of an observation of unit weight:

$$[\sum w(|F_o| - |F_c|)^2 / (N_o - N_v)]^{1/2}$$
 where N_o = number of observations
 N_v = number of variables
- (10) Cromer, D. T. & Waber, J. T.; "International Tables for X-ray Crystallography", Vol. IV, The Kynoch Press, Birmingham, England, Table 2.2 A (1974).

- (11) Ibers, J. A. & Hamilton, W. C.; *Acta Crystallogr.*, 17, 781 (1964).
- (12) Creagh, D. C. & McAuley, W.J .; "International Tables for Crystallography", Vol C, (A.J.C. Wilson, ed.), Kluwer Academic Publishers, Boston, Table 4.2.6.8, pages 219-222 (1992).
- 13) Creagh, D. C. & Hubbell, J.H.; "International Tables for Crystallography", Vol C, (A.J.C. Wilson, ed.), Kluwer Academic Publishers, Boston, Table 4.2.4.3, pages 200-206 (1992).
- (14) teXsan for Windows: Crystal Structure Analysis Package, Molecular Structure Corporation (1997).
- (15) Shannon, R. D. "Revised Effective Ionic Radii and Systematic Studies of Interatomic Distances in Halides and Chalcogenides." *Acta Cryst. A* 32 751-767 (1976).

BIBLIOGRAPHY

- (1) Adams, J. J., Ebberts, C. A., Schaffers, K. I., and Payne, S. A. "Nonlinear optical properties of $\text{LaCa}_4\text{O}(\text{BO}_3)_3$ " *Optics Letters* 26 (4) 217-219 (2001).
- (2) Aka, G., Viegas, N., Kahn-Harari, A., Vivien, D. "Optical Properties of Single Crystals of Gallium-substituted NYAB: $\text{Y}_{1-x}\text{Nd}_x(\text{Al}_{1-y}\text{Ga}_y)_3(\text{BO}_3)_4$." *J. Mater. Chem.* 5 (2) 265-271 (1995).
- (3) Aka, Gerard; Viegas, Nathalie; Teisseire, Beatrice; Kahn-Harari, Andree; and Godard, Jean. "Flux Growth and Characterization of Rare-earth-doped Non-linear Huntite-type Borate Crystals: $\text{Y}_{1-x}\text{Nd}_x(\text{Al}_{0.7}\text{Ga}_{0.3})_3(\text{BO}_3)_4$ and $\text{Y}_{1-x}\text{Yb}_x\text{Al}_3(\text{BO}_3)_4$." *J. Mater. Chem.*, 5 (4) 583-587 (1995).
- (4) Baldwin, George C. "An introduction to nonlinear optics." Plenum Press (1969).
- (5) Belokoneva, E. L., Azizov, A. V., Leonjuk, N. I., Simonov, M. A., Belov, N. V., "The crystal structure of $\text{YAl}_3(\text{BO}_3)_4$." *Zhurnal Strukturnoi Khimii* 22 196-198 (1981).
- (6) Bloembergen, Nicolaas. "Nonlinear optics, 4th Edition." World Scientific. (1996).
- (7) Boyd, Robert W. "Nonlinear optics." Academic Press. (1992).
- (8) CASIX Crystal Guide 1999. contact@casix.com.
- (9) Chai, Bruce H. T. "Advances in bulk inorganic nonlinear optical materials." *Optics & Photonics News* January 31-38 (1999).
- (10) Chani, Valery I.; Shimamura, Kiyoshi; Inoue, Keiji; and Fukuda, Tsuguo "Huntite-borate crystallization in stoichiometric melts." *Journal of Crystal Growth* 133 181-184 (1993).
- (11) Chani, Valery I.; Shimamura, Kiyoshi; Inoue, Keiji; and Fukuda, Tsuguo "Synthesis and search for equilibrium compositions of borates with the huntite structure." *Journal of Crystal Growth* 132 173-178 (1993).
- (12) Chen, C. T., *Development of new nonlinear optical crystals in the borate series*, Harwood Academic Publishers, Langhorne, PA, (1993).
- (13) Chen, C.; Wu, B.; Jiang, A.; and You, G. *Sci. Sin. Ser. B* 28, pp. 235-240, 1985; D. Eimerl, L. Davis, S. Velsko, E.K. Graham, A. Zalkin, "Optical,

- mechanical, and thermal properties of barium borate," *J. Appl. Phys.* **62**, 1968 (1983).
- (14) Chen, C.; Wu, B.; Jiang, A.; You, G.; Li, R.; and Lin, S. "New nonlinear-optical crystal: lithium borate (LiB_3O_5)," *J. Opt. Soc. Amer. B* **6**, pp. 616-621, (1988).
- (15) Cheng, W.D.; Chen, J.T.; Lin, Q.W.; Zhang, Q.E.; and Lu, J.X. "Cluster modeling of electronic structure and nonlinear properties for the optical materials MB_6O_{10} ($\text{M}=\text{Cs}_2, \text{Li}_2, \text{CsLi}$)," *Phys. Rev. B: Condens. Matter Mater. Phys.* **60**, pp. 11747-11754, (1999).
- (16) Creagh, D. C. & Hubbell, J.H.; "International Tables for Crystallography", Vol C, (A.J.C. Wilson, ed.), Kluwer Academic Publishers, Boston, Table 4.2.4.3, pages 200-206 (1992).
- (17) Creagh, D. C. & McAuley, W.J. ; "International Tables for Crystallography", Vol C, (A.J.C. Wilson, ed.), Kluwer Academic Publishers, Boston, Table 4.2.6.8, pages 219-222 (1992).
- (18) Cromer, D. T. & Waber, J. T.; "International Tables for X-ray Crystallography", Vol. IV, The Kynoch Press, Birmingham, England, Table 2.2 A (1974).
- (19) DIFABS: Walker, N. & Stuart, Acta Cryst. A39, 158-166 (1983). An empirical absorption correction program.
- (20) DIRDIF94: Beurskens, P.T., Admiraal, G., Beurskens, G., Bosman, W.P., de Gelder, R., Israel, R. and Smits, J.M.M.(1994). The DIRDIF-94 program system, Technical Report of the Crystallography Laboratory, University of Nijmegen, The Netherlands.
- (21) Dmitriev, V. G.; Gurzadyan, G. G.; Nikogosyan, D. N. "Handbook of nonlinear optical crystals." Springer-Verlag. (1991).
- (22) Emelyanova, E. N., Zigareve, T. A. "Tourmaline growth in hydrothermal conditions." *Kristallografiya* 5 955-957 (1960).
- (23) Ertl, A.; Pertlik, F.; and Bernhardt, H.-J. "Investigations on olenite with excess boron from the Koralpe, Styria, Austria." *Anzeiger Abt. I* 134 3-10 (1995).
- (24) Filimonov, A. A., Leonyuk N. I., Meissner, L. B., Timchenko, T. I., Rez, I. S. "Nonlinear Optical Properties of Isomorphic Family of Crystals with Yttrium-Aluminum Borate (YAB) Structure." *Kristall und Technik* 9 1 63-66 (1974).

- (25) Foit, Franklin F., Jr. "Crystal chemistry of alkali-deficient schorl and tourmaline structural relationships." *American Mineralogist* 74 (3-4) 422-431 (1989).
- (26) Foit, Franklin F., Jr.; Fuchs, Yves; Myers, Paul E. "Chemistry of alkali-deficient schorls from two tourmaline-dumortierite deposits." *American Mineralogist* 74 1317-1324 (1989).
- (27) Foit, Franklin F., Jr.; Rosenberg, Philip E. "The structure of vanadium-bearing tourmaline and its implications regarding tourmaline solid solutions." *American Mineralogist* 64 7-8 788-798 (1979).
- (28) Franken, P. A.; Hill, A. E.; Peters, C. W.; and Weinreich, G. "Generation of optical harmonics." *Physical Review Letters* 7 (4) 118-119 (1961).
- (29) Furusawa, S.; Chikagawa, O.; Tange, S.; Ishidate, T.; Orihara, H.; Ishibashi, Y.; and Miwa, K. "Second harmonic generation in lithium diborate ($\text{Li}_2\text{B}_4\text{O}_7$)," *J. Phys. Soc. Japan* 60, pp. 2691-2696, (1991).
- (30) Gay, P. "An introduction to crystal optics." Longman Group Limited. (1967).
- (31) Giordmaine, J. A. "Mixing of light beams in crystals." *Physical Review Letters*. 8 (1) 19-20 (1962).
- (32) Goerne, G. V., Franz, G., Heinrich, W. "Synthesis of tourmaline solid solutions in the system $\text{Na}_2\text{O-MgO-Al}_2\text{O}_3\text{-SiO}_2\text{-B}_2\text{O}_3\text{-H}_2\text{O-HCl}$ and the distribution of Na between tourmaline and fluid at 300 to 700°C and 200 Mpa." *Contributions to Mineralogy and Petrology* 141 2 160-173 (2001).
- (33) Hawthorne, Frank C.; Henry, Darrell J. "Classification of the minerals of the tourmaline group." *Eur. J. Mineral.* 11 2 201-215 (1999).
- (34) Huard, Serge. "Polarization of light." John Wiley & Sons. (1997).
- (35) Haumesser, Paul-Henri; Gaume, Romain; Viana, Bruno; Antic-Fidancev, Elisabeth; Vivien, Daniel. "Spectroscopic and crystal-field analysis of new Yb-doped laser materials." *J. Phys.: Condens. Matter* 13 23 5427-5447 (2001).
- (36) Haumesser, Paul-Henri; Gaume, Romain; Aka, Gerard; Viana, Bruno; Harari, Andree Kahn; Vivien, Daniel. "Elaboration and spectroscopic analysis of new Yb^{3+} doped double borates." *OSA Trends Opt. Photonics Ser. 34 (Advanced Solid State Lasers)* 555-560 (2000).
- (37) Huebner, K. H. "Borates $2\text{BaO} \cdot 5\text{B}_2\text{O}_3$, $\text{low-BaO} \cdot \text{B}_2\text{O}_3$, $2\text{BaO} \cdot \text{B}_2\text{O}_3$, and $4\text{BaO} \cdot \text{B}_2\text{O}_3$," *Neues Jahrb. Mineral. Monatsh.* 8, pp. 335-342, (1969).

- (38) Ibers, J. A. & Hamilton, W. C.; *Acta Crystallogr.*, 17, 781 (1964).
- (39) Ilyukhin, A. B.; Dzhurinskii, B. F. "Crystal structures of double oxoborates $\text{LnCa}_4\text{O}(\text{BO}_3)_3$ (Ln=Gd, Tb, Lu) and $\text{Eu}_2\text{CaO}(\text{BO}_3)_2$ " *Zhurnal Neorganicheskoi Khimii* 38 917-920 (1993).
- (40) Jung, S. T., Choi, D. Y., and Chung, S. J. "Crystal growth of neodymium yttrium aluminum borate with several neodymium contents." *Materials Research Bulletin* 31 8 1007-1012 (1996).
- (41) Jung, S. T., Choi, D. Y., Kang, J. K., Chung, S. J. "Top-seeded growth of $\text{Nd:YAl}_3(\text{BO}_3)_4$ from high temperature solution." *Journal of Crystal Growth* 148 207-210 (1995).
- (42) Jung, S. T., Yoon, J. T., and Chung, S. J. "Phase Transition of Neodymium Yttrium Aluminum Borate with Composition." *Materials Research Bulletin* 31 8 1021-1027 (1996).
- (43) Kaduk, James A., Pei, Shiyou. "The Crystal Structure of Hydrated Sodium Aluminate, $\text{NaAlO}_2 \cdot \frac{1}{2}\text{H}_2\text{O}$, and Its Dehydration Product" *Journal of Solid State Chemistry* 115, 126-139 (1995).
- (44) Kargaltsev, S. V. "Study of characteristics of growth of synthetic tourmaline crystals." Conference proceedings Fiz.-Khim. Issled. Sulfidnykh silik. Sist. Publisher Akad. Nauk, SSSR. 73-79 (1984).
- (45) Keszer, D.A. "NLO materials for deep UV generation," American Conference on Crystal Growth and Epitaxy, Vail, CO, USA, August 2000; D.A. Kesler, "New materials for high-power laser systems," National Meeting of the Materials Research Society, Boston, MA, USA, December (2000).
- (46) Klein, Cornelis; Hurlbut, Cornelius S. "Manual of Mineralogy, 21st Edition." John Wiley & Sons, Inc. (1993).
- (47) Komatsu, R.; Sugwara, T.; Sassa, K.; Sarukura, N.; Liu, Z.; Izumida, S.; Segawa, Y.; Uda, S.; Fukuda, T.; and Yamanouchi, K. "Growth and ultraviolet application of $\text{Li}_2\text{B}_4\text{O}_7$ crystals: Generation of the fourth and fifth harmonics of $\text{Nd:Y}_3\text{Al}_5\text{O}_{12}$ lasers," *Appl. Phys. Lett.* 70, pp. 3492-3494, (1997).
- (48) Kurtz, S. K., and Perry, T. T. "A Powder Technique for the Evaluation of Nonlinear Optical Materials." *Journal of Applied Physics* 39 8 3798-3813 (1968).
- (49) Kwon, T.Y.; Ju, J.J.; Cha, J.W.; Kim, J.N.; and Yun, S.I. "Linear optical properties and characteristics of critically phase-matched second harmonic

generation of a $\text{Li}_2\text{B}_4\text{O}_7$ crystal grown by the Czochralski method," *Mater. Lett.* **20**, pp. 211-216, (1994).

(50) Least Squares function minimized:

$\Sigma w(|F_o| - |F_c|)^2$ where

$$w = 1/[\sigma^2(F_o)] = [\sigma^2c(F_o) + p^2F_o^2/4]^{-1}$$

$\sigma c(F_o)$ = e.s.d. based on counting statistics

p = p-factor

(51) Leonyuk, N. I., Leonyuk, L. I. "Growth and Characterization of $\text{RM}_3(\text{BO}_3)_4$ Crystals." *Prog. Crystal Growth and Charact.* **31** 179-278 (1995).

(52) Lin, J.; Lee, M.-H.; Liu, Z.-P.; Chen, C.; and Pickard, C. J. "Mechanism for linear and nonlinear optical effects in $\beta\text{-BaB}_2\text{O}_4$ crystals," *Phys. Rev. B: Condens. Matter Mater. Phys.* **60**, pp. 13380-13389, (1999).

(53) Lin, Z.; Lin, J.; Wang, Z.; Chen, C.; Lee, M.-H. "Mechanism for linear and nonlinear optical effects in LiB_3O_5 , CsB_3O_5 , and $\text{CsLiB}_6\text{O}_{10}$ crystals," *Phys. Rev. B: Condens. Matter Mater. Phys.* **62**, 1757-1764, (2000).

(54) MacDonald, Daniel J.; Hawthorne, Frank C. "The crystal chemistry of Si \leftrightarrow Al substitution in tourmaline." *The Canadian Mineralogist* **33** 849-858 (1995).

(55) Maker, P. D.; Terhune, R. W.; Nisenoff, M.; and Savage, C. M. "Effects of dispersion and focusing on the production of optical harmonics." *Physical Review Letters.* **8** (1) 21-22 (1962).

(56) Mashkovtsev, R. I. "Optical absorption in synthetic tourmalines containing Mn, Fe, Ni, and Cu." *Geol. Geofiz.* **36** 4 122-126 (1995).

(57) Mori, Y.; Kuroda, I.; Nakajima, S.; Sasaki, T. and Nakai, S. "Nonlinear optical properties of cesium lithium borate," *Appl. Phys. Lett.* **67**, pp. 1818-1820, (1995).

(58) Morris, P. A. "Defect chemistry of nonlinear optical oxide crystals," *ACS Symp. Ser. (Mater. Nonlinear Opt.)* **455**, pp. 380-393, (1991).

(59) Morris, P. A. "Defects in nonlinear optical oxide crystals," *Ceram. Trans. (Electro-Opt. Nonlinear Opt. Mater.)* **14**, pp. 1451-1465, (1990).

(60) Morris, P. A. "Impurities in nonlinear optical oxide crystals," *J. Cryst. Growth* **106**, pp. 76-78, (1990).

(61) Mougel, F., Aka, G., Kahn-Harari, A., Hubert, H., Benitez, J. M., and Vivien, D. "Infrared laser performance and self-frequency doubling of $\text{Nd}^{3+}:\text{Ca}_4\text{GdO}(\text{BO}_3)_3$ ($\text{Nd}:\text{GdCOB}$)." *Optical Materials* **8** 161-173 (1997).

- (62) Nikolov, V., Peshev, P. "A new solvent for the growth of $Y_{1-x}Nd_xAl_3(BO_3)_4$ single crystals from high-temperature solutions." *Journal of Crystal Growth* 144 187-192 (1994).
- (63) Nye, J. F. "Physical properties of crystals." Oxford University Press Inc. (1985).
- (64) O'Keeffe, M. O.; and Hyde, B. G. *Acta Crystallographica, Section B* 34, 27 (1978).
- (65) Peterson, Gregory A., Keszler, Douglas A., Reynolds, Thomas A. "Stoichiometric, trigonal huntite borate $CeSc_3(BO_3)_4$." *International Journal of Inorganic Materials* 2 101-106 (2000).
- (66) Pieczka, Adam. "Statistical interpretation of structural parameters of tourmalines. The ordering of ions in the octahedral sites." *Eur. J. Mineral.* 11 2 243-251 (1999).
- (67) Piezo Systems, Inc. "History of Piezoelectricity." <http://www.piezo.com/history.html> (2001).
- (68) Prasad, Paras N.; and Williams, David J. "Introduction to nonlinear optical effects in molecules & polymers." John Wiley & Sons, Inc. (1991).
- (69) Reid, A. F.; Ringwood, A. E. *Inorganic Chemistry* 7 443-5 (1968).
- (70) Rosenberg, Philip E.; Foit, Franklin F.; "Synthesis and characterization of alkali-free tourmaline." *American Mineralogist* 64 1-2 180-186 (1979).
- (71) Rosenberg, Philip E.; and Foit, Franklin F., Jr.; "Tourmaline solid solutions in the system $MgO-Al_2O_3-SiO_2-B_2O_3-H_2O$." *American Mineralogist* 70 11-12 1217-1223 (1985).
- (72) Rosenberg, Philip E.; Foit, Franklin F., Jr.; Ekambaram, Vanavan. "Synthesis and characterization of tourmaline in the system $Na_2O-Al_2O_3-SiO_2-B_2O_3-H_2O$." *American Mineralogist* 71 7-8 971-976 (1986).
- (73) Schaffers, Kathleen I. Ph.D. dissertation, Oregon State University, (1992).
- (74) Schaffers, K. I.; Alekel, T.; Thompson, P. D.; Cox, J. R.; and Keszler, D. A. *Journal of the American Chemical Society* 112, 7068-xx (1990).
- (75) Schreyer, Werner; Wodara, Ulrich; Marler, Bernd; VanAken, Peter A.; Seifert, Freidrich; Robert, Jean-Louis. "Synthetic tourmaline (olenite) with excess

boron replacing silicon in the tetrahedral site: I. Synthesis conditions, chemical and spectroscopic evidence.” *Eur. J. Mineral.* 12 3 529-541 (2000).

(76) Shannon, R. D. “Revised Effective Ionic Radii and Systematic Studies of Interatomic Distances in Halides and Chalcogenides.” *Acta Cryst. A* 32 751-767 (1976).

(77) Shao, Zongshu; Lu, Junhua; Wang, Zhengping; Wang, Jiyang; and Jiang, Minhua. “Anisotropic properties of Nd:ReCOB (Re=Y, Gd): A low symmetry self-frequency doubling crystal.” *Process in Crystal Growth and Characterization of Materials* 40 63-73 (2000).

(78) Sheldrick, G.M. “Phase annealing in SHELX-90: direct methods for larger structures,” *Acta Crystallogr., Sect. A*, pp. 467-473 (1990).

(79) Shulze, Gustav E. R.; “Die Kristallstruktur von BPO₄ und BasO₄.” *Z. Physikal. Chem. B* 24 215-240 (1933).

(80) SIR92: Altomare, A., Cascarano, M., Giacovazzo, C., Guagliardi, A. *J. Appl. Cryst.*, 26, 343 (1993).

(81) Smirnov, N.B.; Burmakin, E. I.; Shekhtman, G. Sh.; Stepanov, A. P. *Russ. J. Electrochem.* 36 408-412 (2000).

(82) Smith, A. V. “How to select nonlinear crystals and model their performance using SNLO software,” <http://www.sandia.gov/imrl/XWEB1128/xxtal.htm> (2000).

(83) Standard deviation of an observation of unit weight:

$$[\sum w(|F_o| - |F_c|)^2 / (N_o - N_v)]^{1/2}$$

where N_o = number of observations
 N_v = number of variables

(84) Suwa Seikosha Co., Ltd., Japan. “Growth of synthetic tourmaline single crystals.” Japanese patent JP 59152286 A2 19840830. *Jpn. Kokai tokkyo Koho* (1984).

(85) teXsan for Windows: Crystal Structure Analysis Package, Molecular Structure Corporation (1997).

(86) Thompson, P. D.; Keszler, D. A. “Structure of Sr₃Sc(BO₃)₃.” *Chemistry of Materials* 6 2005-2007 (1994).

(87) Tu, J.M.; and Keszler, D.A. “CsLiB₆O₁₀: A noncentrosymmetric polyborate” *Mater. Res. Bull.* 30, pp. 209-214 (1995).

- (88) Velsko, S.P.; Webb, M.; Davis, L.; and Huang, C. "Phase-matched harmonic generation in lithium triborate (LBO)," *IEEE J. Quant. Electron.* **27**, pp. 2182-2192 (1991).
- (89) Wang, Jiyang; Shao, Zongsu; Wei, Jingqian; Hu, Xiaobo; Liu, Yaogang; Gong, Bo; Li, Guangming; Lu, Junhua; Guo, Ming; and Jiang, Minhua. "Research on Growth and Self-Frequency Doubling of Nd:ReCOB (Re=Y or Gd) Crystals." *Progress in Crystal Growth and Characterization of Materials* **40** 17-31 (2000).
- (90) Wang, Guofu; Han, T. P. J.; Gallagher, H. G.; and Henderson, B. "Crystal growth and optical properties of $\text{Ti}^{3+}:\text{YAl}_3(\text{BO}_3)_4$ and $\text{Ti}^{3+}:\text{GdAl}_3(\text{BO}_3)_4$." *Journal of Crystal Growth* **181** 48-54 (1997).
- (91) Wang, Guofu; He, Meiyun; Chen, Wenzhi; Lin, Zhonbin; Lu, Shaofang; and Wu, Qiangjin "Structure of low temperature phase $\gamma\text{-LaSc}_3(\text{BO}_3)_4$ crystal." *Mat. Res. Innovat.* **2** 341-344 (1999).
- (92) Wang, Pu; Dawes, Judith M.; Dekker, Peter; Knowles, David S.; and Piper, James A. "Growth and evaluation of ytterbium-doped yttrium aluminum borate as a potential self-doubling laser crystal." *J. Opt. Soc. Am. B* **16** 1 63-69 (1999).
- (93) Wang, Pu; Dawes, Judith M.; Dekker, Peter; Piper, James A. "Highly efficient diode-pumped ytterbium-doped yttrium aluminum borate laser." *Optics Communications* **174** 467-470 (2000).
- (94) Webster, Robert. "Gems: Their Sources, Descriptions, and Identification, 5th Edition." Butterworth Heinemann (1994).
- (95) Xue, D., Betzler, K., and Hesse, H. "Structural characteristics and second order nonlinear optical properties of borate crystals." *OSA Trends Opt. Photonics Ser. (Advanced Solid State Lasers)* **34** 542-547 (2000).
- (96) Yariv, Amnon; and Yeh, Pochi. "Optical waves in crystals." John Wiley & Sons, Inc. (1984).
- (97) Zachariassen, W. H.; and Plettinger, H. A. *Acta Crystallographica* **18**, 710 (1965).
- (98) Zernike, Frits; and Midwinter, John E. "Applied nonlinear optics." John Wiley & Sons, Inc. (1973).
- (99) Zhang, Shujun; Cheng, Zhenxiang; Zhou, Guangyong; Sun, Yuming; Hou, Xueyan; Liu, Xuesong; Han, Jianru; Shao, Zongshu; and Chen, Huanchu. "Growth and Properties of $(\text{Cr}^{3+}, \text{Nd}^{3+})$ Doped $\text{GdCa}_4\text{O}(\text{BO}_3)_3$ Crystals." *Progress in Crystal Growth and Characterization of Materials* **40** 81-88 (2000).